ORNL-2199 *4A*
C-84 – Reactors – Special

AEC RESEARCH AND DEVELOPMENT REPORT Features of Aircraft Reactors

INVESTIGATION OF FLUID FLOW IN THE

ART AND OTHER REFLECTOR-MODERATED

REACTOR CORES

G. L. Muller
J. O. Bradfute
F. E. Lynch

OAK RIDGE NATIONAL LABORATORY

operated by

UNION CARBIDE CORPORATION

for the

U.S. ATOMIC ENERGY COMMISSION

Reactor Projects Division

INVESTIGATION OF FLUID FLOW IN THE ART AND OTHER

REFLECTOR-MODERATED REACTOR CORES

G. L. Muller
J. O. Bradfute
F. E. Lynch

DATE ISSUED

APR 9 1959

TABLE OF CONTENTS

INVESTIGATION OF FLUID FLOW IN THE ART AND OTHER
REFLECTOR-MODERATED REACTOR CORES

SUMMARY

The turbulent flow of liquid through ART reflector-moderated reactor cores of annular cross section has been studied because of the need to obtain a steady flow exclusive of the normal unsteadiness of turbulent flow in ducts. This steadiness is important because when a large amount of heat $(100,000,000$ Btu/hr-ft^3) is being generated in the volume of liquid by nuclear fission at high temperatures $(1200^{\circ}F - 1600^{\circ}F)$, low-frequency temperature fluctuations due to unsteady, irregular flow of the liquid can result in hot spots, thermal cycling, and fatigue of the containing materials.

To facilitate the experimental work, studies were made of water flowing through quarter-scale transparent plastic models of the cores so that flow visualization techniques could be used in the work.

An extensive series of tests of many core systems were made over a range of Reynolds moduli based on core midplane dimensions and axial flow rate up to $\sim 90,000$. The corresponding Reynolds modulus for the "21-inch" ART core was $\sim 95,000$, using the properties of fluoride mixture No. 30 at $1425^{\circ}F$. Also, analyses were made of velocity and static pressure data obtained on a full-size "21-inch" ART core model with several different entrance conditions by Whitman, Stelzman, and Furgerson of ARED.

The following conclusions were reached as a result of this series of experiments:

(a) Axial flow through the cores with sufficiently large cross-sectional area expansion rates considered here will always be accompanied by a separation of the forward flow from a point on the outer wall near the inlet and violently unsteady reverse flow in the "separated" region. This separation at the outer wall is due to the large adverse pressure gradient resulting from the large area expansion rate, the lower fluid shear stress at the outer wall than at the inner wall (common to flow through annular ducts), and the curvature of the channel. The flow into the entrance of the core models was always uniform radially and circumferentially, having passed through a calming length of 40 diameters of straight pipe into an annular "nozzle" which was mounted on the core entrance.

(b) Rotational, or spiral, flow through the same cores is always accompanied by separation of the forward flow from a point on the inner wall near the inlet and unsteady reverse flow in the separated region with a velocity component in the direction of the rotation. The separation in this case is caused by the same adverse pressure gradient and the lower fluid shear stress at the inner wall relative to the outer wall (a phenomenon of flow in curved channels). Again, the flow at the core entrance was uniform radially and circumferentially, having passed through 40 diameters of straight pipe into an annular "nozzle" which preceded the turning-vane section which produced the rotational flow.

(c) In rotational flow, the turbulent interchange of momentum and the eddy

conductivity are diminished at the inner wall due to the centrifugal force field set up by the fluid motion; and, therefore, increased temperatures due to volume heat generation can be expected at the inner wall over the temperatures obtained in straight flow at the same rate in an equivalent channel.

(d) If the spiral velocities are very high, frictional forces become of such magnitude that a decay of the spiral velocities becomes noticeable and a backflow due to spiral vortex decay will begin. This was noticed in the high spiral velocity case studied by Whitman, Stelzman, and Furgerson. Backflow occurred on the inner wall at the exit plane.

(e) Turbulence promotion within the cores has been shown to overcome the effects of adverse pressure gradients, but the promoters must be such that they do not introduce unsteady flow; i.e., the scale of the promoted turbulence must be very small. Woven-wire screens and perforated-plate screens of low solidity and small wire diameter (or web thickness) packed into the divergent part of the core flow channels are of such nature. Turbulence promoters such as vortex generators or large obstructions placed in the core entrance cause unsteady flow although they seem to eliminate the separation and the associated backflows.

(f) Straight annular cores and cores of sufficiently low expansion rates can be constructed to give a steady, unseparated flow with axial flow. Calculations show that the maximum midplane-to-inlet area ratio that can be achieved with axial flow through a bare core is 1.33:1 within an 18-in. length of a 21-in.-O.D. core with the same midplane area

as the "21-inch" ART core.

(g) Calculations have shown that a pressure unbalance (4 lb/in.^{2}) due to momentum transfer exists in the header which is of the same order as the friction losses in the core. This pressure discrepancy is in the form of a rise in pressure as the fluid traverses the length of the header from the inlet duct. The unbalance, plus any unsteadiness transmitted to the flow by the fuel pumps, will also create peripheral flow asymmetries and unsteady core flow.

The calculations also point up two considerations. One is that the header pressure unbalances are primarily due to the average fluid velocity level in the headers considered. Thus, header fluid velocities should be kept as low as practicable. The core pressure loss should also be as large as practical to keep the relative importance of the header unbalances small.

(h) Since screen packing in the core has been shown to eliminate the unsteady flow, which is an inherent characteristic of the core shape, it is proposed that this system be used in the core. An additional advantage accrues from the use of the screens in an increase in core pressure loss and the related velocity profile flattening. The peripheral asymmetry due to pressure unbalances in the header will then be much less than exists without the screens. It is felt that perforated-plate screens with the same relative pressure loss and mesh size as the wire screens tested would be more advantageous from the structural and fabrication standpoint than the wire screens.

The heat-transfer characteristics of the screens are in the process of being investigated to determine whether any problems exist in this regard.

(i) A header system has been designed which may afford smaller pressure unbalances than the present header system and, being used in conjunction with the screen-packed core, may allow single-pump operation without large peripheral flow asymmetries. Further experimental work is in process to establish the validity of this conclusion and conclusions (g) and (h).

NOMENCLATURE

a	constant, ft^2
A_c	core cross-sectional area perpendicular to core axis, ft^2
A_h	header cross-sectional area perpendicular to flow direction, ft^2
b	constant, ft
c	constant, ft^2/sec
C_1	constant, ft^{-2}
C_2	constant, ft^2
d	typical dimension of screens; wire diameter, bar width, effective web thickness of perforated-plate screen $(d = M - 0.95\,D)$, etc., ft
D	hole diameter in perforated-plate screen, ft
D_h	hydraulic diameter, ft
e	eddy diffusivity, equal to $\frac{\epsilon}{\rho}$, ft^2/sec
f	coefficient of friction in Fanning equation, dimensionless
g_c	gravitational constant, ft/sec^2
h	head, ft
h_1	head at position 1, ft
h_2	head at position 2, ft
l	mixing length according to Prandtl, ft
L	flow path length in core, ft
L_a	axial length of core, ft
L_s	spiral flow path length in core, ft
M	mesh size of screen, ft
N_{Re}	Reynolds modulus, dimensionless

$N_{Re,sc}$	Reynolds modulus based on d, typical dimension of screen, dimensionless
$N_{Re,avg}$	axial flow Reynolds modulus based on average core dimensions and mass flow rate in core, dimensionless
$N_{Re,mid}$	axial flow Reynolds modulus based on core midplane or equator dimensions and mass flow rate in core, dimensionless
p	pressure, lb/ft^2
p_i	pressure at inner core wall, lb/ft^2
p_o	pressure at outer core wall, lb/ft^2
p_1'	pressure at position 1, including pressure due to elevation, lb/ft^2
p_2'	pressure at position 2, including pressure due to elevation, lb/ft^2
p_{0°	pressure at 0-deg plane in header, lb/ft^2 (see Figure 20)
p_{90°	pressure at 90-deg plane in header, lb/ft^2 (see Figure 20)
p_{130°	pressure at 130-deg plane in header, lb/ft^2 (see Figure 20)
Δp	pressure difference, lb/ft^2
Δp_a	axial-flow pressure difference across core, lb/ft^2
Δp_s	spiral-flow pressure difference across core, lb/ft^2
Q	volume flow rate, ft^3/sec
r	radius, ft
r_i	radius of inner wall of core, ft
r_m	radius of centerline of core flow channel, ft
r_o	radius of outer wall of core, ft
R	ratio of spiral flow path length to core length, dimensionless
s	a length along spiral flow path, ft
t	half-width of core flow channel perpendicular to channel centerline, ft
u'	root-mean-square of fluctuating velocity component in direction perpendicular to plane of channel walls in two-dimensional flow, ft/sec

v_a axial component of velocity in core, ft/sec

$v_{a,avg}$ average of above, ft/sec

v_h fluid velocity in header, ft/sec

v_{hi} fluid velocity at inlet of header, ft/sec

v_m mean velocity in channel at any cross section, ft/sec

v_{max} maximum of above, ft/sec

$v_{s,avg}$ average spiral velocity in core, equal to $\sqrt{v_{t,avg}^2 + v_{a,avg}^2}$, ft/sec

v_t peripheral, rotational, or tangential velocity component, ft/sec

$v_{t,avg}$ average of tangential velocity component in core, ft/sec

v_1 velocity at position 1, ft/sec

v_2 velocity at position 2, ft/sec

v' root-mean-square of fluctuating velocity component in direction of flow, ft/sec

w mass flow rate in header, lb/sec

w_i mass flow rate at inlet of header, lb/sec

x distance parallel to channel wall in direction of flow, ft

x_c distance from core inlet along core axis, ft

x_h distance from header 0-degree plane along mean length of header, ft (see Figure 20)

x_s distance downstream from screen plane, ft

X mean length of header, ft

Δx differential element of length in direction of flow, ft

y distance from channel wall perpendicular to plane of channel wall, ft

Δy differential element of length perpendicular to plane of channel wall, ft

z distance from core midplane parallel to core axis, ft

α angle between spiral-flow component and plane perpendicular to core axis, deg

γ density, lb/ft^3

δ boundary layer thickness, ft

ϵ turbulence factor, equal to $\rho l^2 \frac{dv}{dy}$, $lb\text{-}sec/ft^2$

θ momentum thickness of boundary layer, equal to $\int_0^\delta (1 - \frac{v}{v_{max}}) \frac{v}{v_{max}} dy$, ft

μ coefficient of viscosity, $lb\text{-}sec/ft^2$

ν kinematic viscosity, equal to $\frac{\mu}{\rho}$, ft^2/sec

ρ mass density, $lb\text{-}sec^2/ft^4$

τ shear stress, lb/ft^2

INTRODUCTION

Statement of Problem

The design of circulating-fuel nuclear reactor systems which must operate at high power densities ($\sim$100,000,000 Btu/hr-ft^3) and at temperatures near to the limits of endurance of their containers (1200°F - 1600°F) places special emphasis on the detailed knowledge of the behavior of the circulating-fuel temperatures with respect to position and time.

According to analyses on forced-convection heat transfer with volume heat sources within the liquid,[1, 2, 3] the temperature distribution depends upon the velocity distribution, the heat-generation rate, the heat-removal rate at the wall, and the molecular and turbulent heat transport properties of the liquid. If the velocities and turbulent heat-transfer properties are unstable with time and asymmetric with respect to the channel center and core circumference, then fluctuating temperature distributions and hot spots will occur due to the asymmetrical heat removal from the core. The magnitude of the temperature oscillations and hot spots may or may not exceed the endurance limits of the containing materials.

The problem took two parts: the first, to find some way of obtaining stable and peripherally symmetrical flow in the ART cores proposed by A. P. Fraas and W. T. Furgerson of the Oak Ridge National Laboratory Aircraft Reactor Engineering Division; and second, to investigate other designs for reflector-moderated reactor cores in an effort to find some configurations which would not have unstable flow.

Development of Project and Statement of Purpose

In 1952, R. E. Ball[4] observed the flow of air through a configuration

called the "Fireball" reactor core which had an annular cross section prepen-dicular to the flow. The center-to-inlet (or exit) area ratio was 5.4:1 while the total length of the varying cross section was 24.6 in. A section parallel to the core axis is seen in Figure 1.

Ball found that the forward flow separated from the outer shell at approx-imately 5.3 in. from the inlet and that the separation increased in severity with distance along the flow path. By filling in the region of separation using plasticene, Ball was able to provide a flow contour which reduced the amount of reverse flow. Since the velocities, as measured with a pitot tube, were still low near the walls, vanes were added in the inlet which, after some experimen-tation, produced a fairly flat velocity distribution. However, no observations were made to determine fluctuations in the velocity with time.

Ball states that some pecularities in forming the Plexiglas outer shell of the core resulted in a greater rate of divergence than anticipated. However, since the originally designed rate of divergence was so much greater than the limiting maximum value of 8 deg included angle for a conical diffuser in which no separation takes place, separation would have occurred even without the vari-ations introduced in fabrication. Filling in the flow passage reduced the rate of divergence of the channel.

Evidently, Ball's results were deemed inconclusive either because of the inaccuracies in fabricating the Plexiglas core shells or because of the reduced core diameter resulting from the "filling in", since another investigation was begun by Stumpf of ARED.[26] During the second quarter of 1954, the experimental study reported here was initiated by J. O. Bradfute[5] and H. F. Poppendiek.

ORNL-LR-DWG 22449
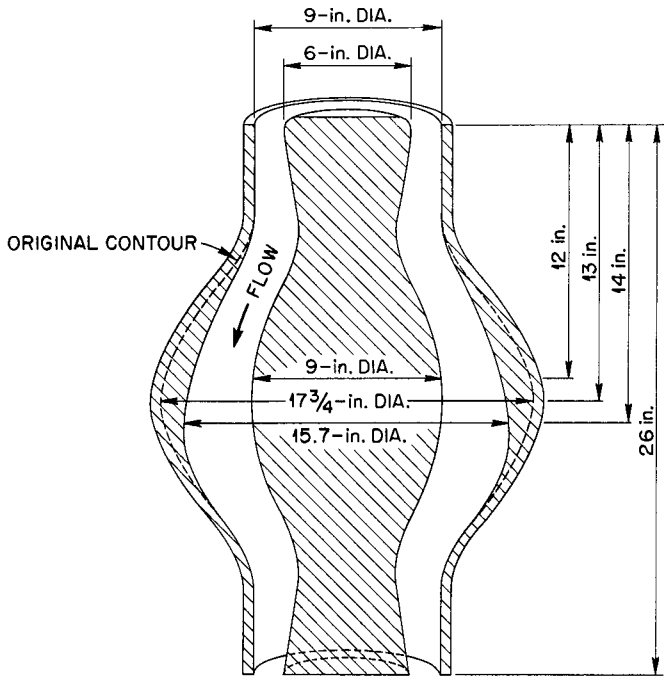
Fig. 1. Cross-Section of Model of "Fireball" Reactor Core (Reference 4)
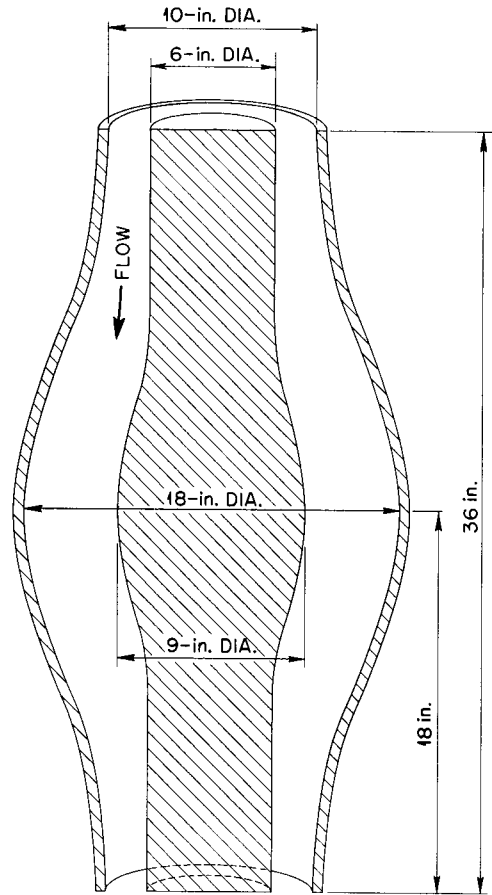
Fig. 2. Cross-Section of 18-in. ART Core Flow Channel
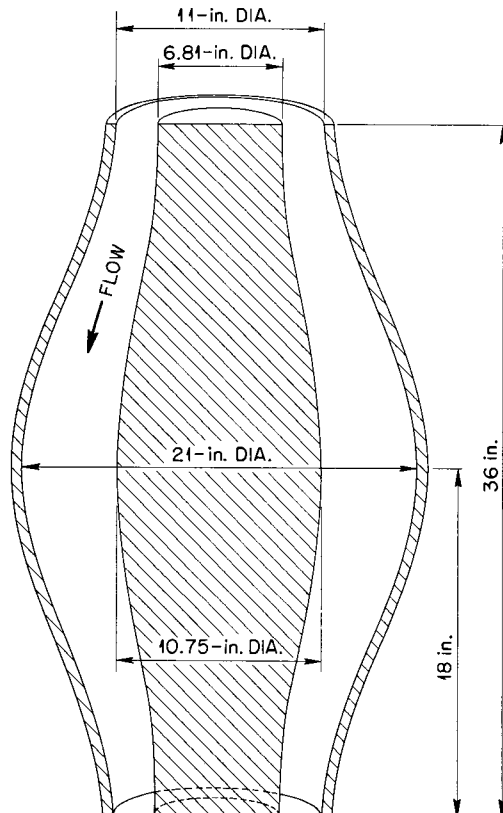
Fig. 3. Cross-Section of 21-in. ART Core Flow Channel

Bradfute studied the flow of water through a quarter-scale model of a core with an equatorial outer diameter of 18 in. This core was assembled using stainless steel for the inner shell and Plexiglas for the outer shell, both shells being carefully machined to the correct contours. The shape of this "18-inch" core differed from that studied by Ball and is shown in Figure 2. The full-scale core had a midplane-to-inlet area ratio of 3.8:1 and an over-all length of 36 in. The reduction in the area expansion ratio was effected by increasing the outer shell diameter at the inlet from 8 in. to 10 in. This change, coupled with an increase in core length, resulted in a reduction in the channel divergence angle.

It was later found[32] that the "18-inch" core required a larger UF_4 concentration (6.5 to 9 mole %) than was originally calculated (~4 mole %). The new calculations showed that a 21-in.-dia core would be required to obtain the 4 mole % concentration. The core shape was proposed by W. T. Furgerson. This design had a midplane-to-inlet area ratio of 4.36:1 in the same length as the "18-inch" core. This core is shown in Figure 3. Early in 1955 work was initiated on a 10/44-scale model of this "21-inch" core.

Parallel to this investigation, full-size "21-inch" core mock-up studies were carried out by G. D. Whitman, W. J. Stelzman, and W. T. Furgerson using the header and pump system designed by Furgerson et al.

Studies of circulating-fuel reactor core hydrodynamics have also been made at Pratt and Whitney Aircraft in conjunction with their reactor research program.[33-44] Mention of these studies is made so that a complete reference to all published reports known to the authors on this subject is at hand.

Due to the lack of an adequate analytical technique for establishing velocity distributions in geometries as complex as those of the ART cores, recourse was made to the experimental solution of the problem. The techniques described were developed to provide a means for rapid qualitative examination of the velocity distributions in the test core geometries.

Since it was felt that the phenomena of separation, backflow, and large-scale unsteady flow observed in the "18-inch" and "21-inch" cores were undesirable for a high-temperature, high-power-density core, much emphasis was placed on the effort to find reflector-moderated reactor core systems which possessed steady flow.

Most of the velocity distributions shown were sketched from visual observations of the deformation of a glowing band of excited phosphor particles as they moved with the water through the core models. Measurements of the velocity distributions for the case of axial flow through the "18-inch" ART core model were made by the stroboscopic photography of tobacco seeds suspended in the flowing water.

Analyses of the data obtained by the group studying flow in the full-size model of the "21-inch" core with several different entrance systems are also presented.

EXPERIMENTAL APPARATUS

Flow System

The experimental flow system consisted of a recirculating loop containing fluid reservoirs, a centrifugal pump, flow and temperature measurement and control devices, and a test section containing the core models and associated entrance and exit regions. A schematic drawing of the system is shown in Figure 4. Further details regarding the system components are presented in Appendix B.

Water was used as the working fluid. Both stroboscopic particle photography and phosphorescent particle visualization techniques were used to establish the local velocities and flow characteristics of the core regions. These methods are discussed in greater detail in Appendix A. The over-all friction losses in the cores were determined using a 30-in., U-tube mercury-manometer. Inlet and exit fluid temperatures were measured with mercury-glass thermometers. The core models and entrance systems studied are described in the following paragraphs.

The Core Models

The core models studied are tabulated below:

a. A 1/4-Scale Model of the "18-inch" ART Core. The outer shell was machined from a solid Plexiglas piece and the island was machined from stainless steel. Figure 5 shows a cross-sectional view of this test section with a table of typical dimensions. The dimensions of the inner and outer walls of the full-size core are obtained from the cylinders of revolution described

SURGE CHAMBER

ORIFICE

STIRRER

MERCURY
MANOMETER

TANK

TEST SECTION

CONTROL
VALVES

CENTRIFUGAL
PUMP

TO DRAIN
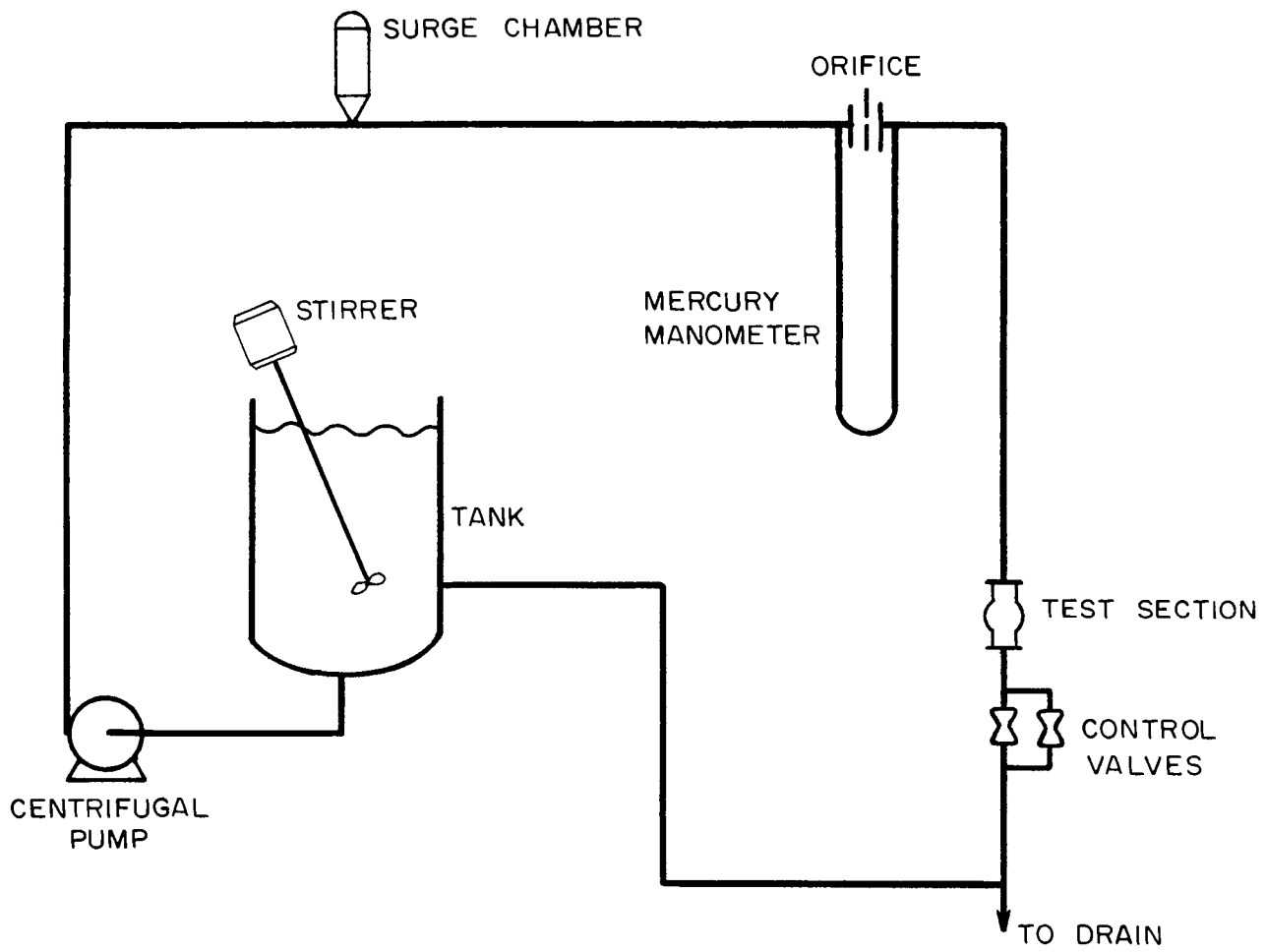
Fig. 4. Schematic Drawing of Experimental Flow System.

ORNL—LR—DWG 2244

DISTANCE FROM MIDPLANE (in.)
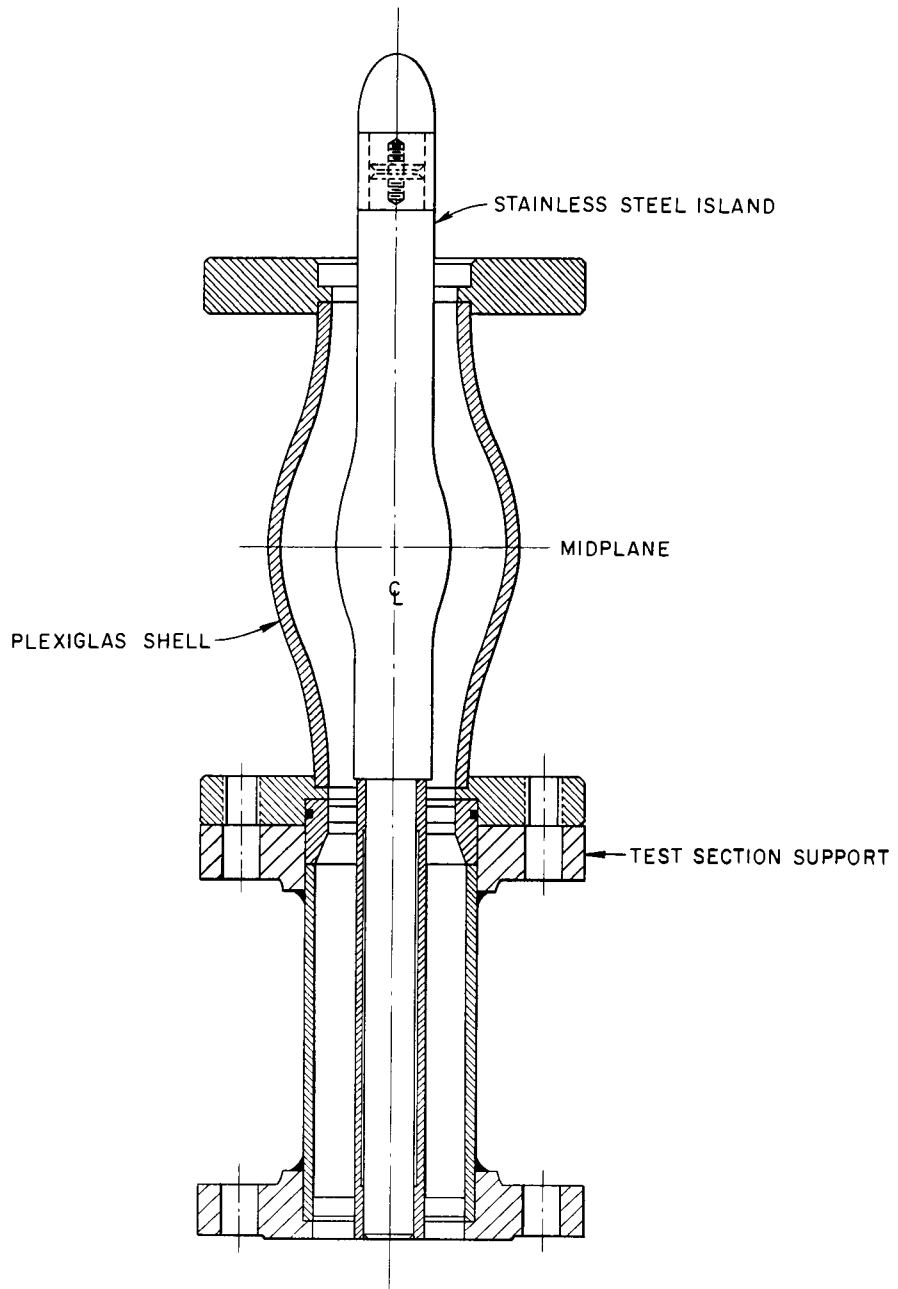
DISTANCE FROM MIDPLANE (in.)	0	0.5	1.0	1.5	2.0	2.5	3.0	3.5	4.0	4.5
INNER DIAMETER (in.)	2.250	2.162	1.940	1.688	1.523	1.500	1.500	1.500	1.500	1.500
OUTER DIAMETER (in.)	4.500	4.421	4.198	3.870	3.493	3.133	2.851	2.692	2.574	2.500

Fig. 5. Cross Section of Quarter-Scale 18-in. ART Core Model.

by the equations,

$$\text{Outer Wall} \begin{cases} r_o = 1.8230 \cos \frac{\pi z}{15} + 7.1770 & \text{for } 0 \le z \le 13.5 \\ r_o = 7.0360 - 0.11799\, z & \text{for } 13.5 \le z \le 16.5 \\ r_o = 1.8230 \cos \frac{\pi(z - 3)}{15} + 6.8230 & \text{for } 16.5 \le z \le 18 \end{cases} \quad (1)$$

$$\text{Inner Wall} \begin{cases} r_i = 0.7500 \cos \frac{\pi z}{9} + 3.7500 & \text{for } 0 \le z \le 9 \\ r_i = 3.000 & \text{for } 9 \le z \le 18 \end{cases} \quad (2)$$

All dimensions are in inches. The midplane-to-inlet area ratio was 3.8:1.

b. A 10/44-Scale Model of the "21-inch" ART Core. The outer shell and island of this model were constructed as in a. Figure 6 shows a cross section of this core. The dimensions of the core model are also given. The centerline of the full-size flow passage is described by a cylinder of revolution generated by the equation,

$$r_m = 1.719 \cos \frac{\pi z}{18} + 6.219 \quad . \quad (3)$$

The midplane-to-inlet area ratio was 4.36:1.

c. A Constant-Gap-Width Core Model using the "Island" of the ART "21-inch" Core and a New Outer Shell. The ratio of the midplane to the inlet areas was 1.443:1. Figure 7 shows a cross section of this core model along with the core dimensions.

d. Another Constant-Gap-Width Core Model using the Outer Shell of the "21-inch" Core and a New Island. The Plexiglas shell was split in two pieces to allow the "island" to be put in place, since it was too large to go through the open end of the shell. Three long bolts compressed a lead gasket between

STAINLESS STEEL ISLAND

MIDPLANE

PLEXIGLAS SHELL

TEST SECTION SUPPORT
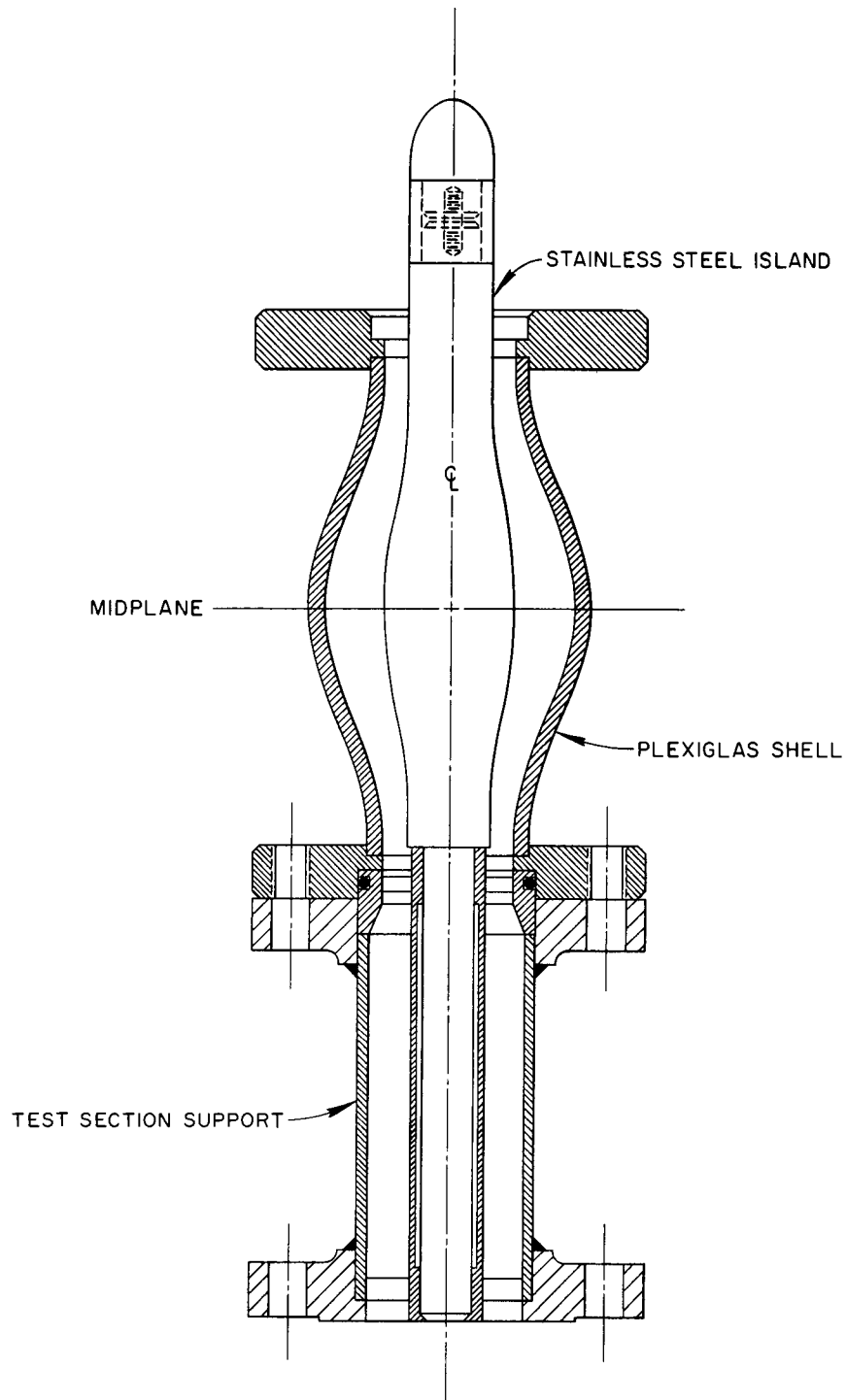
DISTANCE FROM MIDPLANE (in.)	0	0.454	0.909	1.364	1.818	2.273	2.727	3.182	3.636	4.09
INNER DIAMETER (in.)	2.444	2.426	2.361	2.247	2.091	1.891	1.718	1.598	1.548	1.54
OUTER DIAMETER (in.)	4.773	4.707	4.525	4.237	3.887	3.514	3.163	2.861	2.639	2.5C

Fig. 6. Cross Section of $^{10}/_{44}$ Scale 21-in. ART Core Model.
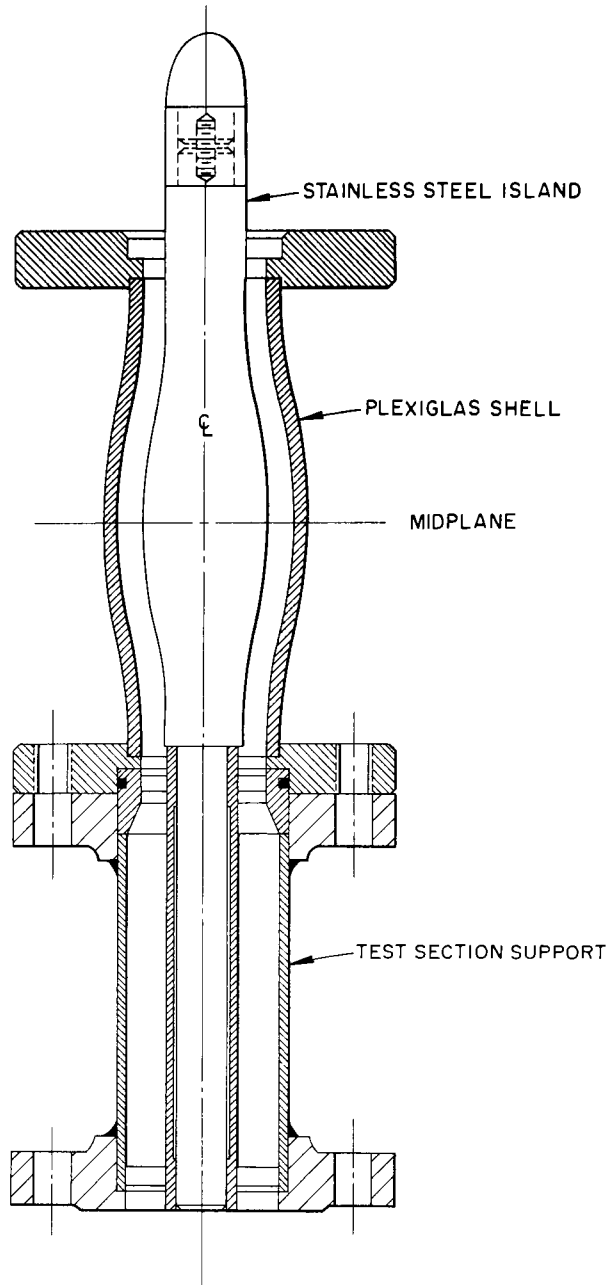
ORNL-LR-DWG 22445

STAINLESS STEEL ISLAND

PLEXIGLAS SHELL

MIDPLANE

TEST SECTION SUPPORT

ISTANCE FROM MIDPLANE (in.)	0	0.454	0.909	1.364	1.818	2.273	2.727	3.182	3.636	4.091
INNER DIAMETER (in.)	2.444	2.426	2.361	2.247	2.091	1.891	1.718	1.598	1.548	1.548
OUTER DIAMETER (in.)	3.396	3.378	3.321	3.211	3.060	2.864	2.686	2.554	2.500	2.500

Fig.7. Cross Section of Constant-Gap-Width Core; Area Ratio -1.443:1

the two halves of the shell to seal the test section. Figure 8 shows the dimensions and a cross-sectional view of the core model. The midplane-to-inlet area ratio was 2.133:1.

e. A Straight-Channel Annular Core Model with a Rapid Area Expansion at the Entrance and a Rapid Area Contraction at the Exit. Provisions were made for positioning screens across the divergent part of the flow channel near the inlet. The shell was split into two pieces to allow the placing of the screens across the flow channel and also to allow the "island", which was too large to go through the open end of the outer shell, to be placed in position. The same method was employed to seal the test section as in case d. Figure 9 shows a cross-sectional view and the dimensions of the core model. The ratio of midplane-to-inlet cross-sectional area was 3.77:1.

f. A "21-inch" ART Core Model with Provisions for Positioning Screens Across the Divergent Channel in the Inlet Half of the Core. The Plexiglas shell was split into halves to allow the screens to be placed in the flow channel. Sealing the test section was accomplished as in case d. Figure 10 shows a cross-sectional view and dimensions.

Core Entrance Systems

A calming length of 40 diameters of straight pipe followed by a convergent "nozzle" transition piece preceded the core model entrance as shown in Figure 11. This insured an axial flow which was uniform both radially and circumferentially at the core inlet. Other inlets to the core were also used; a turning-vane section could be added at the core inlet to produce rotational flow in the core (Figure 12), a twin tangential inlet similar to the present ART header system was also used (Figure 13), and vortex generators were added at the core inlet (Figure 14).
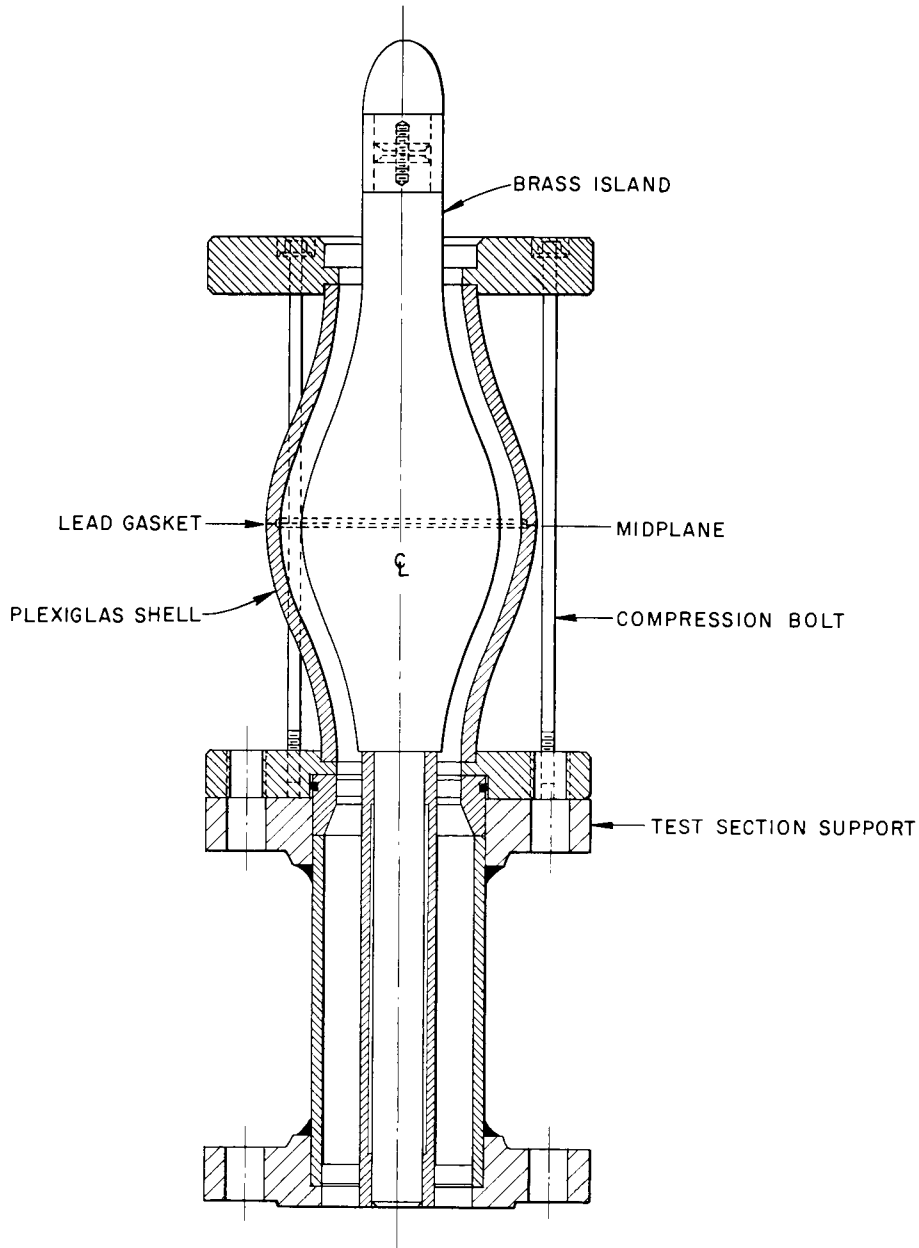
ISTANCE FROM MIDPLANE (in.)	0	0.454	0.909	1.364	1.818	2.273	2.727	3.182	3.636	4.091
INNER DIAMETER (in.)	3.821	3.749	3.540	3.236	2.866	2.491	2.151	1.876	1.669	1.548
OUTER DIAMETER (in.)	4.773	4.707	4.525	4.237	3.887	3.514	3.163	2.861	2.639	2.500

Fig. 8. Cross Section of Constant Gap−Width Core Model; Area Ratio 2.133:1

ORNL-LR-DWG 22447

STAINLESS STEEL ISLAND

SCREENS

LEAD GASKET

PLEXIGLAS SHELL

MIDPLANE

2.727 in.
2.977 in.
3.207 in.
3.465 in.
3.727 in.
4.090 in.

SCREEN POSITIONS

℄

COMPRESSION BOLT

TEST SECTION
SUPPORT
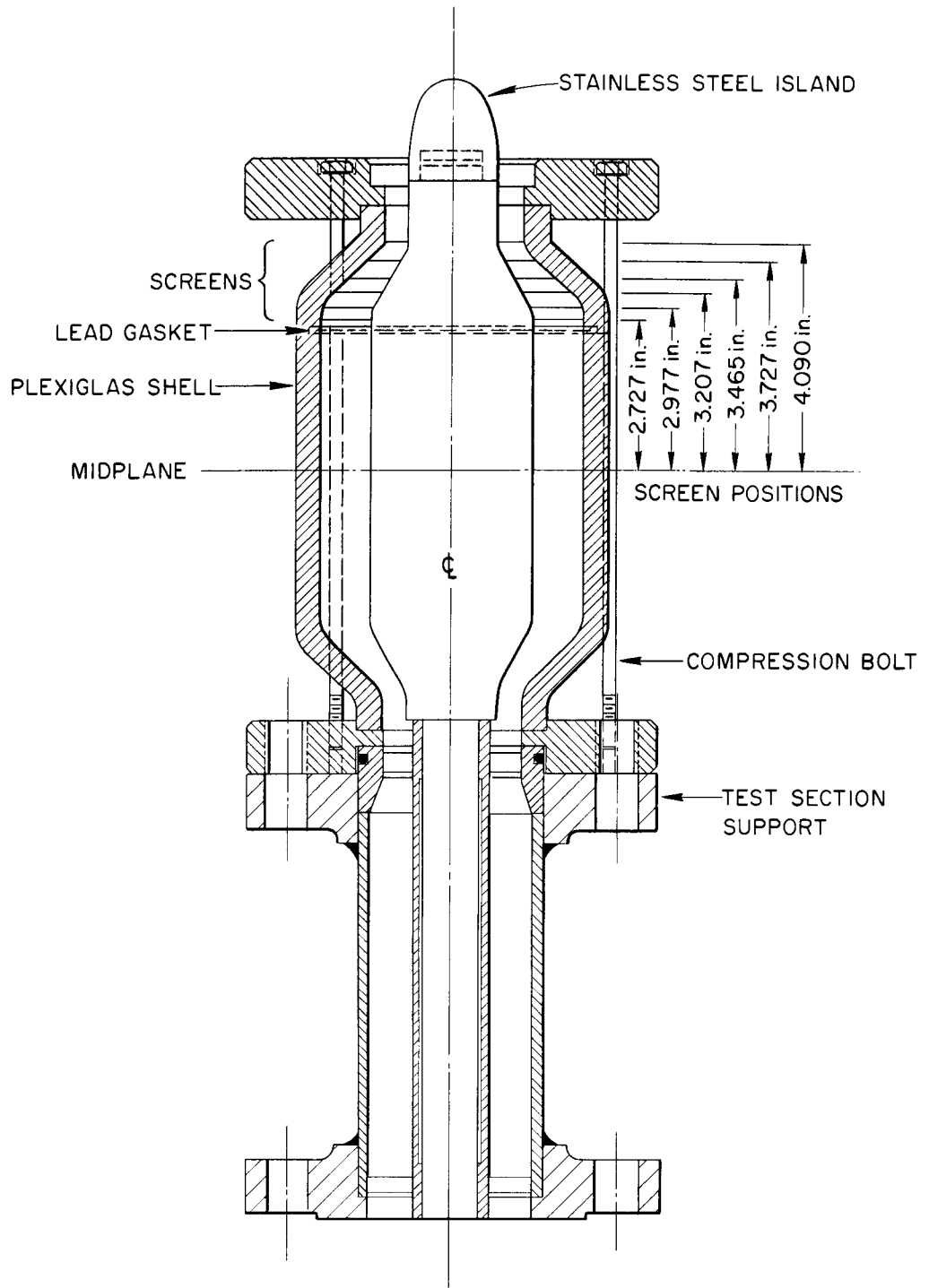
DISTANCE FROM MIDPLANE (in.)	0	2.727	3.000	3.500	4.000	4.136
INNER DIAMETER (in.)	2.954	2.954	2.80	2.18	1.61	1.591
OUTER DIAMETER (in.)	4.773	4.773	4.49	3.42	2.54	2.500

Fig. 9. Cross Section of Straight Core Model Using Screen Packing in Expanding Entrance Channel
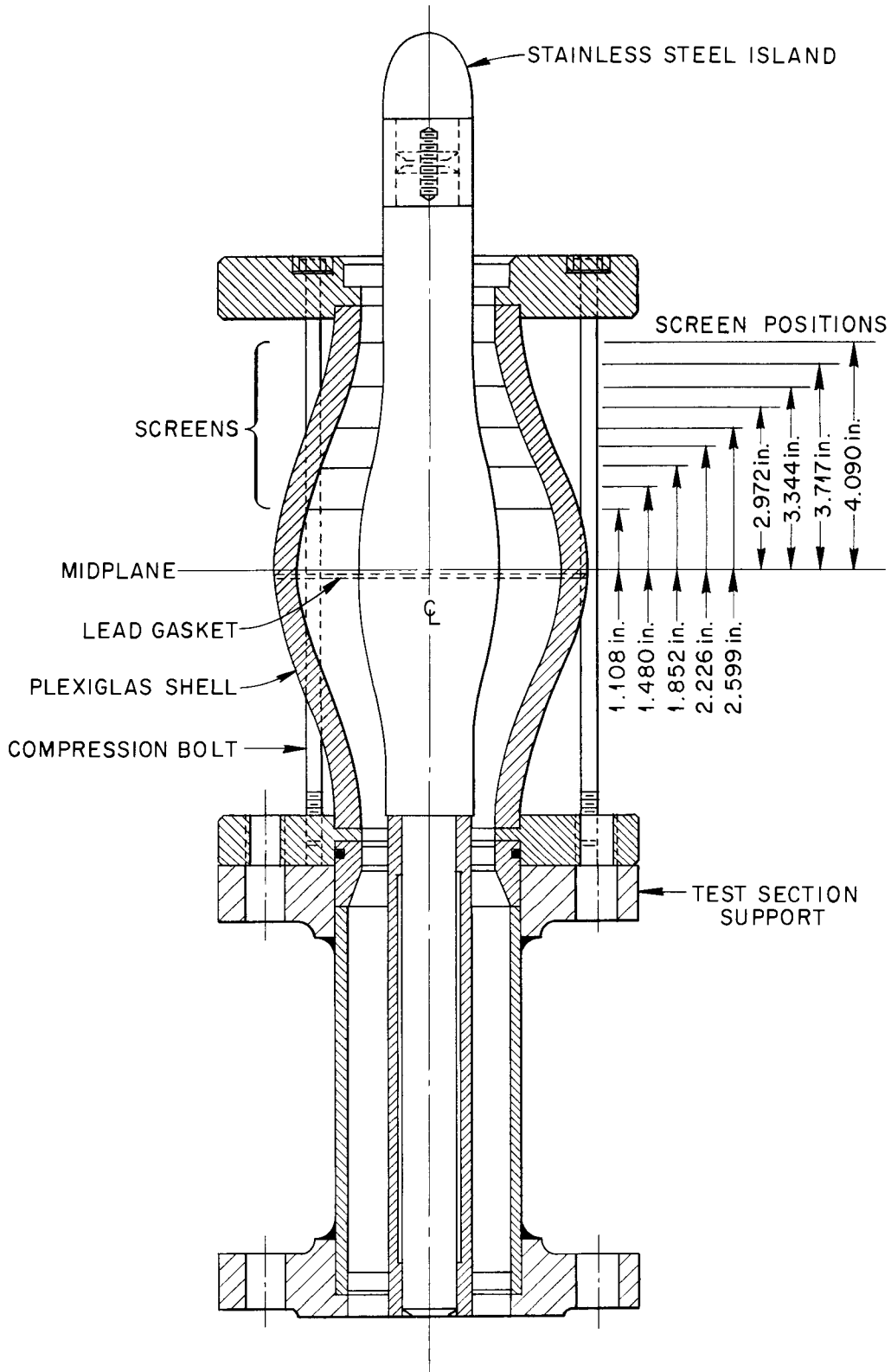
Fig.10. Cross Section of 21-in. ART Core Model Using Screen Packing in Expanding Entrance Half of Channel.

ORNL–LR–DWG 22442
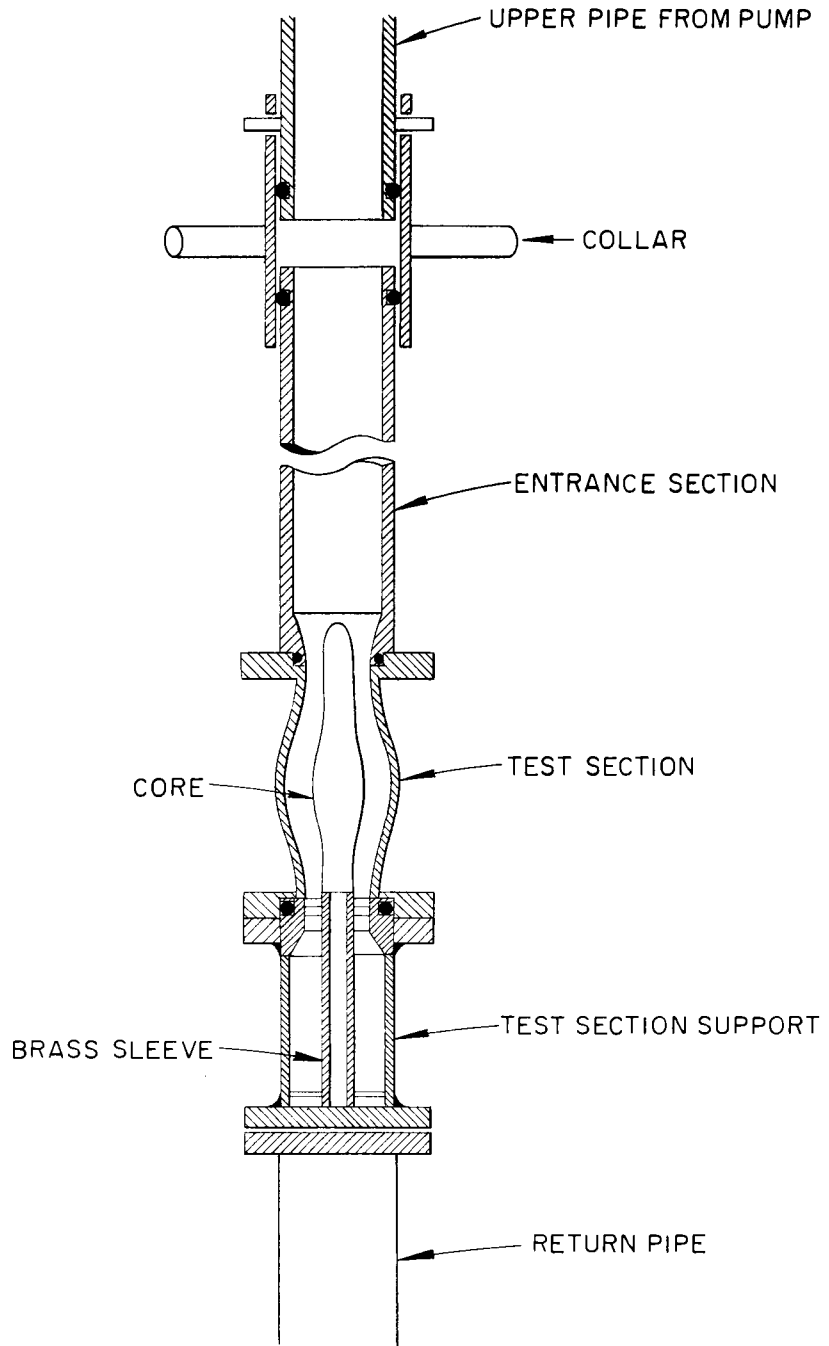
Fig. 11. Test Stand Assembly.
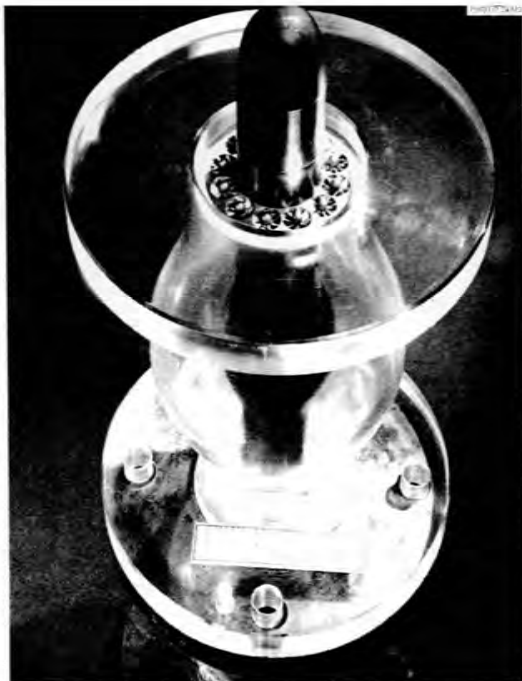
Fig. 14. The Quarter-Scale Model of the 18-in. Core with the Pratt and Whitney
Vortex Generator at the Inlet
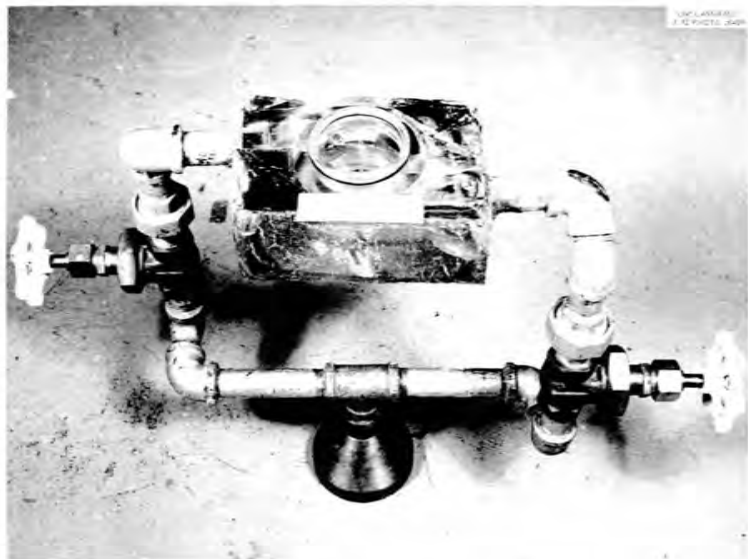
Fig. 13. Twin Tangential-Inlet Header Model
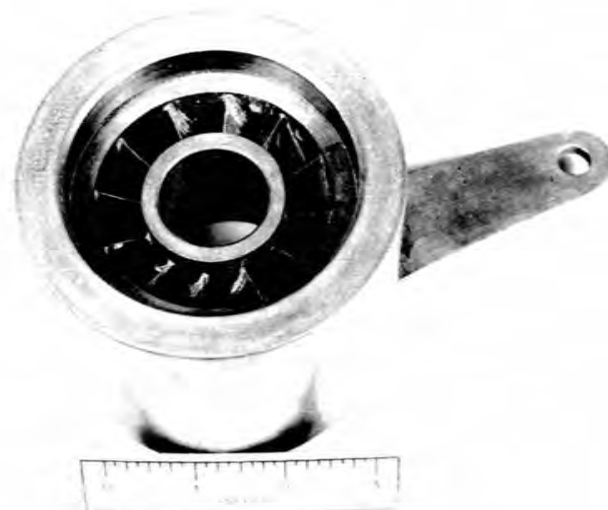
Fig. 12. Turning-Vane Section

MATHEMATICAL ANALYSES

Mean Velocities and Reynolds Numbers in "21-inch" ART Core

Mean axial and rotational components of velocity were obtained for three entrance conditions for the "21-inch" ART core from velocity data taken in the full-size ART core model.[6] The entrance conditions were: (1) a high velocity rotational flow induced by two 2.1 by 2.1-in. tangential entrance ducts directed perpendicular to the core axis, (2) a lower velocity rotational flow induced by two similarly arranged 4.38 by 3.45-in. ducts, and (3) a still lower velocity rotational flow induced by adding turning vanes to the second case.

Axial components were obtained by dividing the volume flow rate by the core cross-sectional areas. Dividing the volume flow rate by the entrance duct areas for the first two cases gave the mean rotational component at the entrance. By assuming conservation of angular momentum, the mean rotational components were computed as a function of axial length. For the third case (turning vanes), the rotational component was obtained from velocity data[6] measured at the core midplane. This data was first adjusted to account for the property differences between fuel No. 30 and water; and then, using angular momentum conservation, the radial component was calculated as a function of axial position. The velocities obtained from these analyses are plotted as a function of axial length in Figure 15.

The velocity results were combined with the core dimensions and the physical properties of fuel No. 30 at 1425°F (Table 1) to obtain the resultant vector Reynolds moduli.
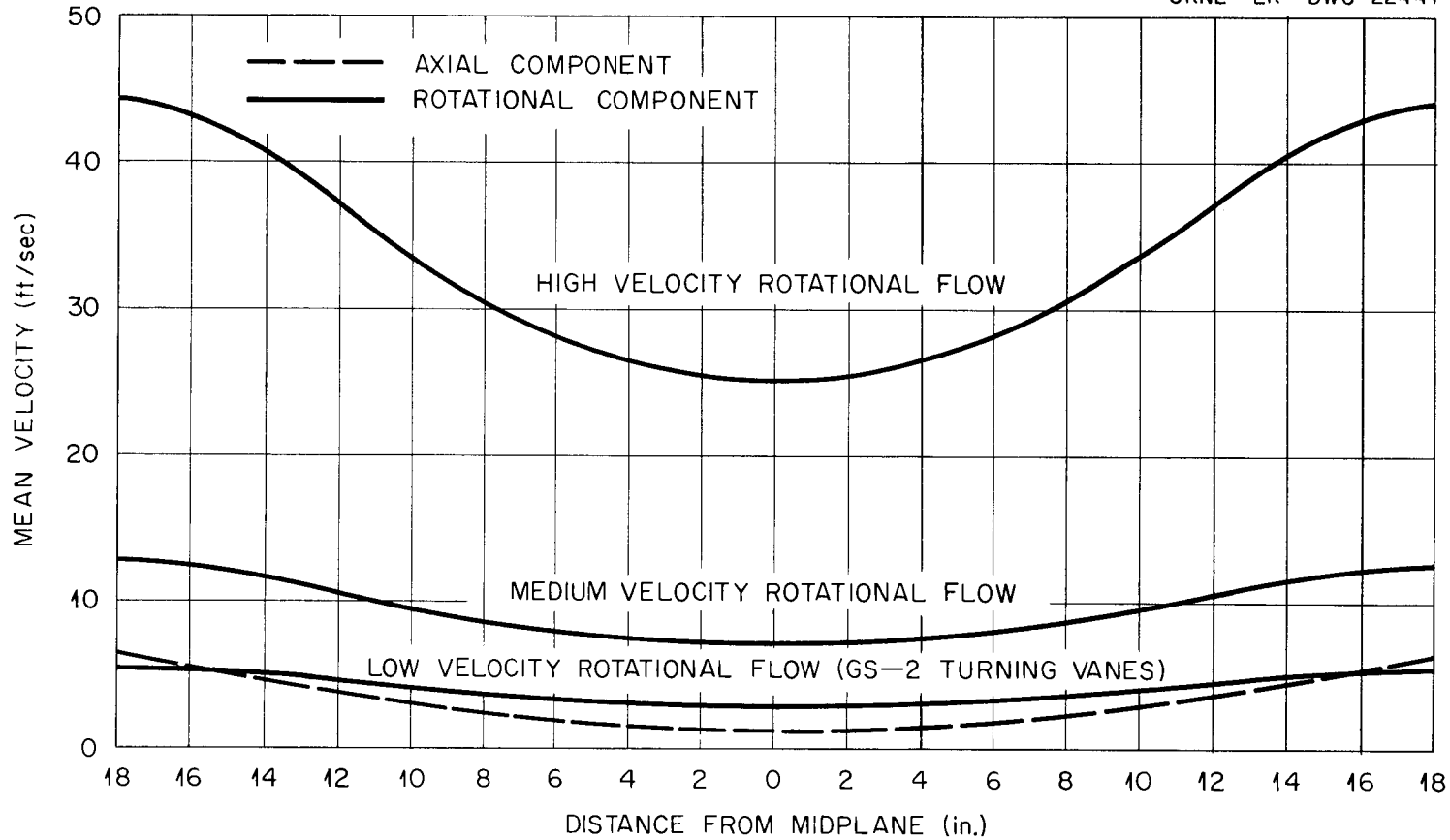
Fig. 15. Prediction of Mean Velocity Components in 21—Inch ART Core with Several Entrance Conditions for Flow of Fluoride Composition No. 30 at ART Design Flow Rate (1200 gal/min).

TABLE 1

Physical Properties of Fluoride Mixture No. 30 at 1425°F

Viscosity = 9.73 lb/ft-hr

Density   = 200 lb/ft^3

The vector Reynolds moduli for the three cases studied are shown as a function of axial position in Figure 16. The Reynolds moduli for axial flow are also shown.

Pressure Distributions in ART Core

To find the pressure losses in the ART core for the first two cases mentioned above, the calculated mean velocity components were used to determine the mean flow angles relative to the horizontal plane.

The ratio of the spiral flow path length to the axial length at a point is $\frac{\Delta s}{\Delta z} = \csc \alpha$, approximately.[*] Letting $\Delta z \longrightarrow 0$, there is obtained $\frac{ds}{dz} = \csc \alpha$. Then, the flow path length, L, is found by integration of the $\csc \alpha$ over the axial length z. Thus,

$$L = \int_{-18}^{18} \csc \alpha \, dz = \int_{-18}^{18} f(z)dz \tag{4}$$

The function f(z) is plotted in Figure 17 for the two cases. The integration was performed graphically.

The ratio of spiral flow path length to axial length $\left(\dfrac{L_s}{L_a} = R \right)$ thus

---

[*]Calculations show that the length of the axial flow path is only 2% longer (36.78 in.) than the axial length of the core, so that the equation is a good approximation.
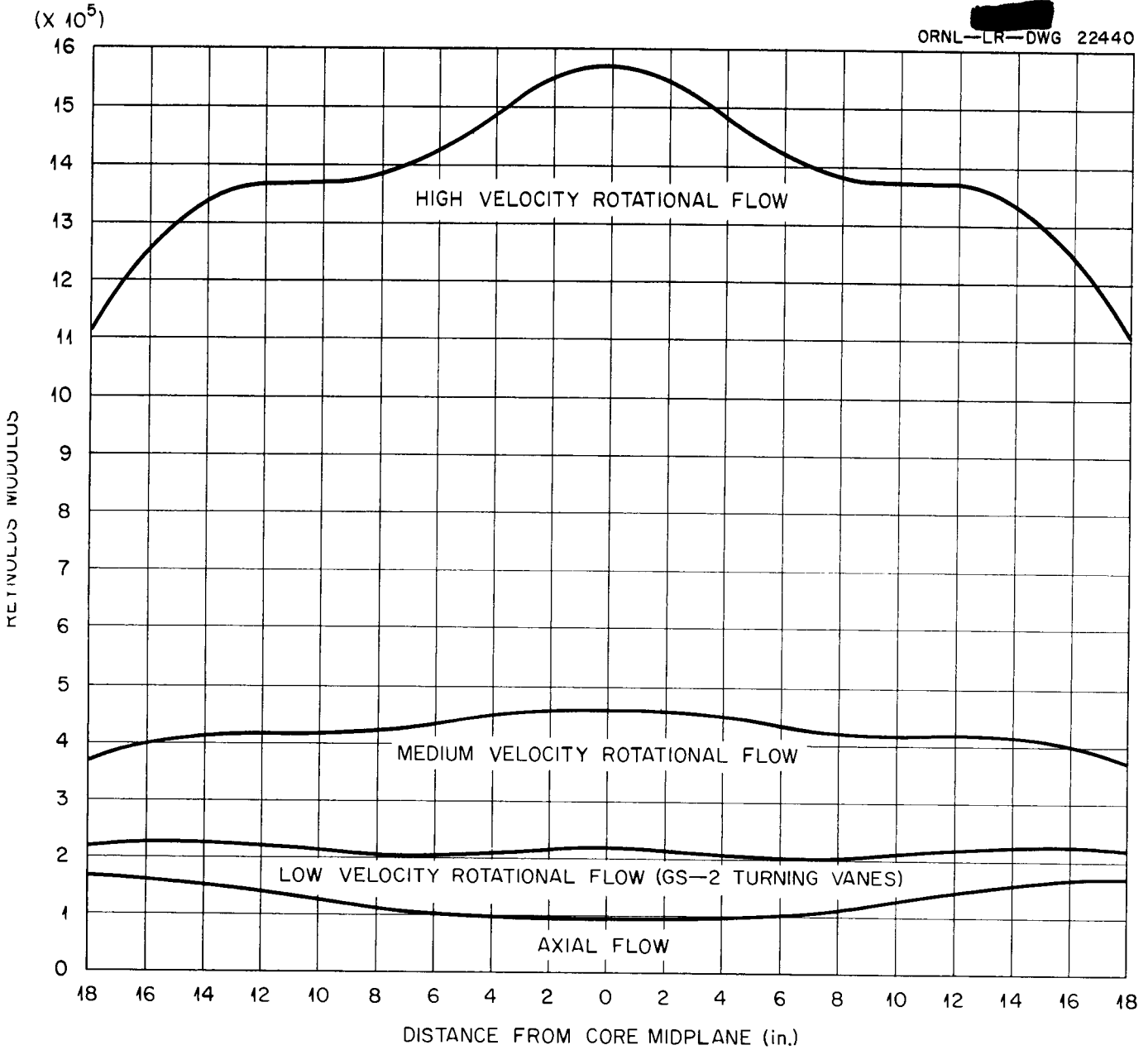
Fig. 16. Prediction of Resultant Vector Reynolds Moduli in 21-Inch ART Core for Flow of Fluoride Composition No. 30 at 1200 gal/min.
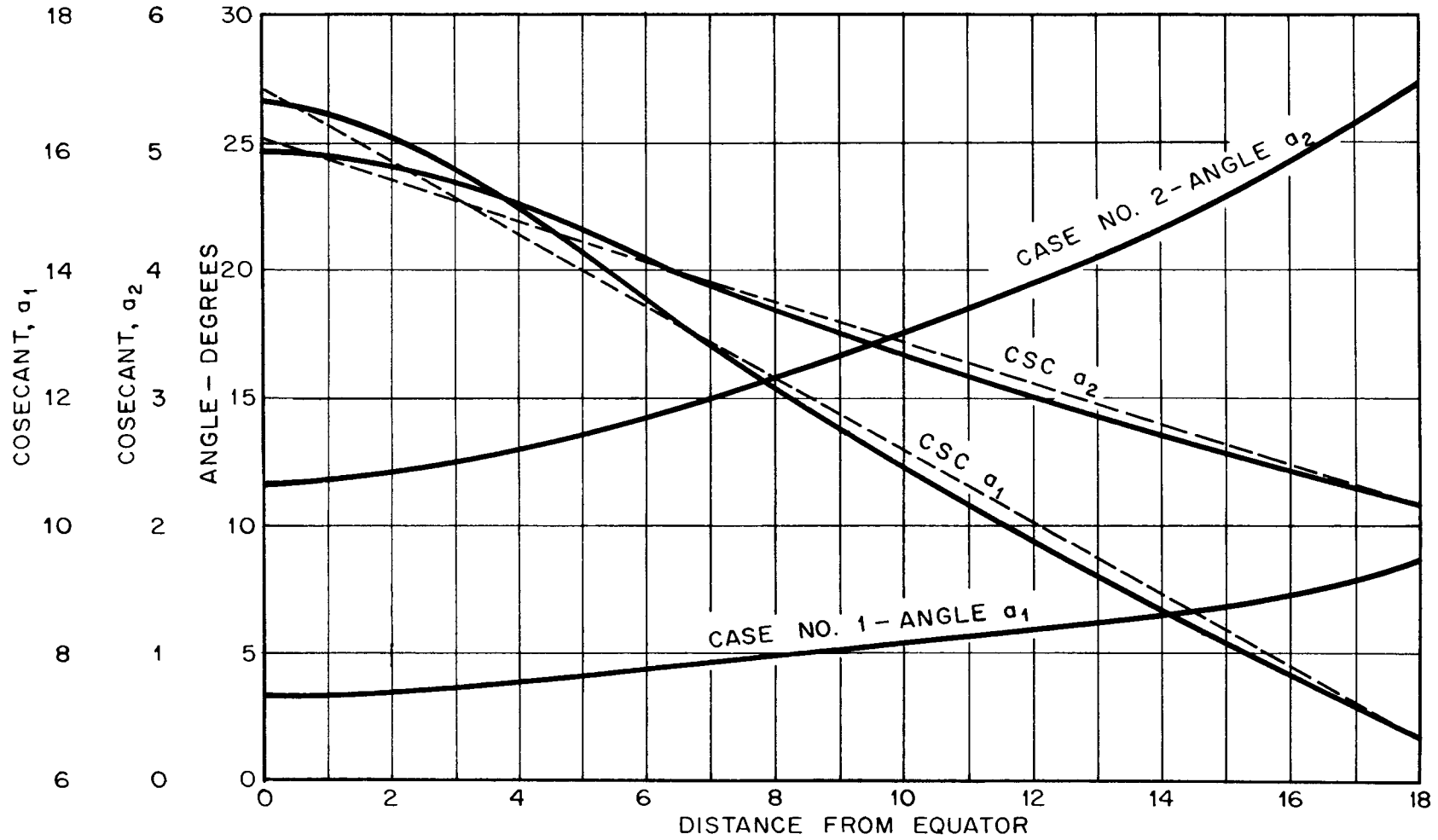
Fig. 17. The Cosecant α as a Function of z.

determined was used to calculate the ratio of rotational flow pressure loss to axial flow pressure loss according to the equation,

$$\frac{\Delta p_s}{\Delta p_a} = \frac{L_s \ v_{s,avg}^{1.75}}{L_a \ v_{a,avg}^{1.75}} = R \left(\frac{v_{s,avg}}{v_{a,avg}}\right)^{1.75} \qquad . \qquad (5)$$

Since the average core velocity is directly proportional to the flow path length, it follows, assuming equal volumetric flow rates that

$$\frac{v_{s,avg}}{v_{a,avg}} = R$$

and hence,

$$\Delta p_s = \Delta p_a \cdot R^{2.75} \qquad . \qquad (6)$$

The axial flow pressure loss was calculated for an annulus of the following average ART dimensions:

$$r_o \qquad = 8.427 \text{ in.}$$

$$r_i \qquad = 4.653 \text{ in.}$$

$$L_a \qquad = 34.3 \text{ in.}$$

and for

$$v_{a,avg} \qquad = 2.5 \text{ ft/sec}$$

then

$$N_{Re,avg} \qquad = 116,500$$

$$f \qquad = 0.018$$

from which

$$\Delta p_a = f \ \frac{L_a}{D_h} \ \frac{\gamma \ v_{a,avg}^2}{2 g_c} = 0.011 \text{ lb/in.}^2 \qquad (7)$$

The ratio R for case 1 was found to be 11.7 and for case 2, 3.6. The calculated spiral-flow pressure drops are then 9.7 lb/in.^{2} for case 1 and

0.41 lb/in.^{2} for case 2.

The core entrance losses were determined using the Darcy-Weisbach equation for the friction losses in the entrance ducts and the pressure data from case 2 for the losses incurred as the fluid turns into the core. Since there were no similar data for case 1, it was assumed that the turning losses were proportional to the square of the velocity coming from the entrance ducts. Table 2 gives the resulting core entrance losses.

TABLE 2

Core Entrance Pressure Losses

Flow Rate - 1200 gpm

	Case No. 1	Case No. 2
Friction loss in ducts between pumps and core	3.0 lb/in.^{2}	0.2 lb/in.^{2}
Turning loss	36.6 lb/in.^{2}	3.1 lb/in.^{2*}

Radial Pressure Differences

To obtain some idea as to the effect of the rotational component of velocity on the radial pressure distribution, it was assumed:

(a) that a free vortex-type rotational velocity component exists; i.e., $v_t = \frac{c}{r}$; and,

(b) that the total contribution to the radial pressure difference is the rotational velocity component; thus, $\frac{dp}{dr} = \rho \frac{v_t^2}{r}$.

Integrating between the inner and outer walls, there results

$$p_o - p_i = \frac{1}{2} c^2 \rho \left(\frac{1}{r_i^2} - \frac{1}{r_o^2} \right) \quad . \tag{8}$$

*Measured pressure loss from reference 6.

In Figure 18 the predicted radial pressure difference between the outer and inner walls, $p_o - p_i$, is shown for both case 1 and case 2.

Core Design Using the Nikuradse-Buri Parameter Γ for Flow in Divergent Channels

Buri's corrections[7] of Nikuradse's results[8] for turbulent flow in divergent channels show that the wall shear stress drops to zero, indicating boundary layer separation, when the dimensionless parameter

$$\Gamma = \frac{\theta}{v_{max}} \frac{dv_{max}}{dx} N_{Re,\theta}^{0.25} \tag{9}$$

has a minimum value of - 0.060, where

$$N_{Re,\theta} = \frac{v_{max} \theta}{\nu} .$$

Taking $\Gamma = - 0.057$ and using the ratios $\frac{v_m}{v_{max}} = 0.735$ and $\frac{t}{\theta} = 6.80$ as found by Nikuradse, equation (9) can be rewritten to give

$$\Gamma' = \frac{t}{v_m} \frac{dv_m}{dx} \left(\frac{v_m t}{\nu}\right)^{0.25} = - 0.574 . \tag{10}$$

This new parameter, Γ', can then be used to design a convergent-divergent core having no flow separation at the walls.

From continuity requirements,

$$A_c v_m = Q = \text{a constant} \tag{11}$$

for all flow cross sections.

Then equation (10) becomes

$$\Gamma' = - \frac{t}{A_c} \frac{dA_c}{dx} \left(\frac{Qt}{\nu A_c}\right)^{0.25}$$
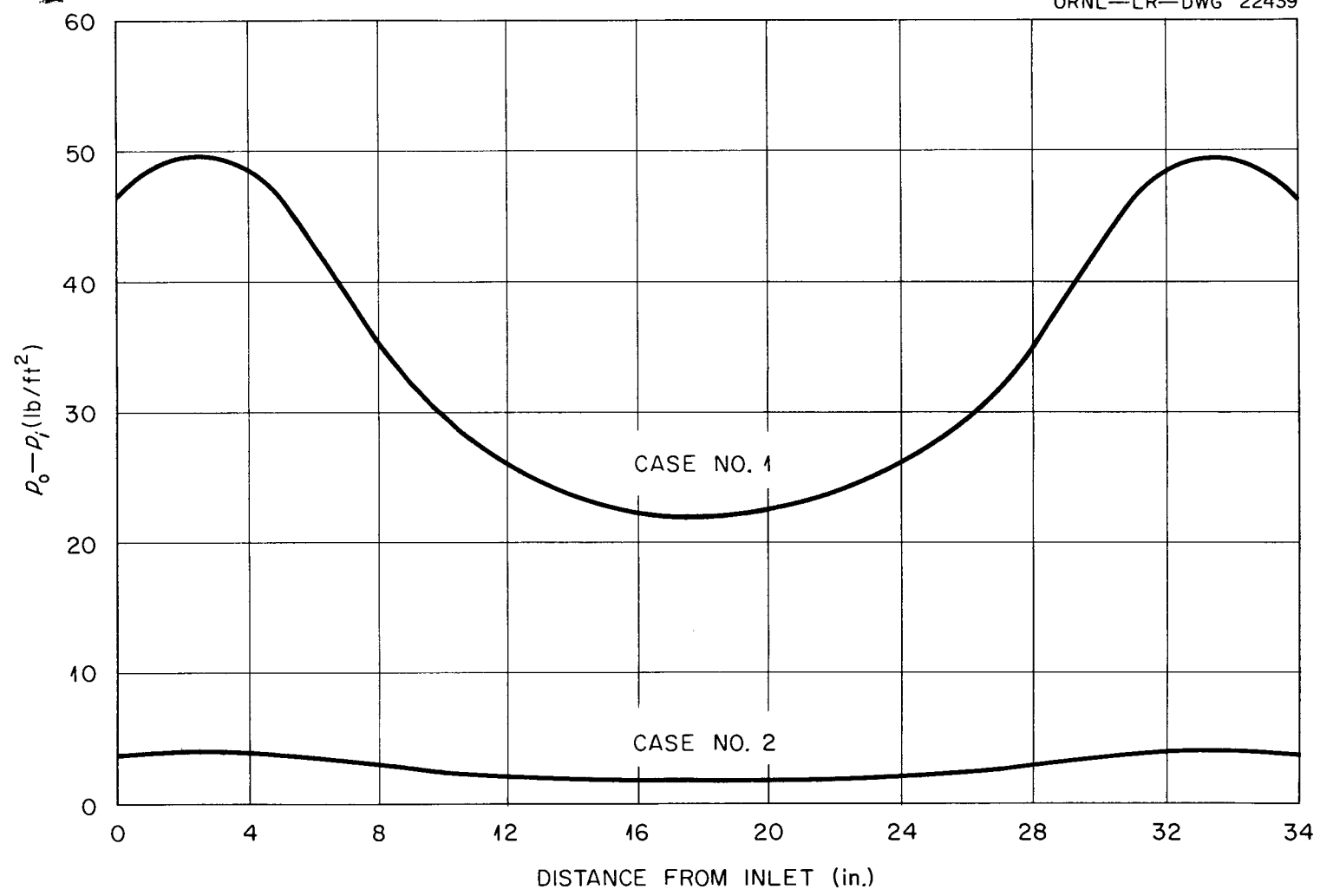
Fig. 18. Predicted Pressure Difference Between Outer and Inner Core Walls for Flow of Fluoride Composition No. 30 at 1200 gal/min.

or on substituting,

$$A_c = 4\pi r_m t \ , \ x_c \cong x$$

$$\frac{dr_m}{r_m^{1.25}} = \frac{0.574}{t} \cdot \left(\frac{4\pi\nu}{Q}\right)^{0.25} dx_c \tag{12}$$

Integrating equation (12) under the conditions that

(1) the core midplane area is same as that of the ART (1.775 ft^2),

(2) the outer shell diameter is 1.833 ft at the midplane,

(3) the channel half-thickness, t, is 0.196 ft,

(4) the flow rate, Q, is 2.70 ft^3/sec,

(5) the fluid is the fluoride mixture No. 30 at $1425^\circ F$; hence,

$\nu = 1.35 \times 10^{-5}$ ft^2/sec; and,

(6) $r_m = 0.721$ ft at $x_c = 1.5$ ft.

$$\int_{0.721}^{r_m} \frac{dr_m}{r_m^{1.25}} = \int_{1.5}^{x_c} \frac{0.574}{t} \left(\frac{4\pi\nu}{Q}\right)^{.25} dx_c$$

$$- 4 \left(r_m^{-.25} - 1.085\right) = 5.5 \left(\frac{\nu}{Q}\right)^{.25} (x_c - 1.5)$$

or

$$r_m = \left[\frac{4}{- 0.2605 \ (x - 1.5) + 4.340}\right]^4 \cdot \tag{13}$$

Table 3 shows the results of the evaluation of equation (13).

TABLE 3

Variation of r_m as a Function of x_c

x_c (ft)	r_m (ft)
0	0.512
0.3	0.546
0.6	0.585
0.9	0.627
1.2	0.672
1.5	0.721

Figure 19 presents the resulting core geometry as constructed graph-ically from the information of Table 3. Near the core midplane, the walls are rounded off to give a smooth transition to the symmetrical exit half. The re-sulting midplane outer diameter is 1.75 ft (21 in.) and the midplane-to-inlet area ratio is 1.33:1. Without rounding-off at the midplane, the ratio would be 1.41:1. In comparison, the "18-inch" and "21-inch" ART cores have area ratios of 3.80:1 and 4.36:1, respectively, for the same length as the 1.33:1 area ratio core.

Pressure Distribution in ART Heads

Pressure unbalances in entrance regions such as the ART core inlet head are caused by friction losses and momentum changes. For the systems under study, friction losses were found to be small as compared to the pressure changes due to momentum transfer. The pressure variations due to momentum

ORNL—LR—DWG 22438
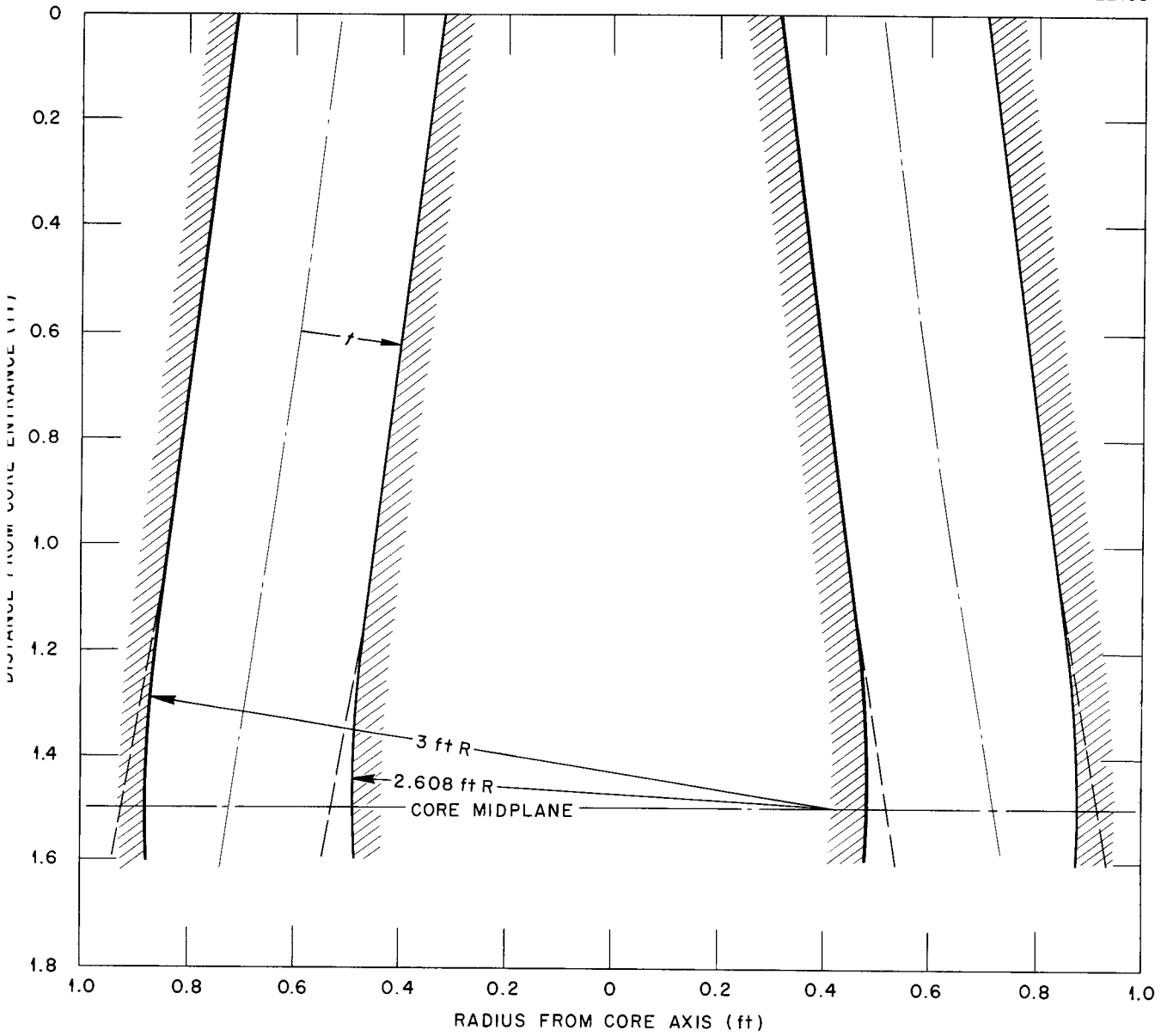
Fig. 19. Cross Section of Inlet Half of Annular Flow Channel of Core Constructed from Γ-Function.

changes have two sources. One is the Bernoulli effect, in which a velocity change in the fluid is accompanied by a pressure change. The second is the momentum transfer that occurs as the fluid leaves the header and turns into the core. While data of other investigators[9] indicate that the momentum transfer is less than perfect, a 100% effectiveness was assumed for simplicity and conservatism in computing the pressure changes. Then, the equation,

$$dp = - \frac{d(wv_h)}{A_h g_c} \tag{14}$$

is obtained, assuming that the flow is withdrawn uniformly per unit head area. Integrating equation (14),

$$\Delta p = - \frac{1}{g_c} \int \frac{d(wv_h)}{A_h} = - \frac{1}{\gamma g_c} \int \frac{1}{A_h} d\left(\frac{w^2}{A_h}\right) . \tag{15}$$

With uniform flow withdrawal per unit head area, the flow through the header at any position, x_h, is described by

$$w = \left(1 - \frac{x_h}{X}\right) w_i . \tag{16}$$

A good approximation is that the cross-sectional header area varies linearly with distance from inlet; i.e.,

$$A_h = a - bx_h . \tag{17}$$

Substituting equations (16) and (17) into equation (15) and rearranging,

$$\Delta p = - \frac{w_i^2}{\gamma g_c X^2} \int_0^X \frac{2ax_h - 2aX - bx_h^2 + bX^2}{(a - bx_h)^3} dx_h . \tag{18}$$

Using the method of partial fractions,

$$\Delta p = - \frac{w_i^2}{\gamma g_c X^2} \left[\frac{1}{b^2} \int_0^X \frac{- b dx_h}{a - bx_h} - \left(\frac{a^2}{b} + bX^2 - 2aX \right) \int_0^X \frac{- b dx_h}{(a - bx_h)^3} \right] \quad . \quad (19)$$

This becomes

$$\Delta p = - \frac{w_i^2}{\gamma g_c X^2} \left[C_1 \ln \left(\frac{a - bX}{a} \right) - C_2 \left(\frac{1}{2a^2} - \frac{1}{2(a - bX)^2} \right) \right] \quad (20)$$

where

$$C_1 = \frac{1}{b^2}$$

$$C_2 = - \frac{a^2}{b^2} - X^2 + \frac{2aX}{b} \quad .$$

Evaluating equation (20) for the header shown in Figure 20(a) with

$$X \quad = 0.742 \text{ ft}$$

$$a \quad = 0.152 \text{ ft}^2$$

$$b \quad = 0.0539 \text{ ft}$$

$$w_i^2 = 71,500 \text{ lb}^2/\text{sec}^2$$

$$\gamma \quad = 200 \text{ lb/ft}^3 \quad .$$

The pressure difference, $p_{130^\circ} - p_{0^\circ}$, is found to be 3.6 lbs/in.^{2}. Similarly, for the header shown in Figure 20(b), with

$$X \quad = 0.98 \text{ ft}$$

$$a \quad = 0.072 \text{ ft}^2$$

$$b \quad = 0.049 \text{ ft}$$

$$w_i^2 = 71,500 \text{ lb}^2/\text{sec}^2$$

$$\gamma \quad = 200 \text{ lb/ft}^3 \quad ,$$
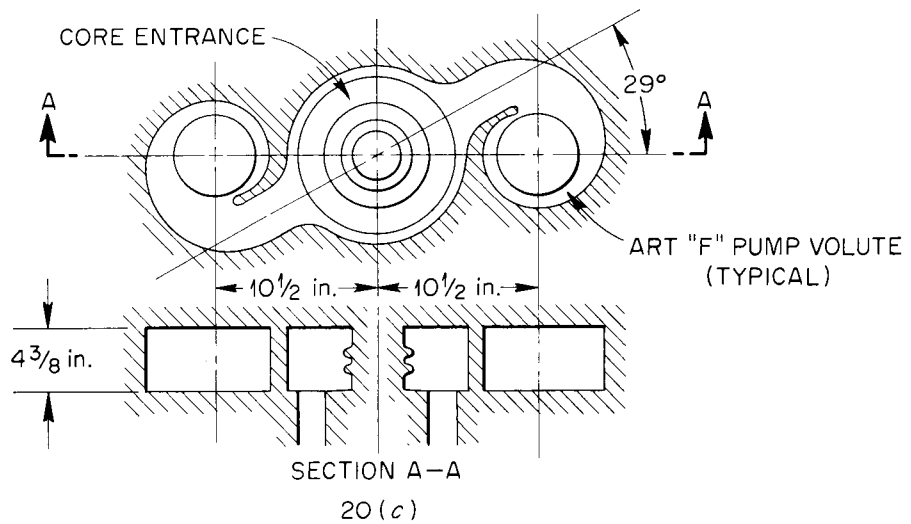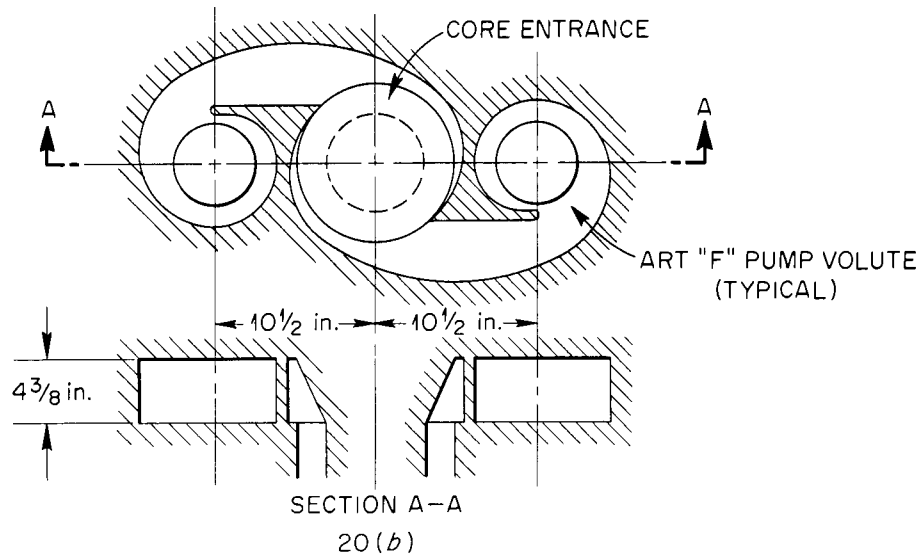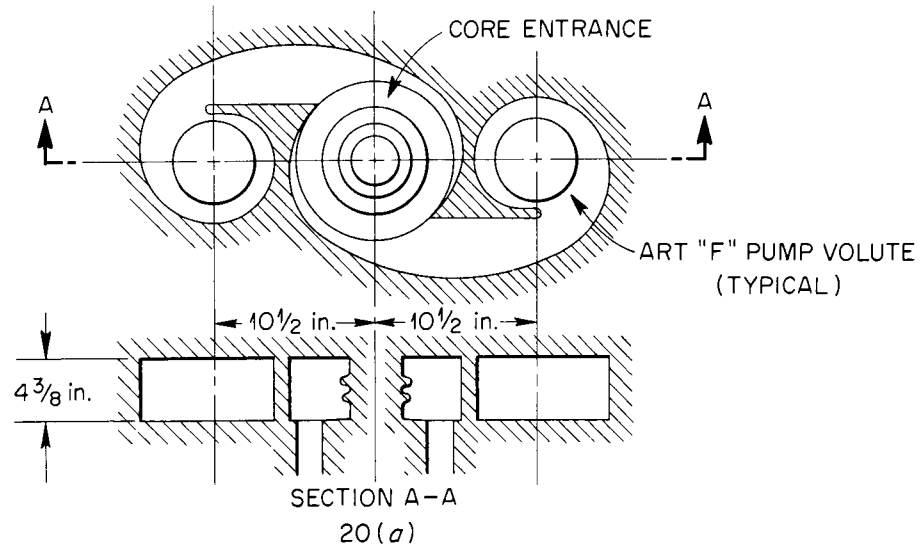
Fig. 20. Core Entrance Header Configurations.

$$p_{130^\circ} - p_{0^\circ} = 20 \text{ lb/in.}^2 .$$

The header shown in Figure 20(c) is of constant cross-sectional flow area. Thus, equation (14) becomes

$$dp = - \frac{\gamma}{g_c} d(v_h^2) \quad . \tag{21}$$

Integrating equation (21), there is obtained

$$\Delta p = - \frac{\gamma}{g_c} \int_{v_{hi}}^{0} v_h \ dv_h = \frac{\gamma v_{hi}^2}{g_c} \quad . \tag{22}$$

Then for

$$v_{hi} = 5.14 \text{ ft/sec}$$
$$\gamma = 200 \text{ lb/ft}^3 ,$$

$$p_{90^\circ} - p_{0^\circ} = 1.14 \text{ lb/in.}^2 .$$

The pressure variation as a function of circumferential position for the three headers considered is shown in Figure 21.

ORNL-LR-DWG 22436
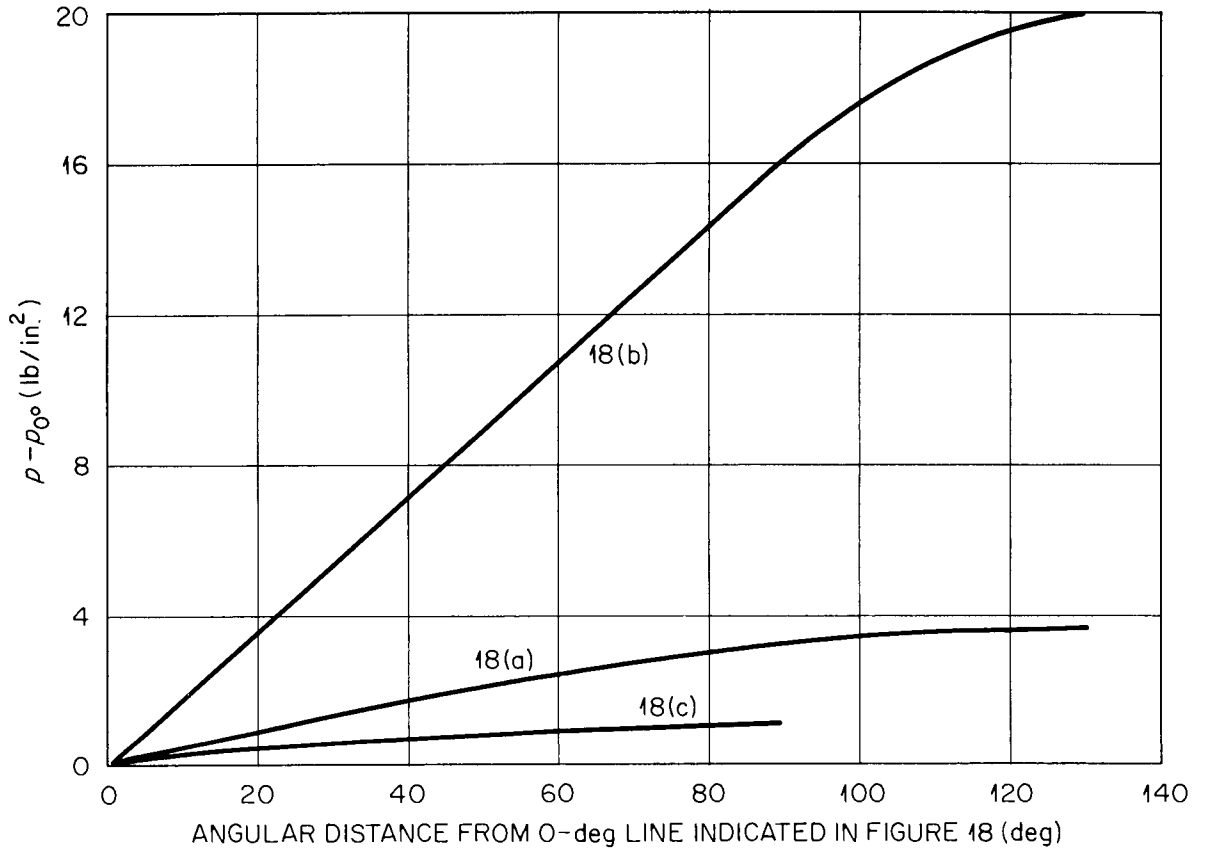
Fig. 21. Header Static Pressure as a Function of Circumferential Position for Fluoride Mixture No. 30 Flow at ART Design Flow Rate.

EXPERIMENTAL RESULTS

Axial Flow Through Cores

(a) The qualitative velocity distributions for axial flow through a quarter-scale model of the "18-inch" ART core[10] are shown in Figure 22 along a vertical section through the flow channel for a midplane Reynolds modulus of 3,000. These distributions represent the visual impressions of velocity profiles obtained using the phosphorescent particle flow visualization technique described in Appendix A. Although there were some differences of opinion among three independent observers regarding a few details such as the exact shape of the profiles, there was unanimous agreement concerning the gross features of the flow.

(b) Velocity measurements obtained[11] by the stroboscopic photography of particles suspended in the water flowing through the "18-inch" core model at a higher flow rate (N_{Re} = 10,000) verified the qualitative observations made earlier. Figure 23 shows these profiles. The stroboscopic particle photography technique is described in Appendix A.

(c) The qualitative velocity distributions in a 10/44-scale model of the "21-inch" ART core[12] are shown in Figure 24. These profiles were obtained visually as in case (a) for a midplane N_{Re} = 2,800. In addition, the gross features (flow separation, etc.) were obtained at a midplane N_{Re} = 18,500 by visually observing the particle motion under a strong light. This method is also described in Appendix A. Figure 25 shows the gross flow features observed under these conditions.

ORNL—LR—DWG 22433

VELOCITY IS QUITE LOW
AND MAY BE NEGATIVE
INDICATING SEPARATION

NEGATIVE PROFILES DIFFICULT
TO OBSERVE DUE TO LARGE
SCALE TURBULENCE

LIMIT OF MAXIMUM PENETRATION
OF TURBULENT EDDIES IS OBSCURE
DUE TO ONSET OF INTENSE TURBU-
LENCE
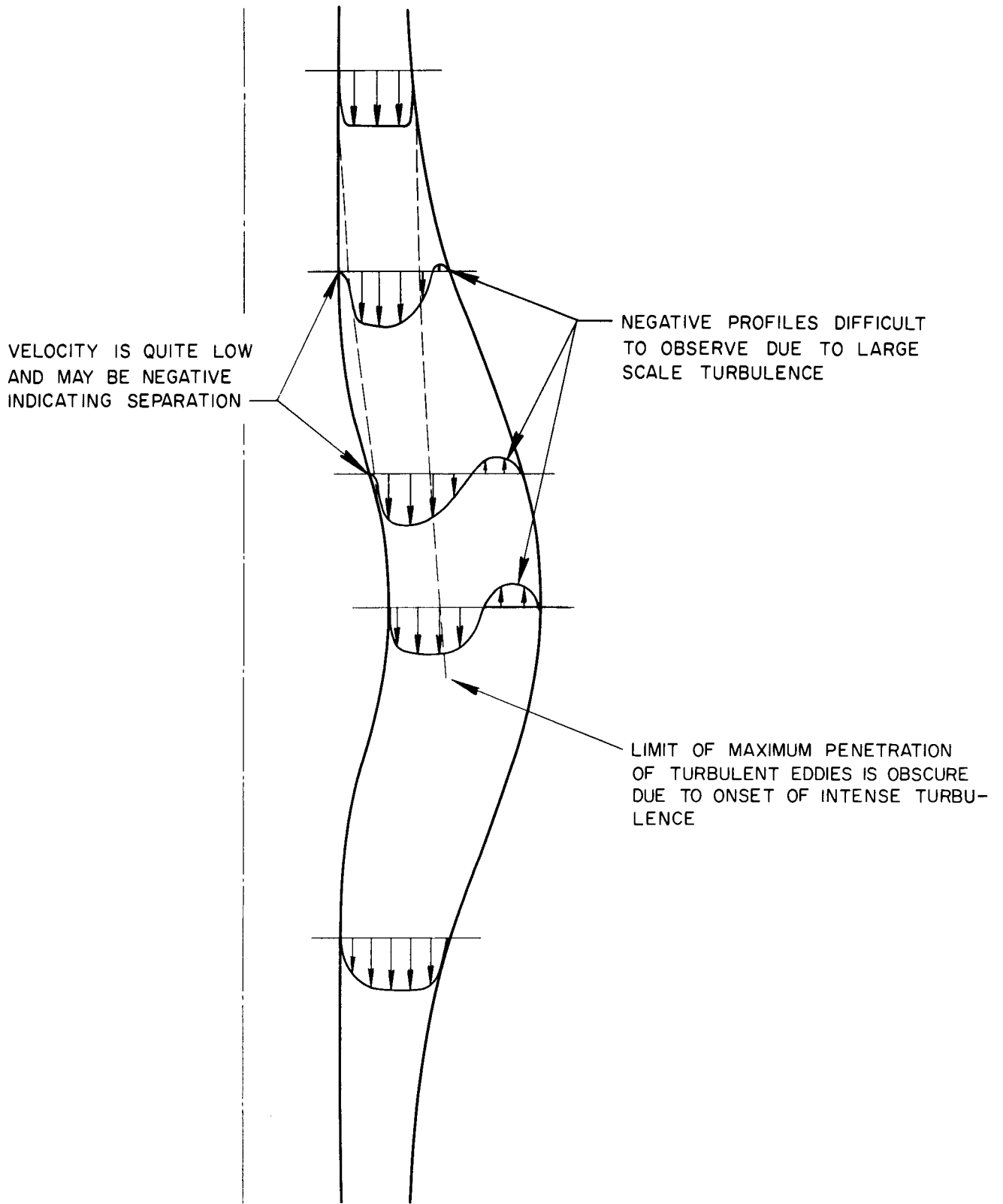
Fig. 22. Qualitative Estimate of Axial-Flow Velocity Profiles in the Quarter-Scale Model of 18-Inch ART Core at $N_{Re, mid}$ = 3,000.

ORNL-LR-DWG 7197

INLET

REYNOLDS NUMBER   10,000

FLOW RATE   1140 cm^3/sec

VELOCITY SCALE $\dfrac{30\ cm^3/sec}{1\ ft/sec}$

LINEAR SCALE   1 cm / .5 in.
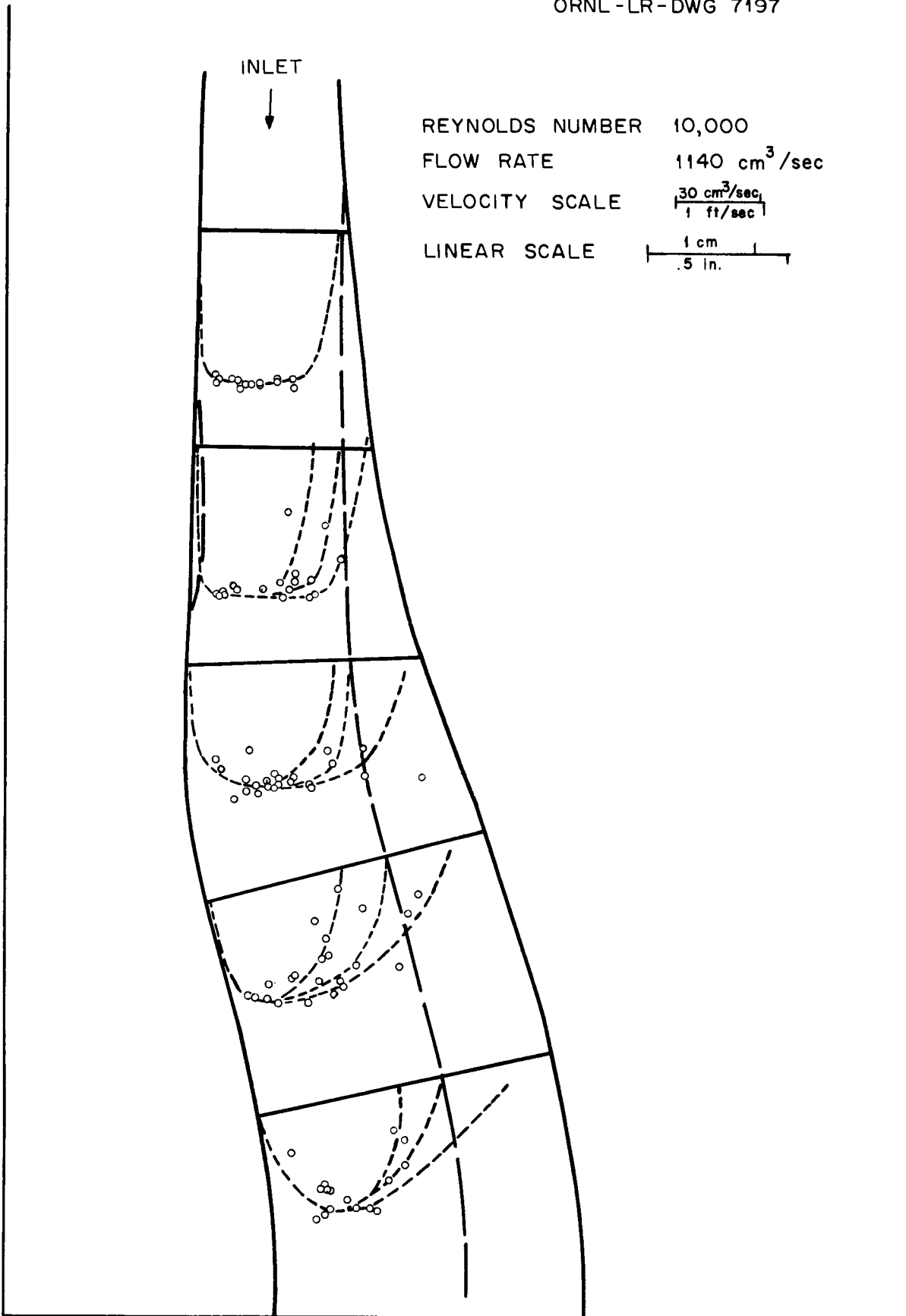
Fig. 23.   Velocity Distribution in the Quarter-Scale Model of the 18-Inch ART Core.
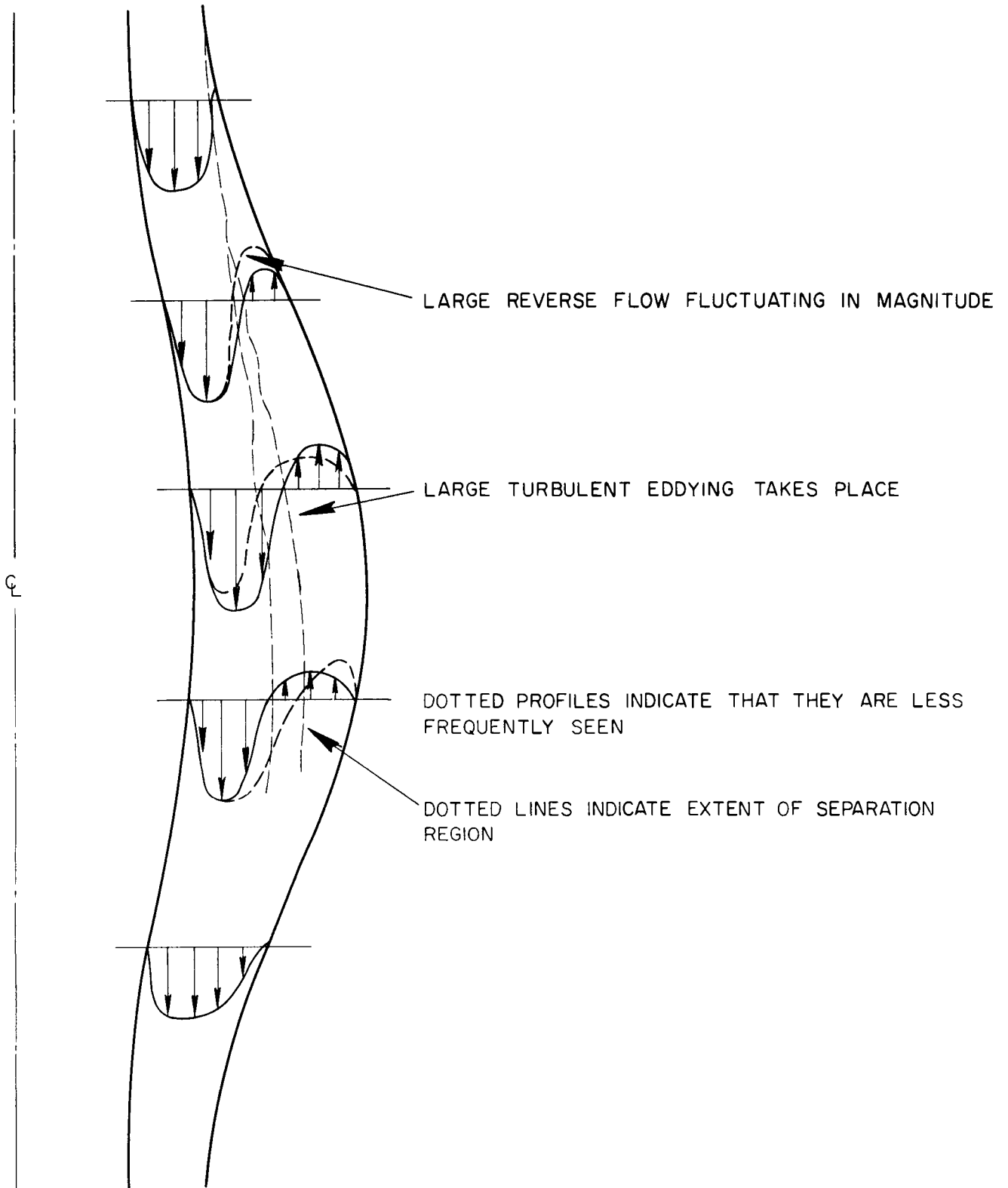
Fig. 24. Qualitative Observations of Velocity Distribution for Axial Flow Through the "21-Inch" ART Core at $N_{Re, mid}$ = 2,800.

ORNL—LR—DWG 22435

DOTTED LINES INDICATE EXTENT
OF SEPARATION REGION.

ARROWS INDICATE GENERAL
DIRECTION OF FLOW.

FLUCTUATING, TURBULENT EDDIES
LARGE AREA OF BACKFLOW.
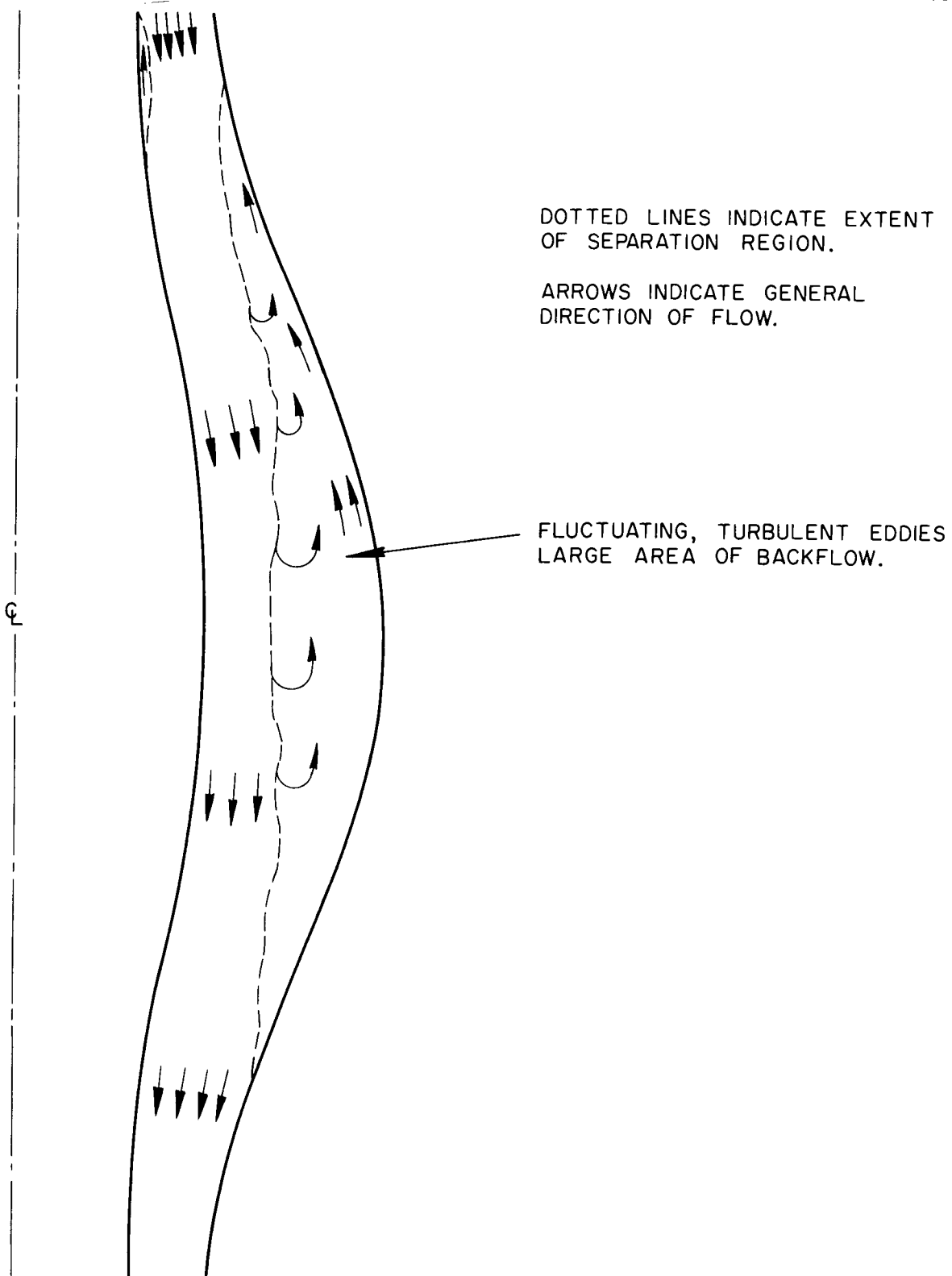
Fig. 25. Gross Flow Features of Axial Flow Through the 21-Inch ART Core at $N_{Re, mid}$ = 18,500.

(d) Visually observed qualitative velocity distributions in a constant-gap-width core of midplane-to-inlet area ratio of 1.443:1[13] are shown in Figure 26. The gross flow features were obtained by observing the particle motion in the water up to $N_{Re, mid}$ = 30,000. The variation of the separation point with $N_{Re, mid}$ is also tabulated in Figure 26.

(e) Qualitative velocity distributions are shown for a 2.133:1 midplane-to-inlet area ratio core[13] in Figure 27. The velocity distributions were obtained visually using the phosphorescent particle technique at a $N_{Re, mid}$ = 3,000, and the gross flow features were observed at $N_{Re, mid}$ up to 20,000.

Rotational Flow Through Cores

(a) Qualitatively observed axial velocity components of the rotational flow through the "18-inch" core model[14] are shown in Figure 28. The rotational component was added to the flow by a set of turning vanes designed to give a velocity of constant scalar magnitude at an angle of 45 deg from a horizontal plane at the core inlet.

(b) Rotational flow was also observed in the 10/44-scale "21-inch" core model.[15] The qualitative axial velocity component distributions are shown in Figure 29. Approximate flow angles obtained with the phosphorescent particle technique are also given. The inlet turning vanes (designed by G. F. Wislicenus), which add the rotational component, were shaped such that the trailing edges of the vanes gave a greater rotational component at the channel center than near the walls. The average core inlet flow angle was approximately 45 deg. Figure 30 shows a photograph

ORNL–LR–DWG 22431

REYNOLDS NO.	SEPARATION POINT (DISTANCE FROM INLET) (in.)
3000	$2\frac{5}{8}$
5000	$2\frac{1}{2}$
7000	$2\frac{1}{4}$
10,000	$1\frac{3}{4}$
15,000	$1\frac{11}{16}$
20,000	$1\frac{5}{8}$
30,000	$1\frac{3}{8}$

SEPARATION STARTS AT ABOUT THIS POINT AND ENDS AT THE EQUATOR OR JUST BELOW IT

LOW NEGATIVE FLOW NEAR THE SHELL WALL

LOW FLOW NEAR THE SHELL WALL BUT NOT NOT NEGATIVE
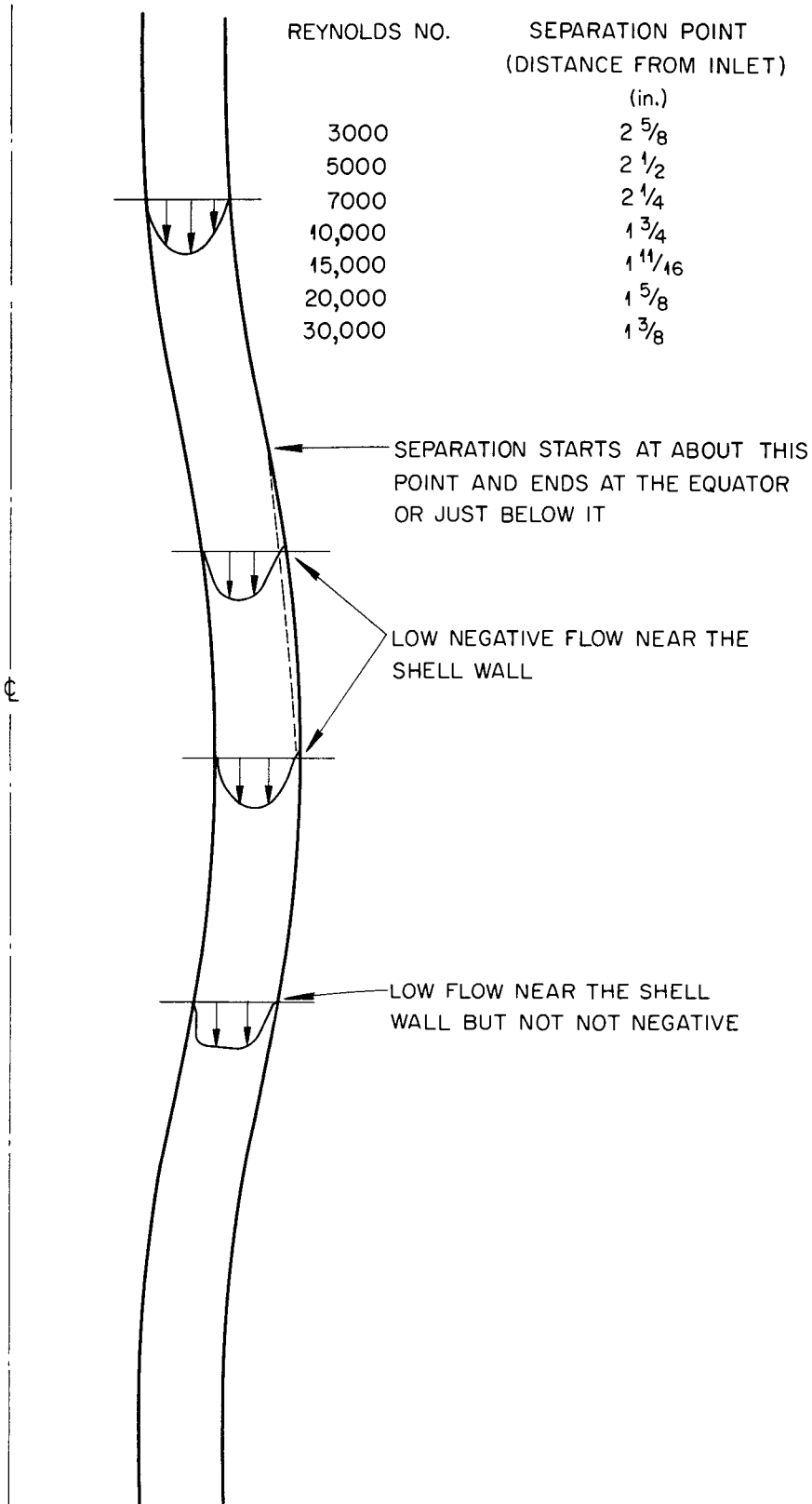
Fig. 26. Qualitative Velocity Distributions at $N_{Re,\ mid}$ = 3,000 and General Flow Features at Midplane Reynolds Numbers up to 30,000 for 1.443:1 Constant-Gap-Width Core Model.

ORNL-LR-DWG 22432
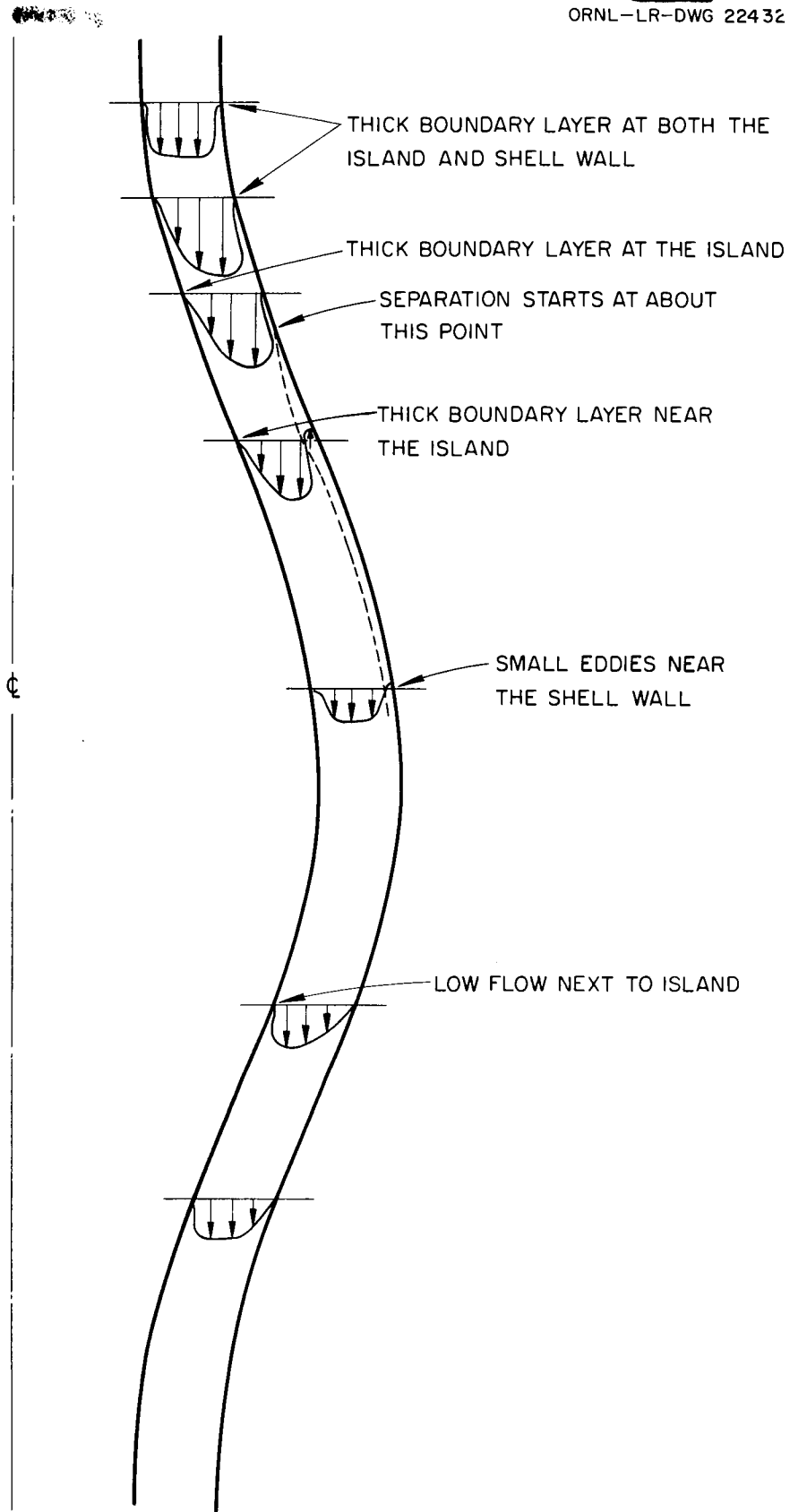

Fig. 27. Qualitative Velocity Distributions at $N_{Re, mid}$ = 3,000 and General Flow Features at Midplane Reynolds Numbers up to 20,000 for 2.133:1 Constant-Gap-Width Core Model.

ORNL—LR—DWG 22429

INTERMITTENT REVERSE FLOW
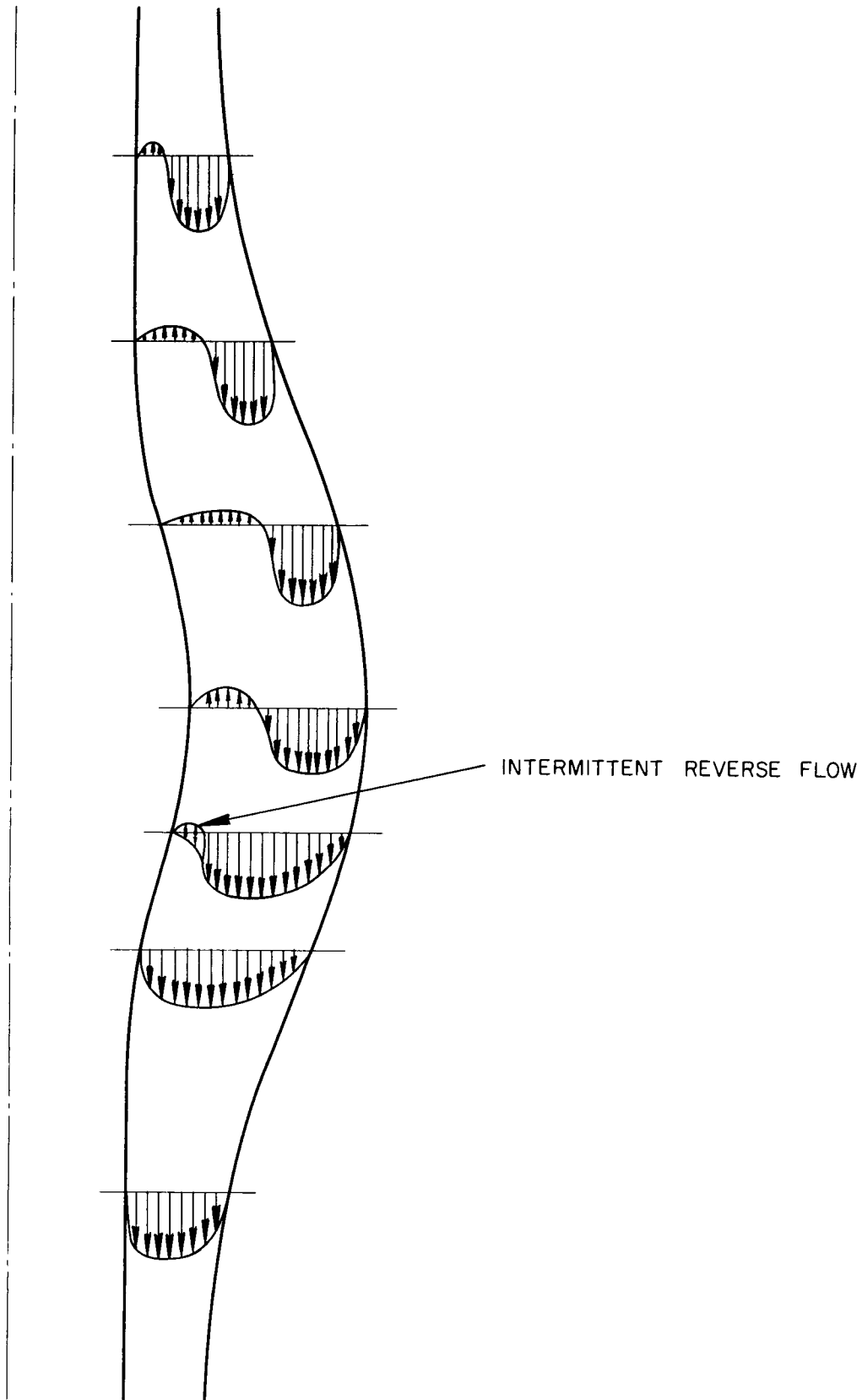
Fig. 28. Qualitative Estimate of Axial Component of Velocity Distribution at Axial $N_{Re, mid}$ = 3,000 for Rotational Flow Through ART "18-Inch" Core Model.

ORNL—LR—DWG 22430

ANGLE OF FLOW REFERRED TO HORIZONTAL PLANE

LARGE TURBULENT EDDIES
NEAR ISLAND WALL ANGLE ~ O deg TO —20 deg
NEAR SHELL WALL ANGLE ~ +50 deg

DASHED LINE INDICATES SEPARATION REGION

VERY HIGH VELOCITY NEAR THE SHELL WALL

NEAR ISLAND WALL ANGLE ~ —10 deg TO
—90 deg AVE. —28 deg
NEAR SHELL WALL ANGLE ~ +60 deg

NEAR ISLAND WALL ANGLE ~ O deg TO —30 deg
NEAR SHELL WALL ANGLE ~ +54 deg

MANY EDDIES IN THIS REGION

NEAR ISLAND WALL ANGLE ~ O deg TO +28 deg
NEAR SHELL WALL ANGLE ~ +26 deg

+29 deg

Fig. 29. Qualitative Axial Velocity Component Distribution for Axial $N_{Re, mid}$ = 3,000 for Rotational Flow Through ART "21-Inch" Core Model.

Fig. 30. "21-Inch" ART Core Model with Turning-Vane Section at the Inlet.

of both the vanes and the core model.

Flow Through 10/44-Scale ART "21-inch" Core - Twin Tangential Entrance
Header - One-Pump Operation

The gross flow features of a 10/44-scale "21-inch" ART core with twin tangential entrance ducts (scaled from the ART medium rotational velocity entrance) were obtained by observing the motion of phosphorescent particles in the water while simulating single-pump operation. The flow features near the inner and outer walls are indicated in Figure 31. Arrows indicate the main direction of the flow near the walls.

Flow Through Cores with Turbulence Promotion

(a) Axial flow through the "18-inch" ART core model with twelve 16-mesh screens spaced one inch apart in the inlet pipe was studied[16] using the phosphorescent particle flow visualization technique. Figure 32 shows the arrangement of the screens and the core used in this study. Qualitatively sketched velocity profiles are shown in Figure 33 along a vertical section of the flow channel.

(b) The "18-inch" quarter-scale core model was equipped with eight aerofoil-type turbulence promoter vanes attached to the outer wall at the inlet.[17] Figure 34 shows the vanes attached to the outer shell, and the three vertical planes where visual observations were made. The island has been removed to provide a clear view of the vanes. Qualitative velocity profiles in the three planes mentioned are shown in Figure 35 at $N_{Re,\ mid}$ = 5,000. The gross flow features were also observed at $N_{Re,\ mid}$ = 20,000.

-56-

FLOW IN →

REGION OF VIOLENT EDDYING
EXISTS NEAR INNER WALL, BE-
COMING LESS VIOLENT AS THE
DISTANCE FROM THE HEADER
INCREASES

SOLID ARROWS INDICATE GEN-
ERAL FLOW DIRECTIONS NEAR
INNER WALL.
DASHED ARROWS INDICATE
GENERAL FLOW DIRECTIONS
NEAR OUTER WALL.

FLOW IN

FLOW IN →

FIRST VIEW OF CORE MODEL

SECOND VIEW OF CORE MODEL
(90° FROM FIRST VIEW)

FLOW IN

← FLOW IN

THIRD VIEW OF CORE MODEL
(180° FROM FIRST VIEW)

FOURTH VIEW OF CORE MODEL
(270° FROM FIRST VIEW)

Fig. 31. Flow Features Near the Inner and Outer Wall of the "21-in." ART Core Model
while Simulating Single-Pump Operation

ORNL-LR-DWG 22425

12-16 MESH SCREENS

PLEXIGLAS TEST SECTION
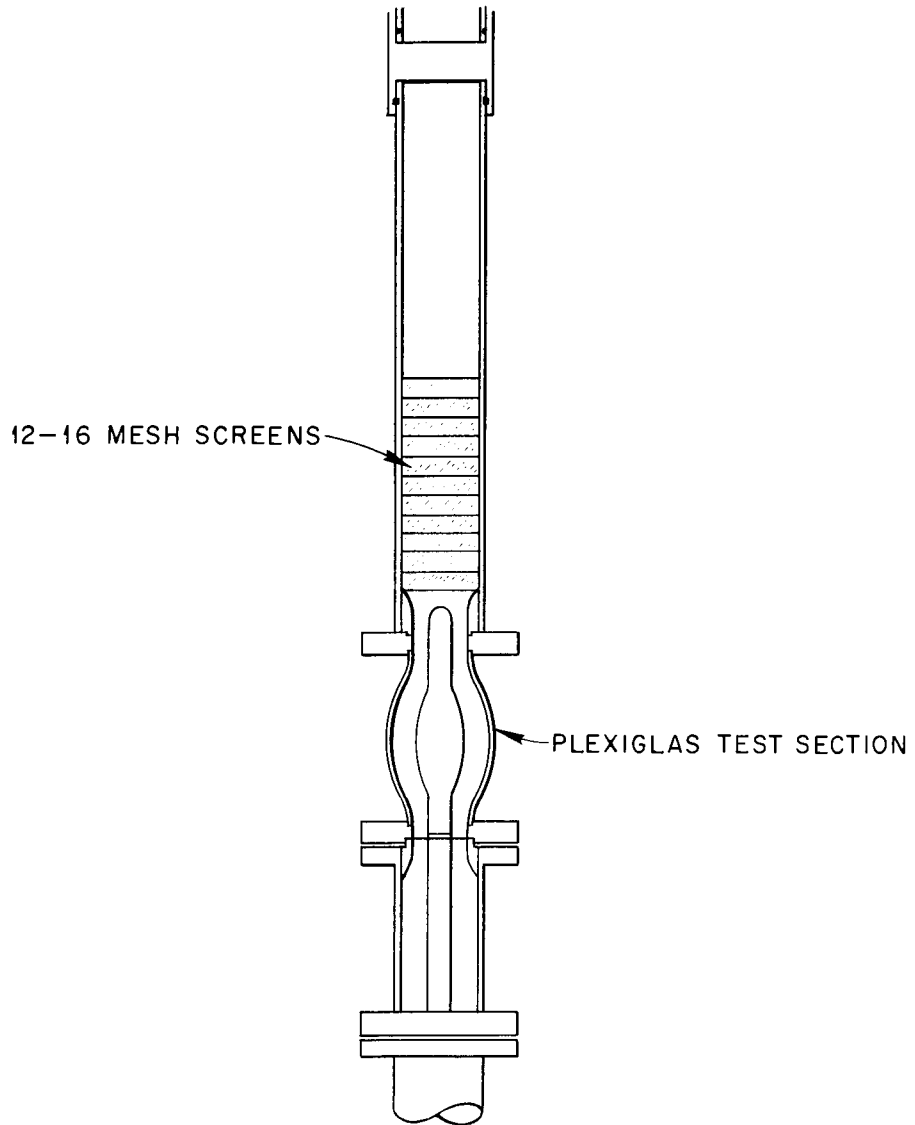
Fig. 32. Sketch of Core Model Assembly Showing Location
and Spacing of Screens in Inlet Pipe.

ORNL—LR—DWG 22426

NEGATIVE PROFILES EASY
TO OBSERVE.
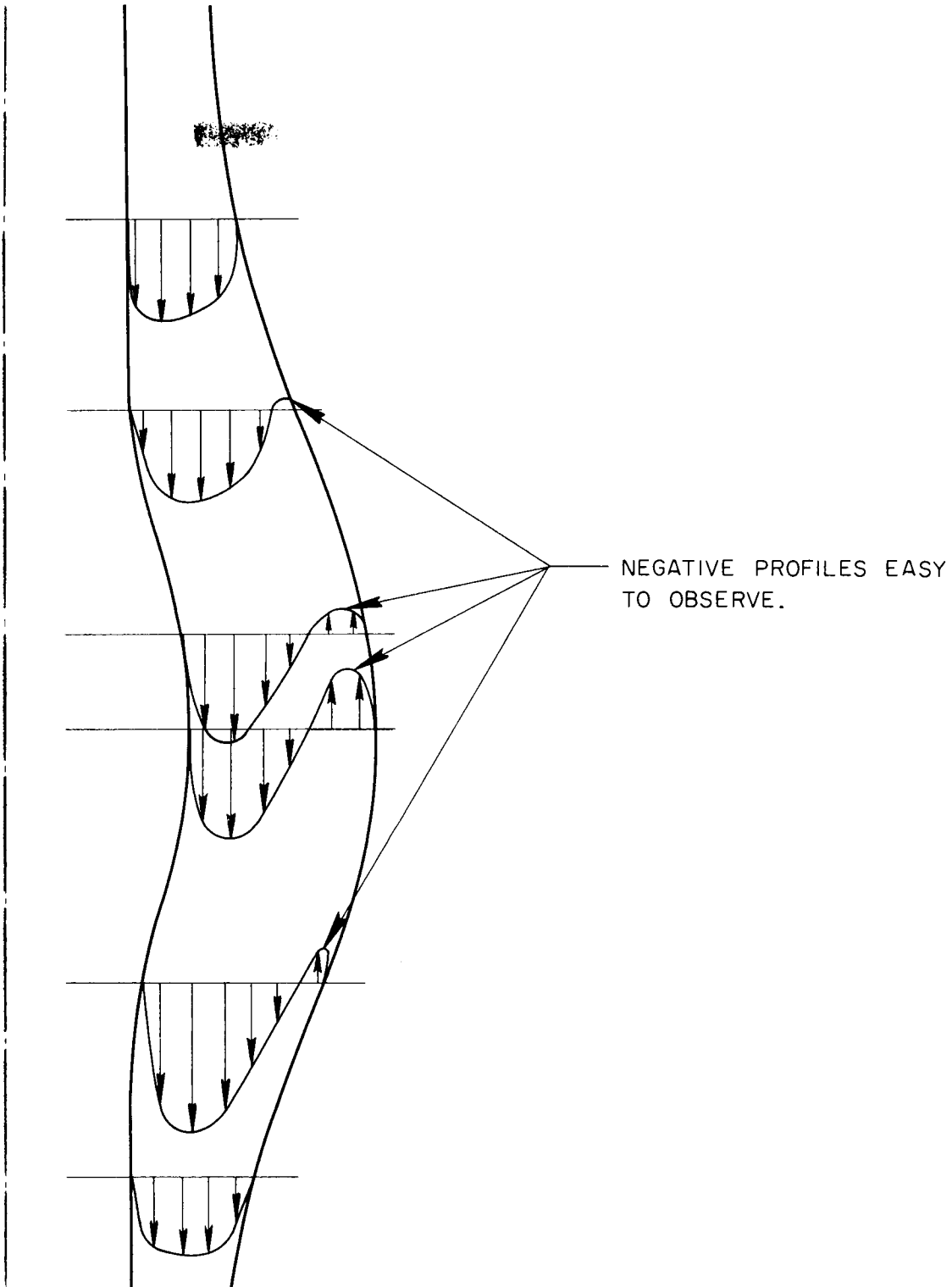
Fig. 33. Qualitative Estimate of Velocity Distribution for Axial Flow Through "18-Inch"
ART Core Model with Screens at the Inlet $N_{re, mid}$ = 3,000.
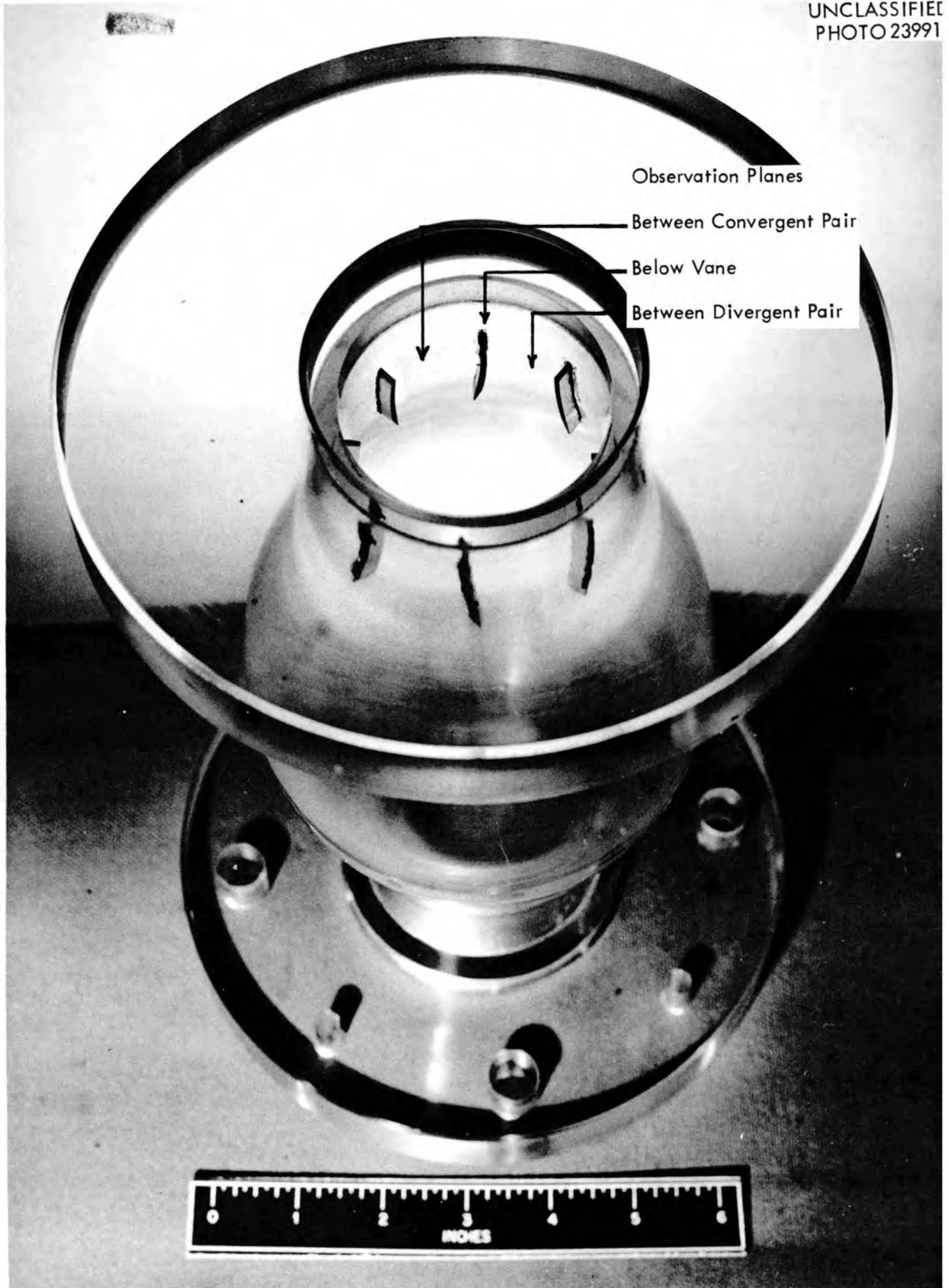
Fig. 34. Plastic Outer Core Shell with Turbulator Vane Set No. 1.

ORNL-LR-DWG 22427
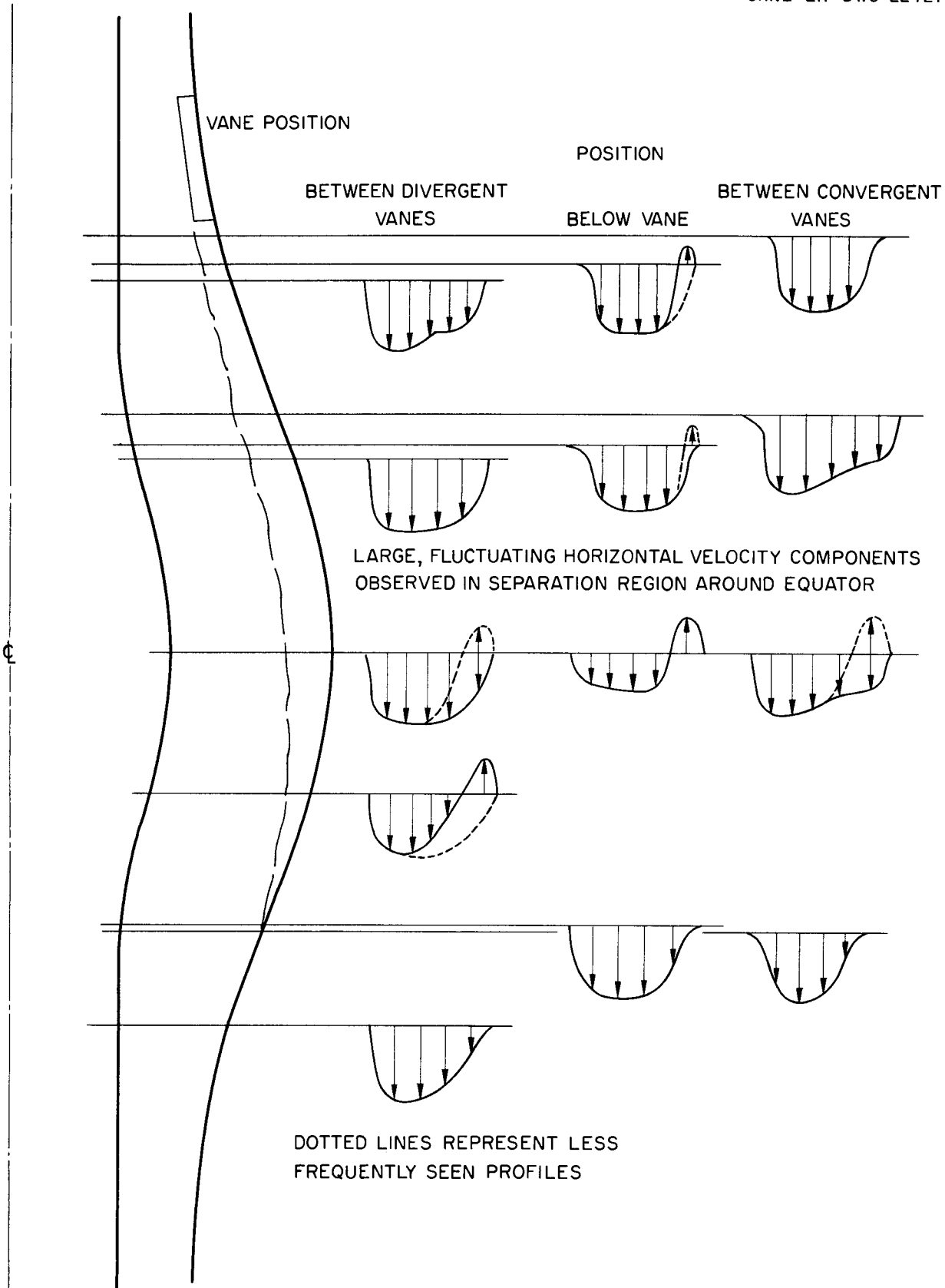
Fig. 35. Qualitative Estimates of Velocity Distribution and General Flow Features Through the "18-Inch" ART Core Model with Turbulator Vane Set No. 1 at Midplane Reynolds Numbers from 5,000 to 20,000.

(c) Eight aerofoil turbulence promoters of sharper curvature and wider span were also tried.[18] Observations of velocity profiles were made along the vertical planes shown in Figure 36. This figure is a photograph of the core shell with the vanes attached. Figures 37 and 38 show the velocity profiles obtained qualitatively at $N_{Re, mid}$ = 5,000 and the gross flow features observed at $N_{Re, mid}$ = 20,000.

(d) Qualitative axial velocity profiles were obtained using the phosphorescent particle technique for the "18-inch" ART core model with the Pratt and Whitney Aircraft vortex generator in the entrance.[19] Figure 14 shows the generators mounted on the core, and Figure 39 shows a photograph of the generator. The vanes for this test were set at a 45-deg angle with the core axis. Figure 40 shows the qualitative velocity profiles obtained. Average profiles are shown since variability existed in the flow. General flow features were also observed up to $N_{Re, mid}$ = 20,000.

(e) The Pratt and Whitney Aircraft vortex generators used in case (d) above were also tried with the "21-inch" ART core model.[19] The axial velocity profiles are shown in Figure 41. The dashed lines indicate other instantaneous profiles observed at different times. The general flow features were observed up to $N_{Re, mid}$ = 20,000.

(f) Experiments were conducted on the "21-inch" ART core model with Pratt and Whitney vortex generators of 50-, 55-, 60-, 65-, and 70-deg vane angles relative to the direction of the core axis. Unsteady flow (large-scale fluctuating eddies) was observed using the phosphorescent particle flow visualization method for all cases. The results were very similar to
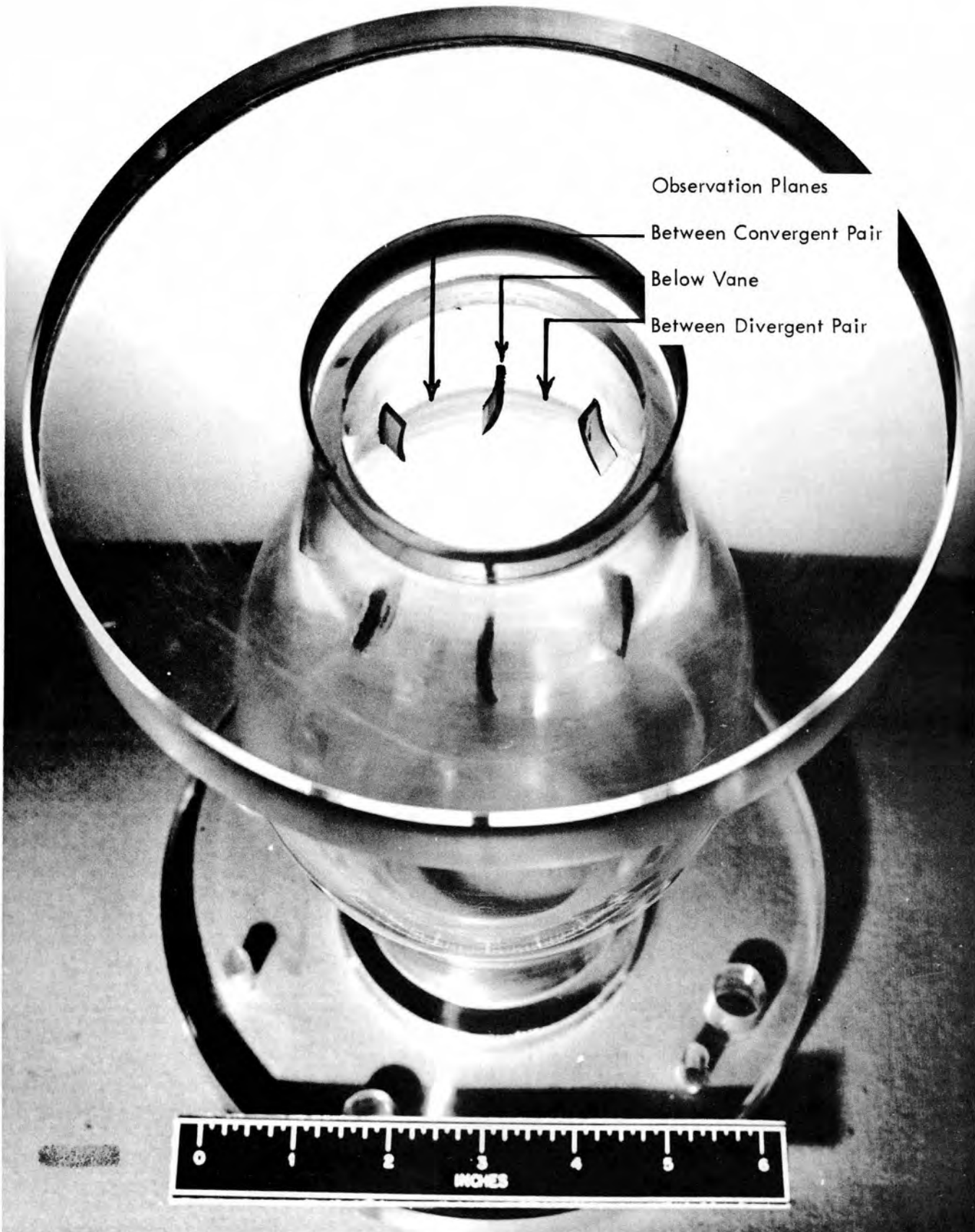
Fig. 36. Plastic Core Shell with Turbulator Vane Set No. 2.

ORNL—LR—DWG 22423
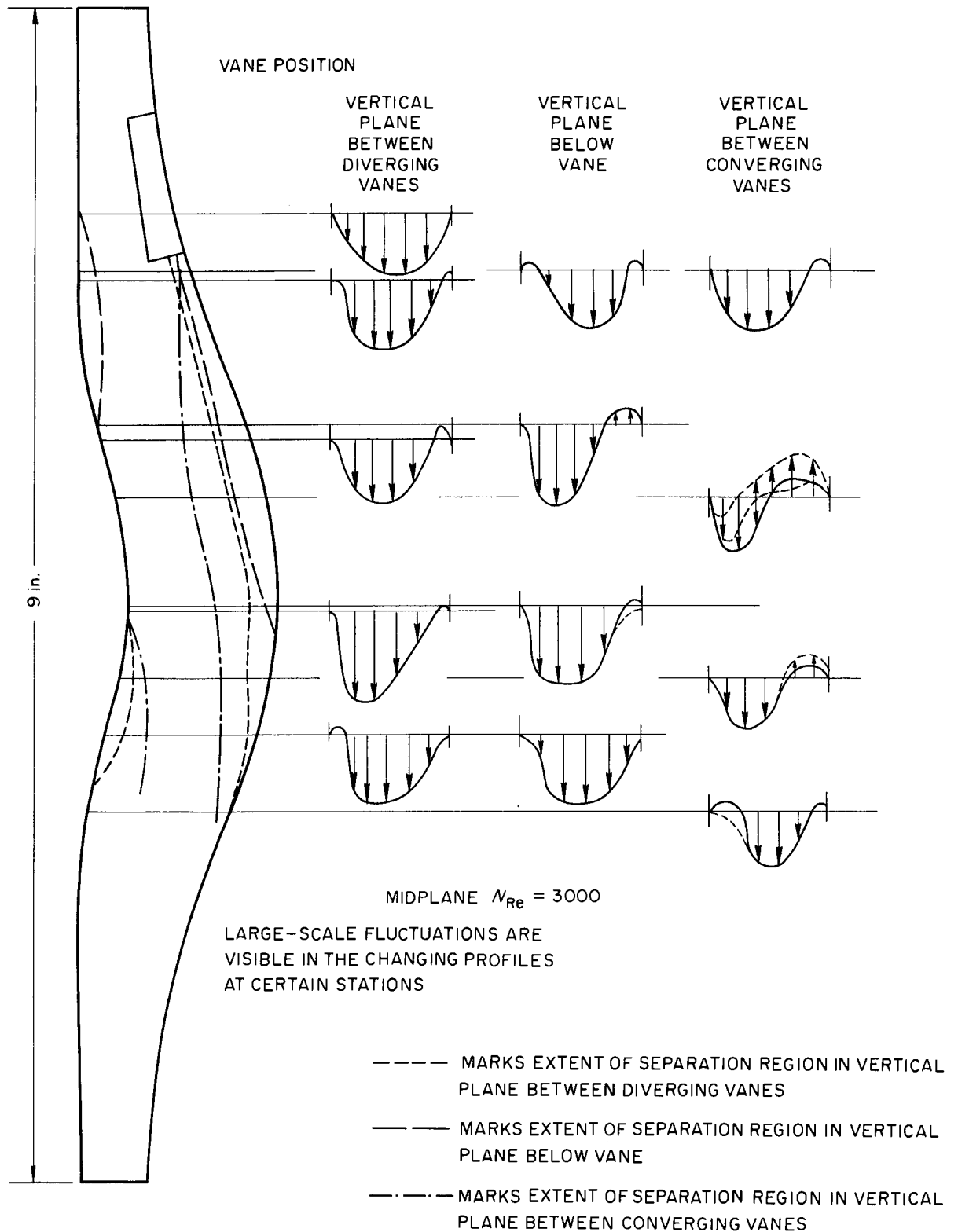
Fig. 37. Qualitative Estimate of Velocity Profiles Observed in Axial Flow Through the "18-Inch" ART Core Model with Turbulator Vane Set No. 2 at $N_{Re, mid}$ = 3,000.

ORNL-LR-DWG 22424

BETWEEN DIVERGING
VANES

BELOW VANE

BETWEEN CONVERGING
VANES
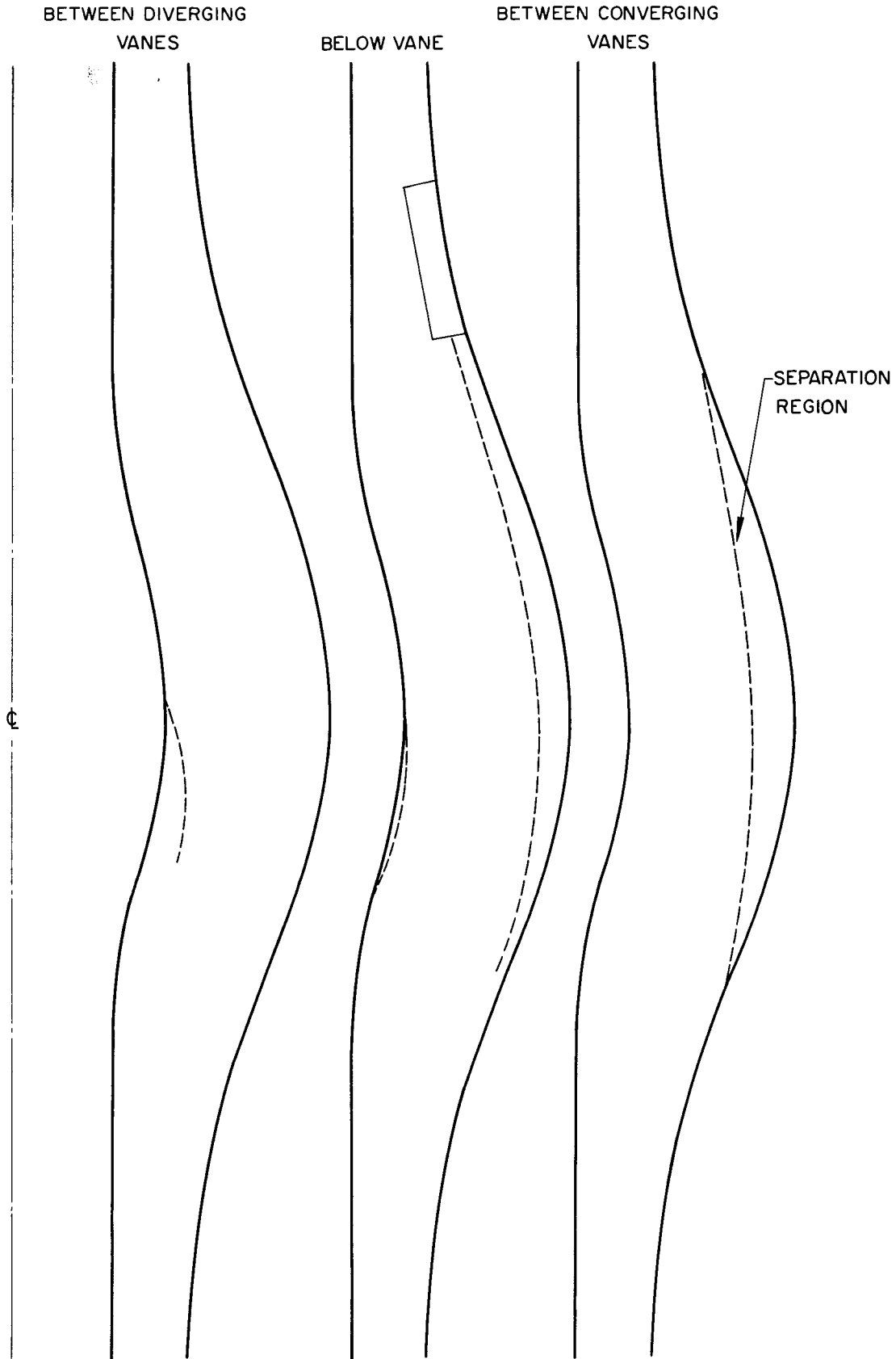
SEPARATION
REGION

Fig. 38. Qualitative Estimate of Separation Region in Axial Flow Through the "18-Inch" ART Core Model with Turbulator Vane Set No. 2 at $N_{Re, mid} = 20,000$.
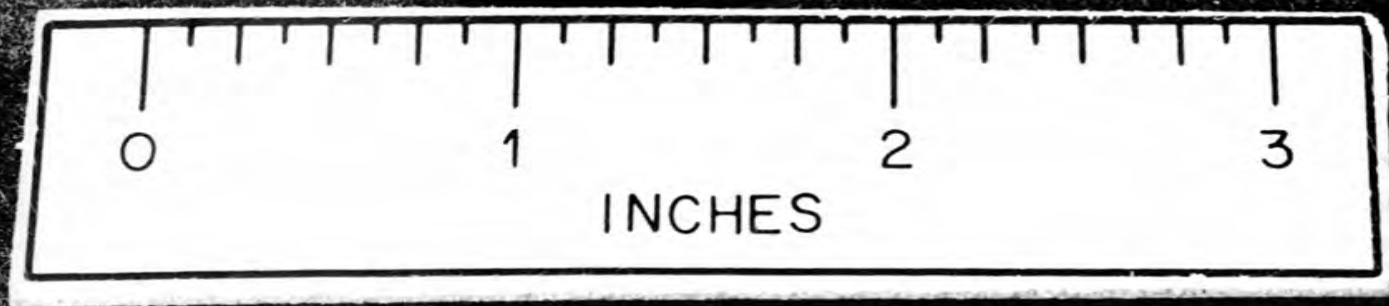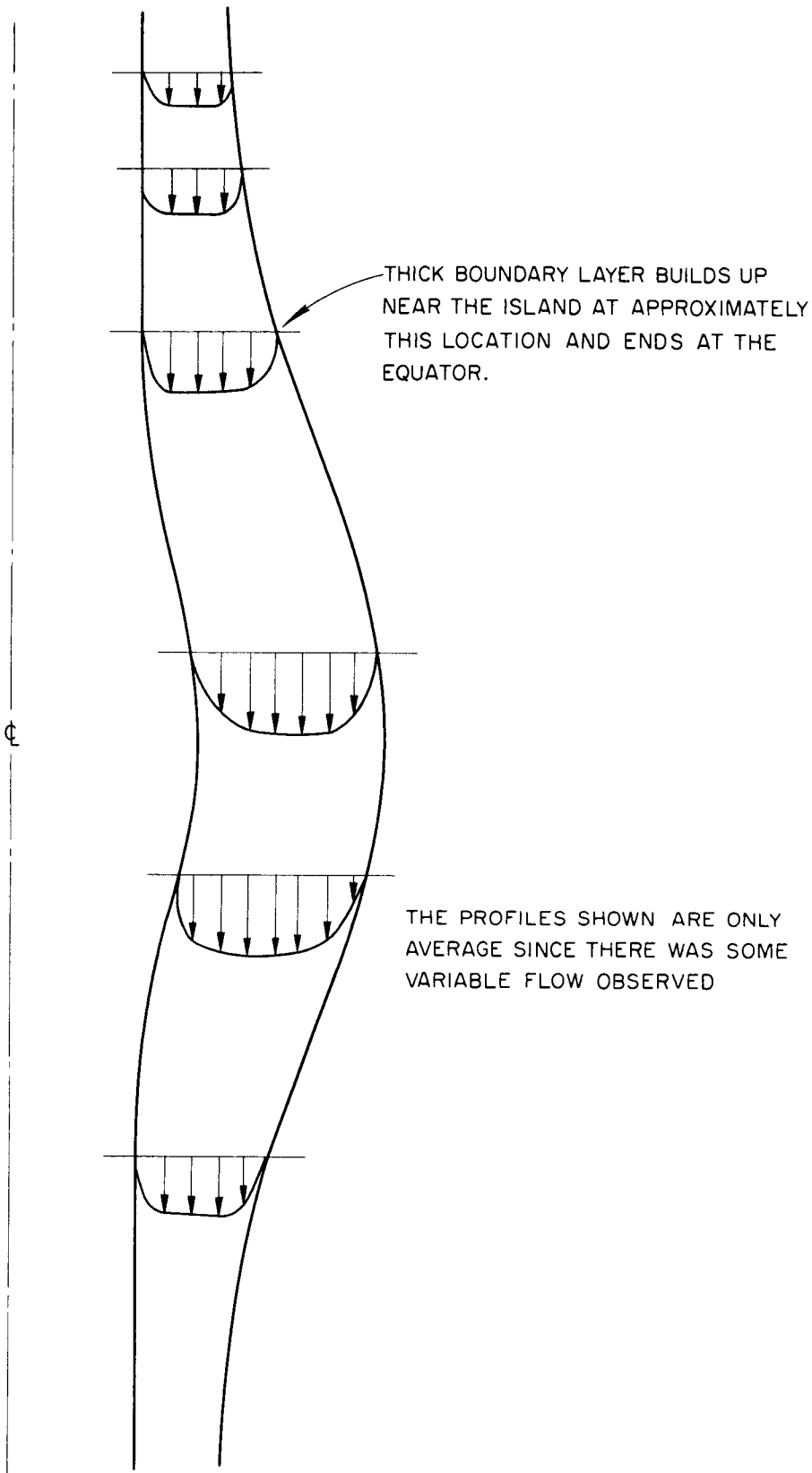
-65-

Fig. 20. The Pratt and Whitney Aircraft Vortex Generator

ORNL-LR-DWG 22421

THICK BOUNDARY LAYER BUILDS UP
NEAR THE ISLAND AT APPROXIMATELY
THIS LOCATION AND ENDS AT THE
EQUATOR.

THE PROFILES SHOWN ARE ONLY
AVERAGE SINCE THERE WAS SOME
VARIABLE FLOW OBSERVED

Fig. 40. Qualitative Estimate of Velocity Profiles Observed in Axial Flow Through the
"18-Inch" ART Core Model with the Pratt and Whitney Aircraft Vortex Generator at the
Inlet.

ORNL-LR-DWG 22422

DASHED PROFILES INDICATE THOSE THAT
ARE LESS FREQUENTLY SEEN.

PULSATING FLOW, VELOCITY NEXT TO THE
ISLAND CHANGES FROM A VERY LOW TO A
NEGATIVE FLOW. A "SQUARE—WAVE" PRO-
FILE WAS ALSO VISIBLE OCCASIONALLY.

THICK BOUNDARY LAYER NEXT TO
THE ISLAND
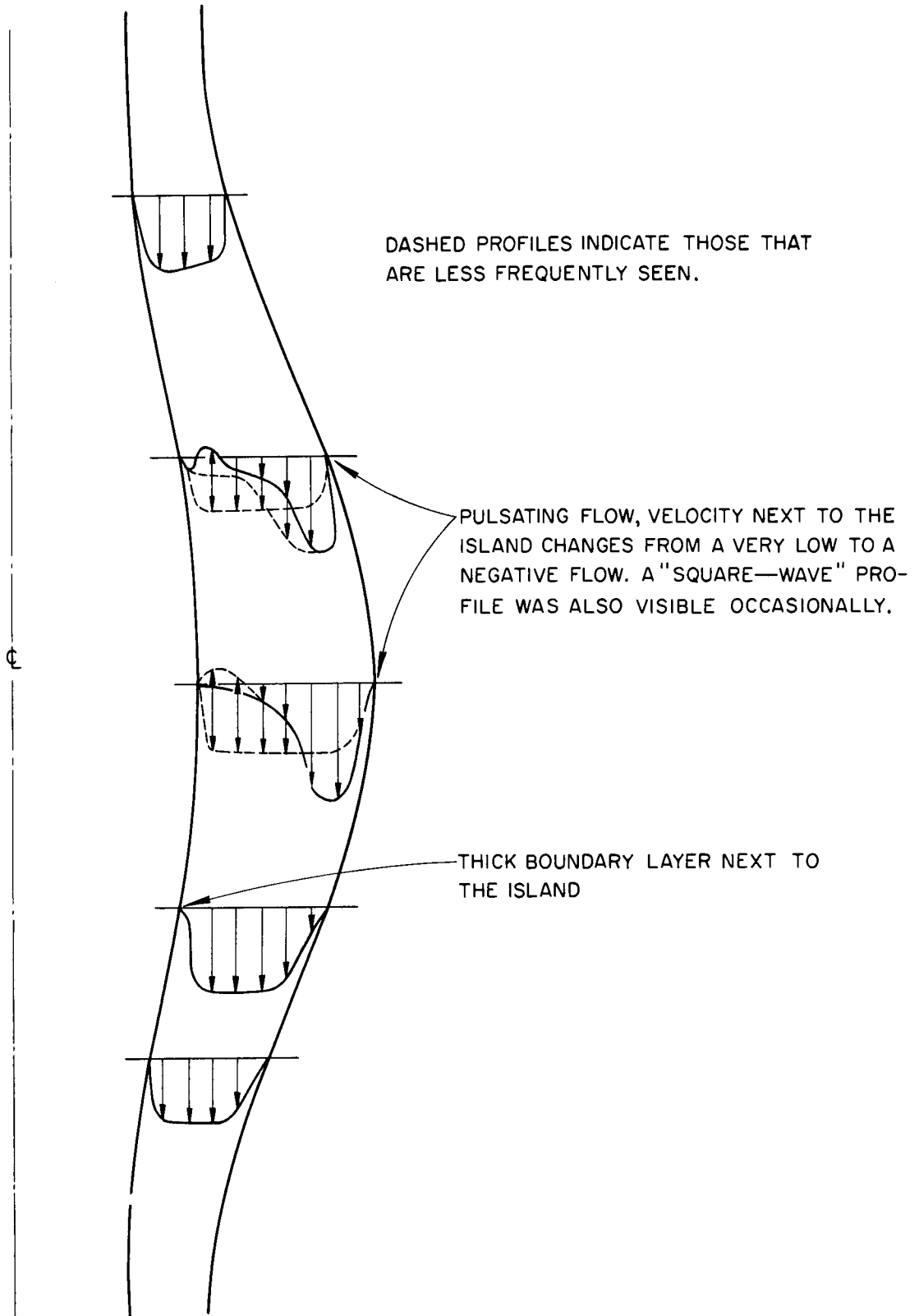
Fig. 41. Qualitative Estimate of Velocity Distribution in Axial Flow Through the
"21-Inch" ART Core Model with the Pratt and Whitney Aircraft Vortex Generator at
the Inlet.

those obtained in case (e). In addition, peripheral asymmetries in the flow rate in the core were observed with the vortex generators, even though the distribution of flow to the vortex generators was even.

(g) The inlet half of the ART "21-inch" core model was packed with combinations of screens of varying solidity ratios.[20] A photograph of the core model with a screen packing combination is shown in Figure 43. The following table lists the screen combinations investigated:

TABLE 4

Screen Packing Combinations for 10/44-Scale "21-inch" Core

Position	Distance from Core Inlet (in.)	Combinations 1	2	3	4	5
1	0				a	a
2	0.373					
3	0.746	a*	a	a	a	a
4	1.118					
5	1.491	a	a	c	a	a
6	1.864					
7	2.238	c			a	a
8	2.610		a	c		
9	2.982				a	b

*a - 0.385 solidity ratio screen, 20 x 20 mesh, 0.0108-in.-dia wire
 b - 0.510 solidity ratio screen, 20 x 20 mesh, 0.0150-in.-dia wire
 c - 0.622 solidity ratio screen, 30 x 30 mesh, 0.0128-in.-dia wire
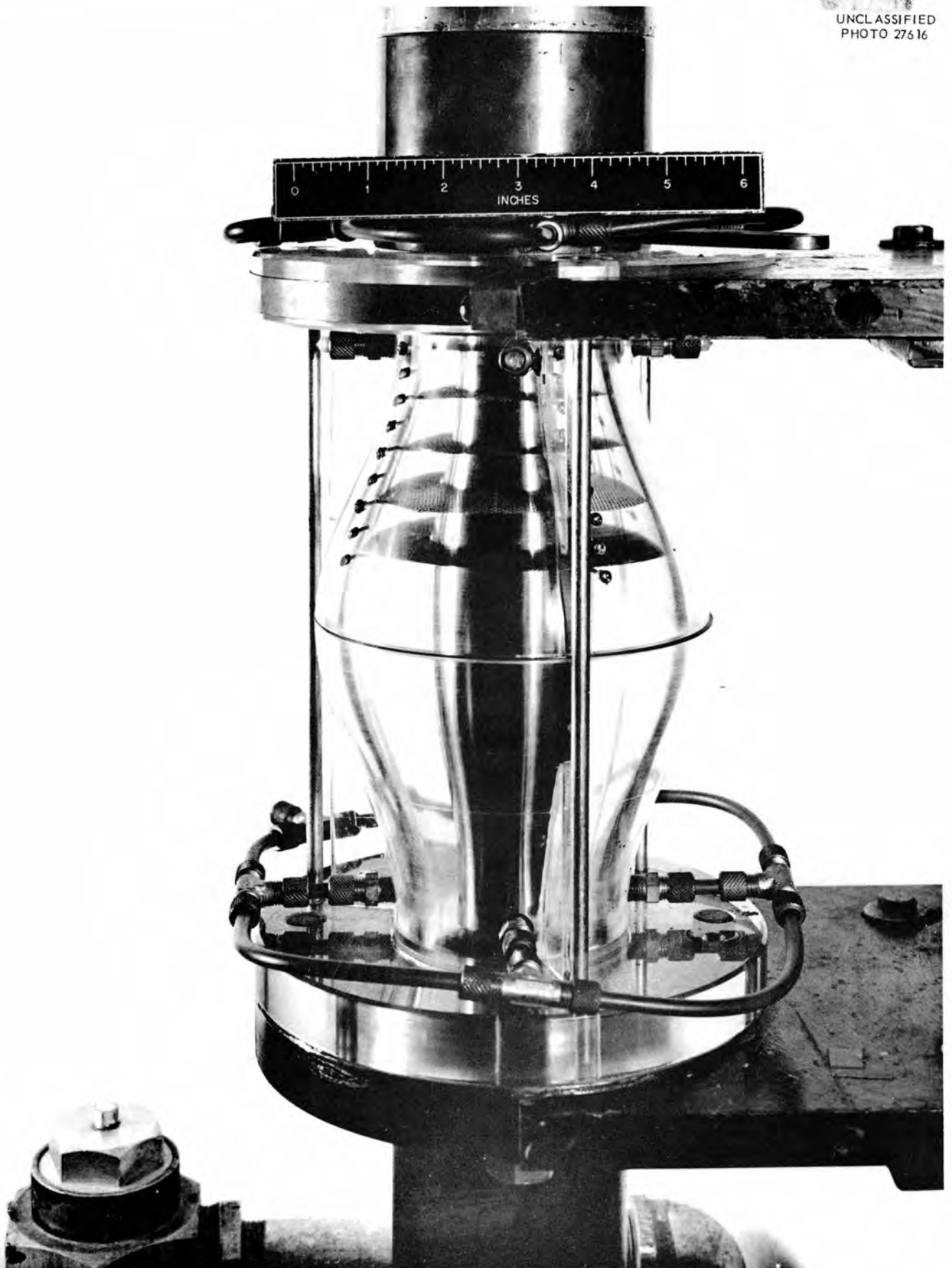
Fig. 42. 10/44-Scale Model of ART Core with Screen Combination Number 5.

Figures 43 through 47 show the flow features and velocity profiles obtained with these screen arrangements using the phosphorescent particle technique. The total relative pressure loss for the five combinations is shown in Figure 48 as a function of core midplane Reynolds modulus. It was found that the combination given by number 5 of Table 4 prevented boundary layer separation and created a fairly uniform velocity field. This is shown in Figure 47.

(h) The inlet area expansion of a 10/44-scale model of a "21-inch" straight annular core was also packed with combinations of screens.[20] A sketch of the flow channel with the screen positions indicated is shown in Figure 49 and a photograph of the core packing in Figure 50. Two combinations were tried: 0.385 solidity ratio screens in positions 1, 2, 3, 4, and 6; and 0.385 solidity ratio screens in all six positions. Figures 51 and 52 show the flow features of these combinations. Plotted in Figure 53 is the relative pressure loss for the second packing combination as a function of core midplane Reynolds modulus. The second packing combination prevented boundary layer separation in the abruptly diverging entrance region and gave a fairly uniform flow throughout the core. The boundary-layer separation region shown in Figure 52 near the exit of the core results from the too abrupt turning angle in this region.

Velocity Fluctuations in the Full-Scale "21-inch" ART Core Model

Motion pictures[21] of dye filaments near the walls in a full-scale model of the "21-inch" ART core were analyzed frame by frame to determine the angle of the dye filament at the point of injection. The results are plotted in

Ornl-Lr-Dwg-17718

BOUNDARY LAYER SEPARATION

0.385

0.385

0.622

BOUNDARY LAYER SEPARATION
IN SMALL AREAS ABOUT
PERIPHERY

$\mathbb{C}_L$

SCREEN POSITIONS INDICATED BY
SHORT ARROWS.

NUMBER NEXT TO ARROW IS SOLIDITY
RATIO OF SCREEN.

VELOCITY PROFILES OBSERVED AT
$Re_{MIDPLANE}$ = 7,650.

PARTICLE MOTION OBSERVED UP TO
$Re_{MIDPLANE}$ = 80,000.

FLOW EXIT
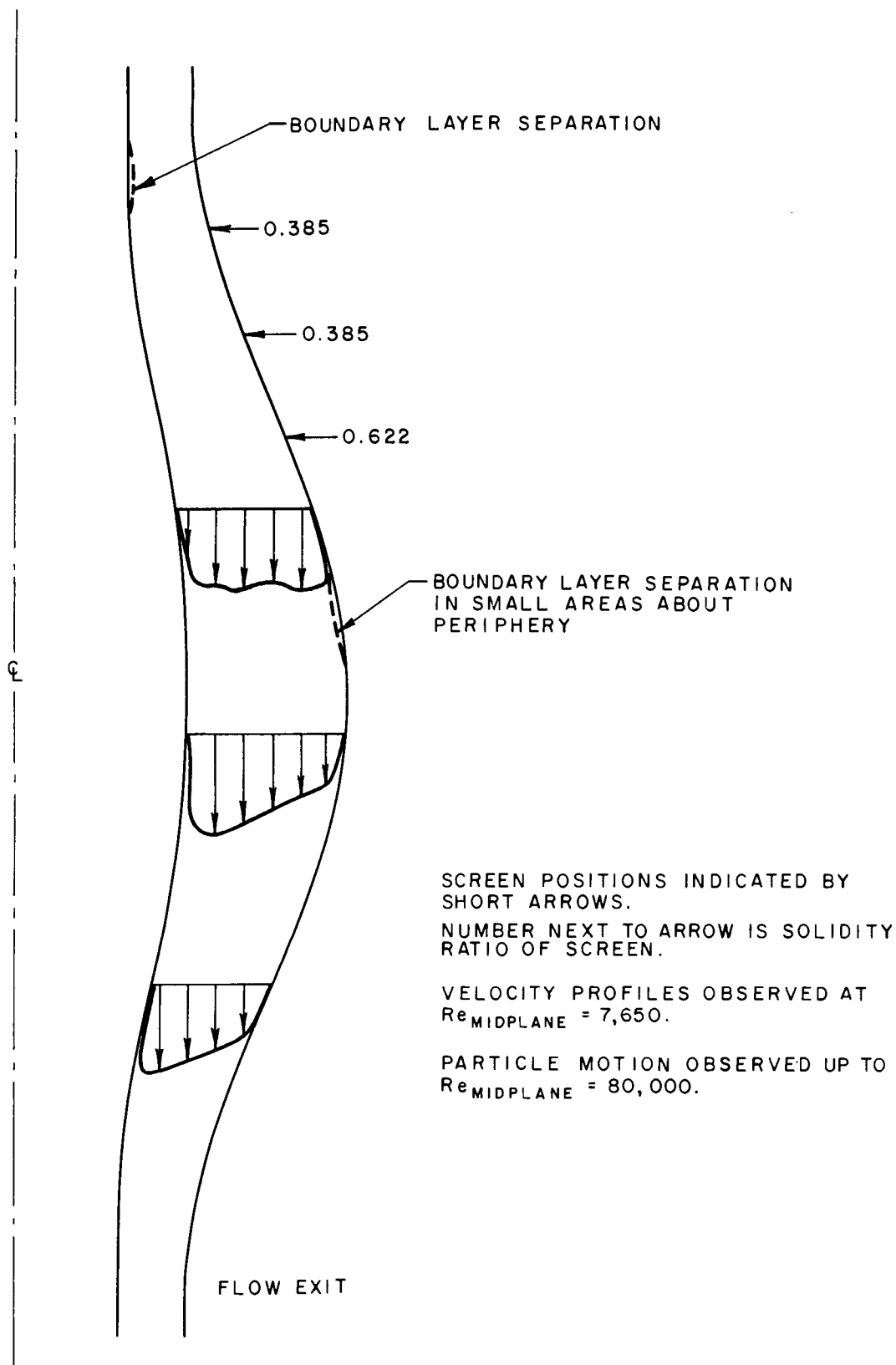
Fig. 43. Qualitative Flow Distribution in ART Core with Screen Combination Number 1.

Ornl-Lr-Dwg-17719

BOUNDARY LAYER SEPARATION

0.385

VELOCITY PROFILES OBSERVED
AT $Re_{MIDPLANE}$ = 5000

SCREEN POSITIONS INDICATED
BY SHORT ARROWS.

NUMBER NEXT TO ARROW IS
SOLIDITY RATIO OF SCREENS.

0.385

0.385

BOUNDARY LAYER SEPARATION AT
SOME POINTS AROUND PERIPHERY

FLOW EXIT
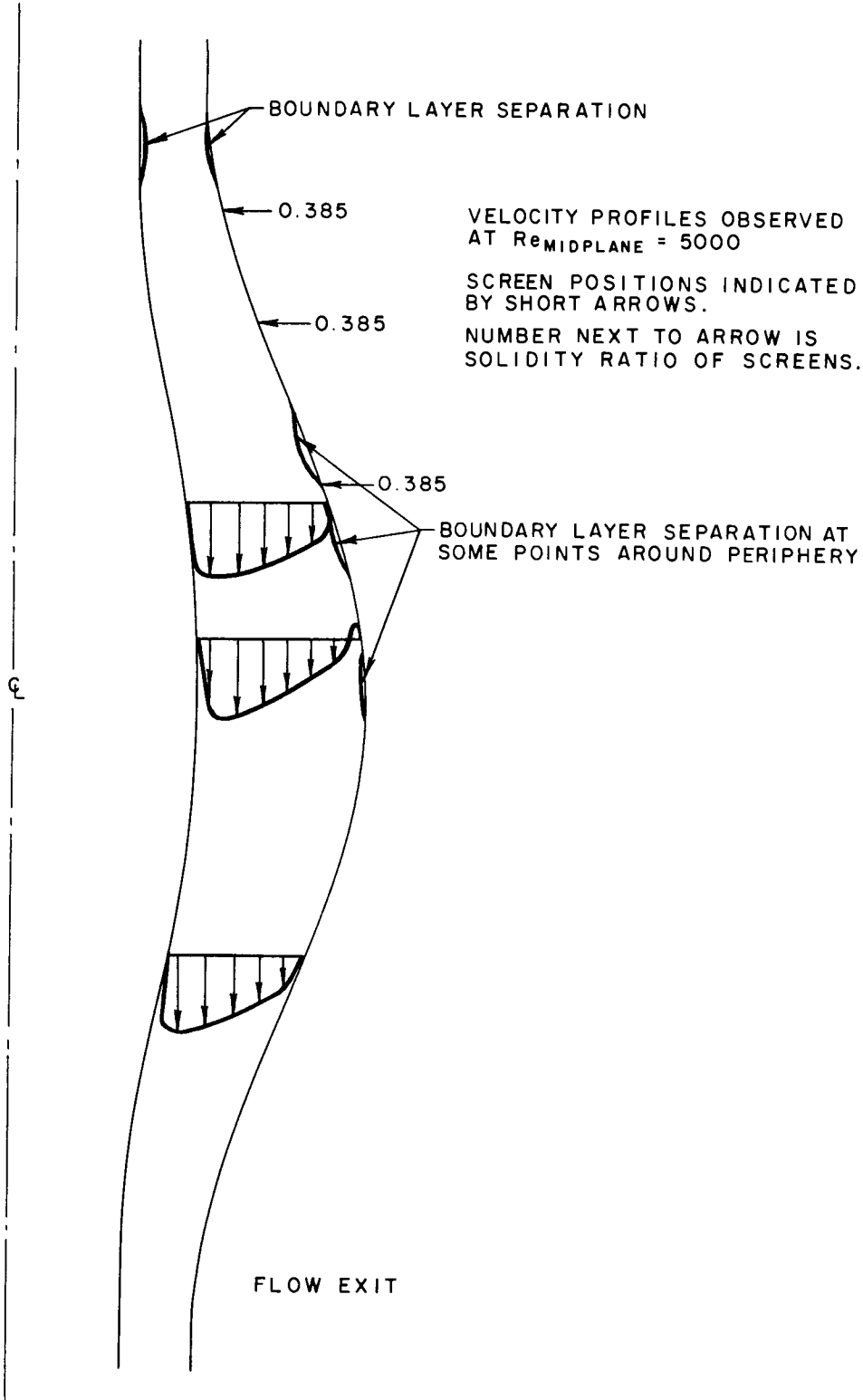
Fig. 44. Qualitative Flow Distribution in ART Core with Screen Combination Number 2.

Ornl-Lr-Dwg-17720

BOUNDARY LAYER SEPARATION

0.385

0.622

0.622

BOUNDARY LAYER
SEPARATION AT SOME
POINTS AROUND
PERIPHERY

PARTICLE MOTION OBSERVED
UP TO $Re_{MIDPLANE}$ = 80,000

SCREEN POSITIONS INDICATED
BY SHORT ARROWS.

NUMBER NEXT TO ARROW IS
SOLIDITY RATIO OF SCREEN
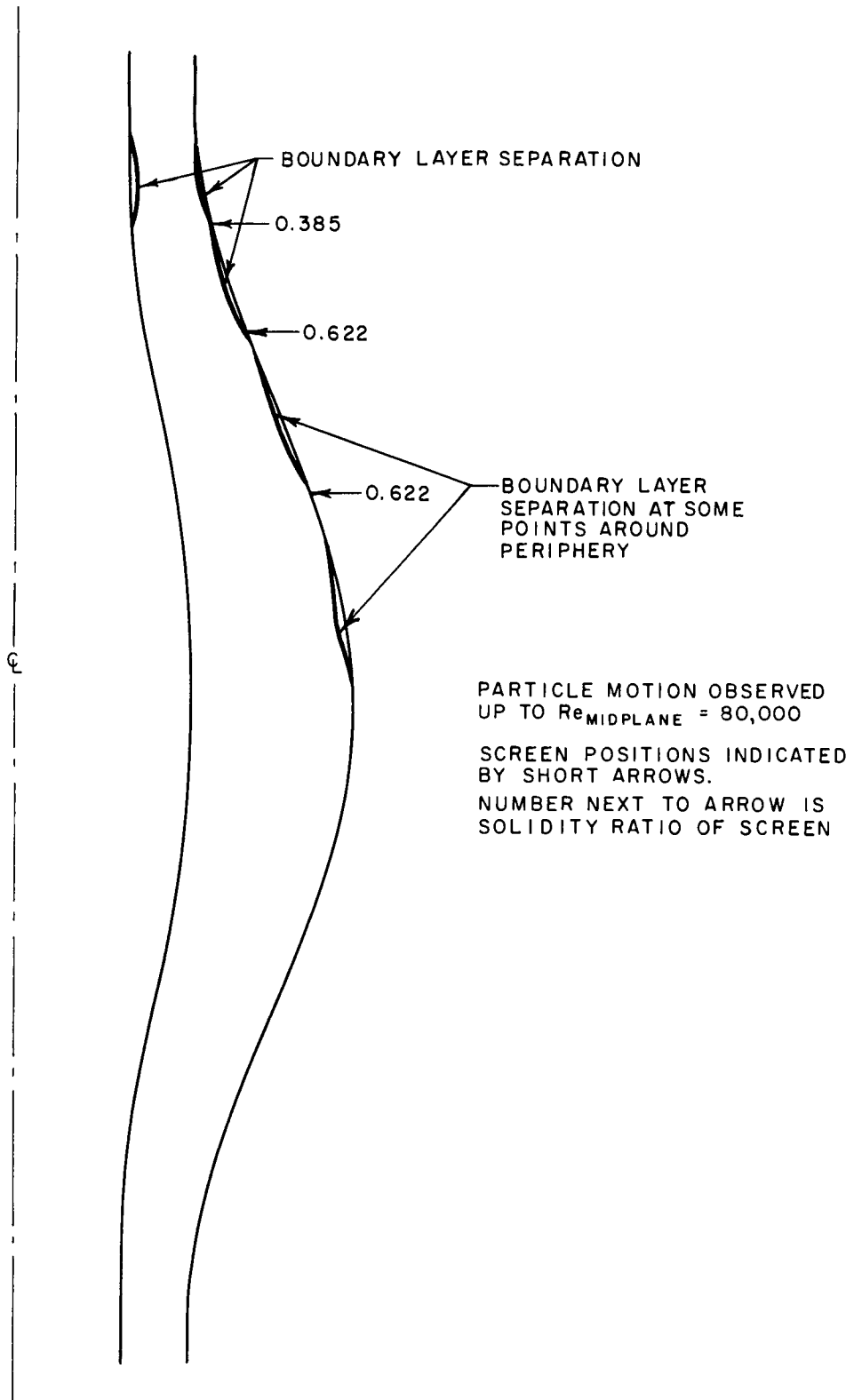
Fig. 45. Qualitative Flow Distribution in ART Core with Screen Combination Number 3.

Ornl-Lr-Dwg-17721

SCREEN POSITIONS INDICATED
BY SHORT ARROWS.

NUMBER NEXT TO ARROW IS
SOLIDITY RATIO OF SCREEN.

VELOCITY PROFILES OBSERVED
AT $Re_{MIDPLANE}$ = 6000.

PARTICLE MOTION OBSERVED UP
TO $RE_{MIDPLANE}$ = 80,000
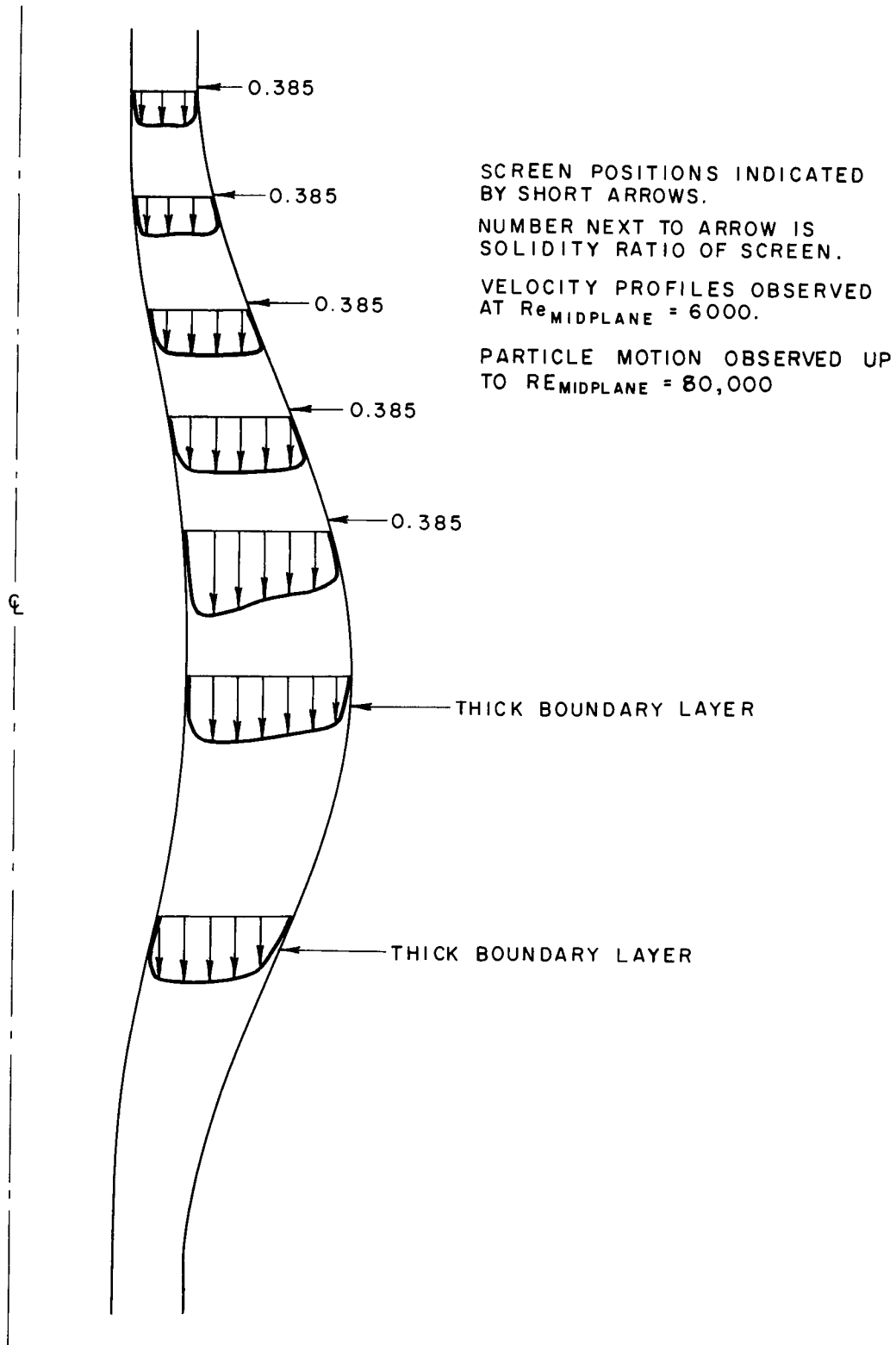
Fig. 46. Qualitative Flow Distribution in ART Core with Screen Combination Number 4.

Ornl-Lr-Dwg-17722

SCREEN POSITIONS INDICATED BY
SHORT ARROWS.

NUMBER NEXT TO ARROW IS
SOLIDITY RATIO OF SCREEN.

VELOCITY PROFILES OBSERVED
AT $3000 < Re_{MIDPLANE} < 5000$

PARTICLE MOTION OBSERVED UP
TO $Re_{MIDPLANE} = 80,000$

NO BOUNDARY LAYER SEPARATION
NOTED

0.385

0.385

0.385

0.385

0.510

FLOW EXIT
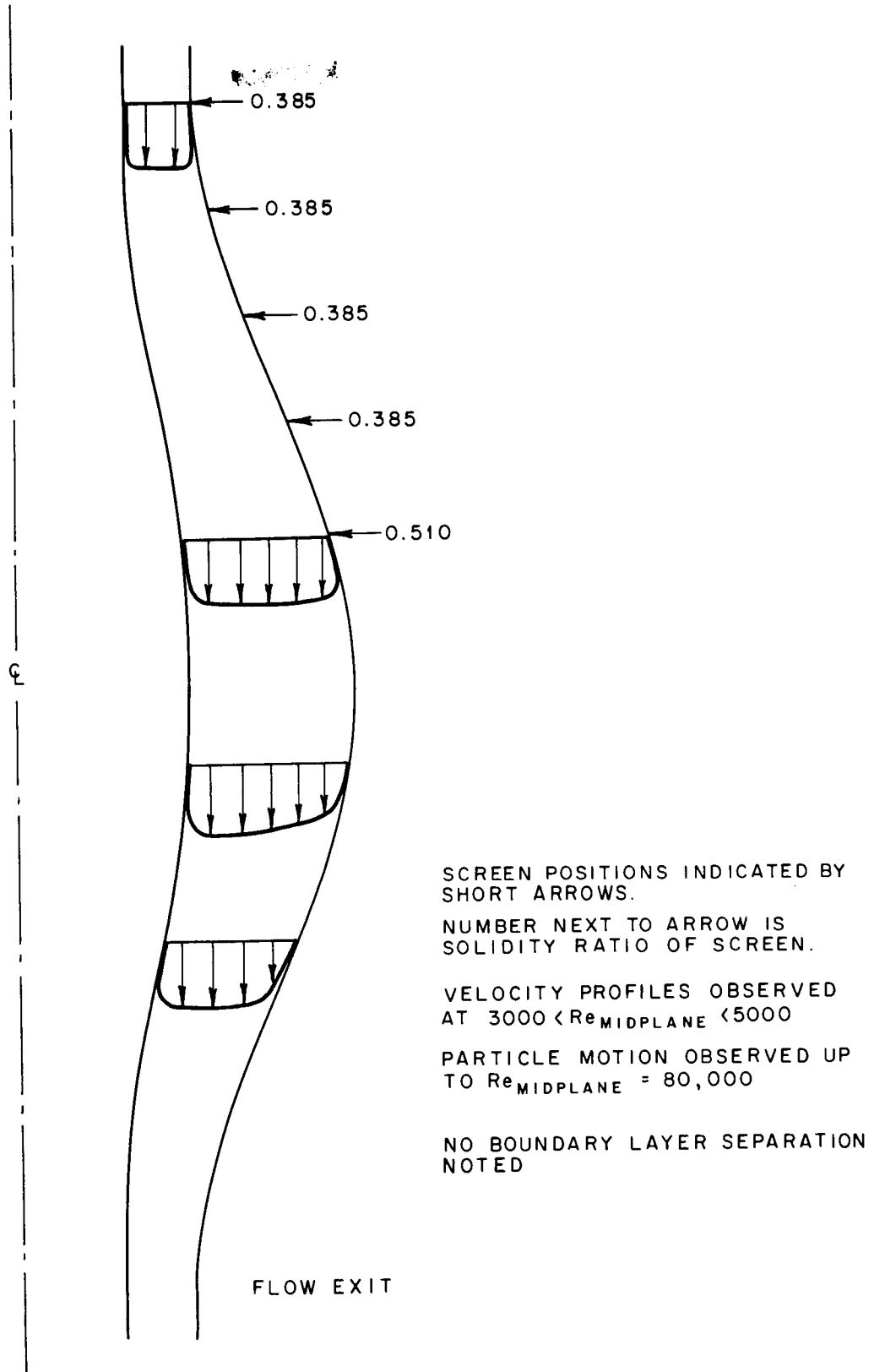
Fig. 47. Qualitative Flow Distribution in ART Core with Screen Combination Number 5.

ORNL-LR-DWG-17723
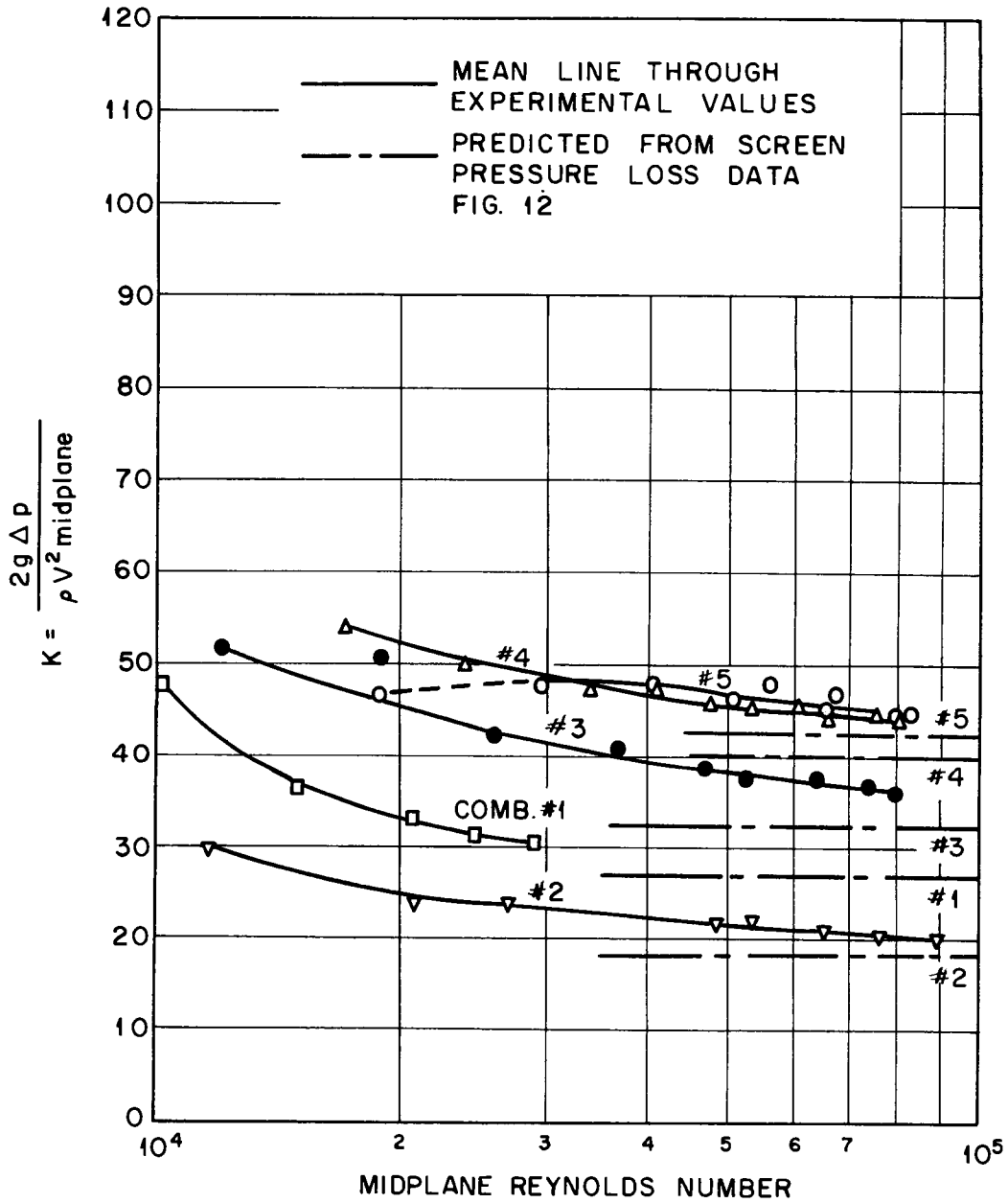
Fig. 48. Relative Core Pressure Loss for Various Screen Combinations in ART Core.

Ornl-Lr-Dwg-17717
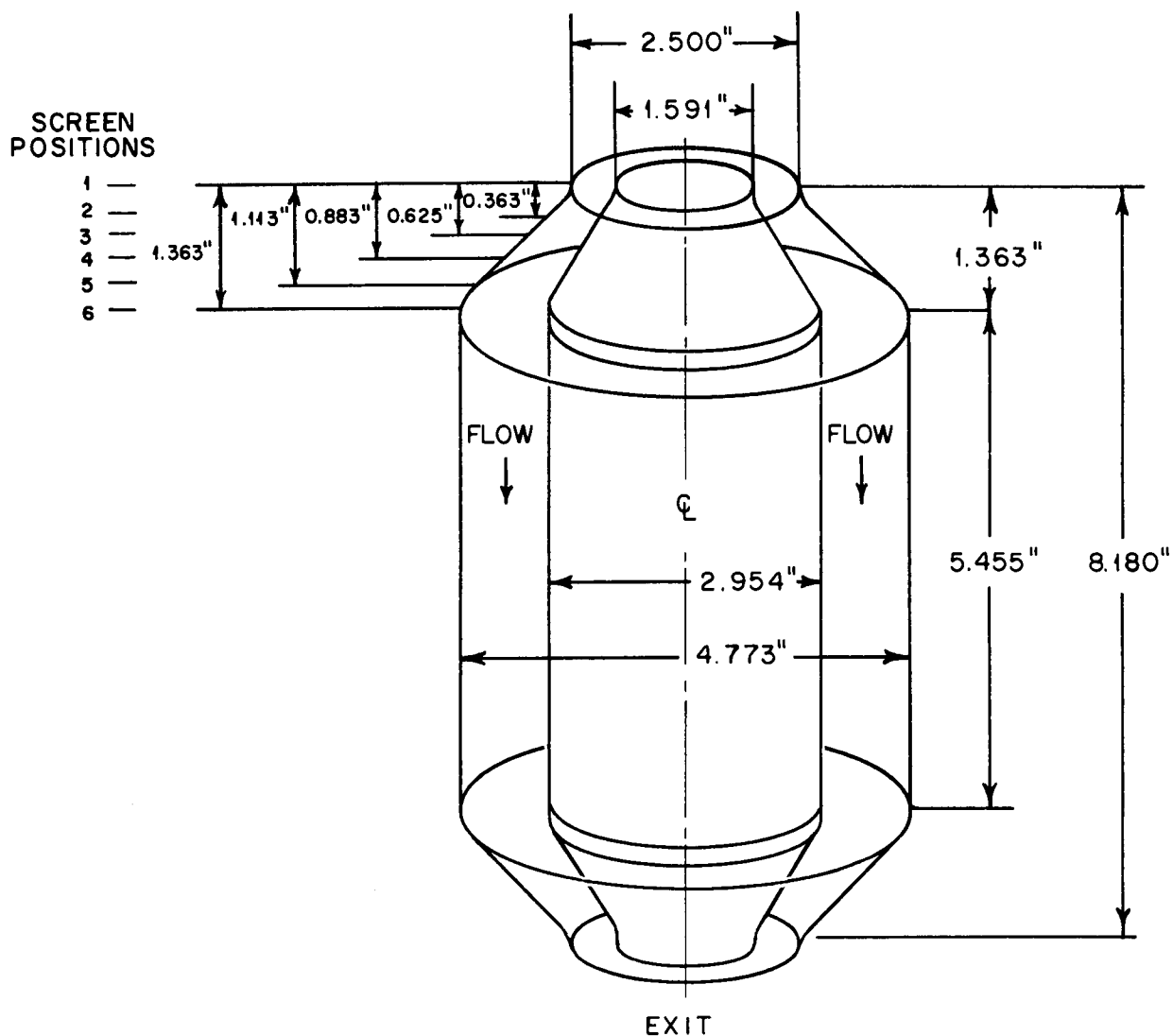
FULL SIZE CORE DIMENSIONS

TOTAL CORE VOLUME = 3.89 ft.^{3}

AREA RATIO OF MIDPLANE TO ENTRANCE = 3.77

MIDPLANE O.D. = 21" ; I.D. = 13"

ENTRANCE O.D. = 11 ; I.D. = 7"

OVERALL LENGTH = 36"

Fig. 49. "21-Inch" Abrupt Expansion Straight Annular Core (10/44-Scale Model).
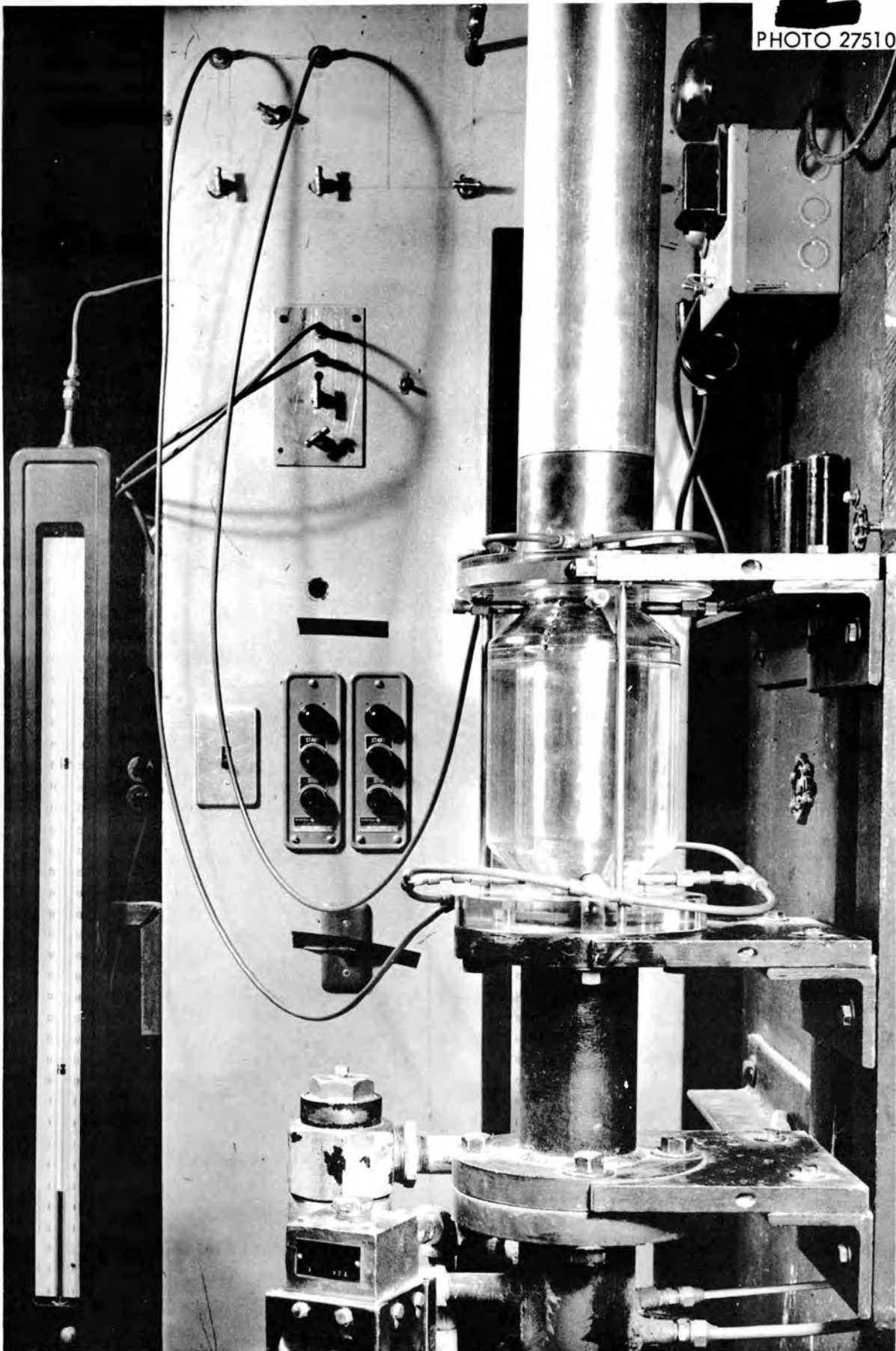
Fig. 50. Assembly of "21-Inch" Abrupt Expansion Straight Annular Core Model with Six 20 x 20 Mesh Screens.

Ornl-Lr-Dwg-17725

0.385

0.385

0.385

0.385

BOUNDARY LAYER SEPARATION

0.385

PARTICLE MOTION OBSERVED
UP TO $Re_{MIDPLANE}$ = 80,000

SCREEN POSITIONS INDICATED
BY SHORT ARROWS.
NUMBER NEXT TO ARROW IS
SOLIDITY RATIO OF SCREEN.

BOUNDARY LAYER SEPARATION

FLOW EXIT
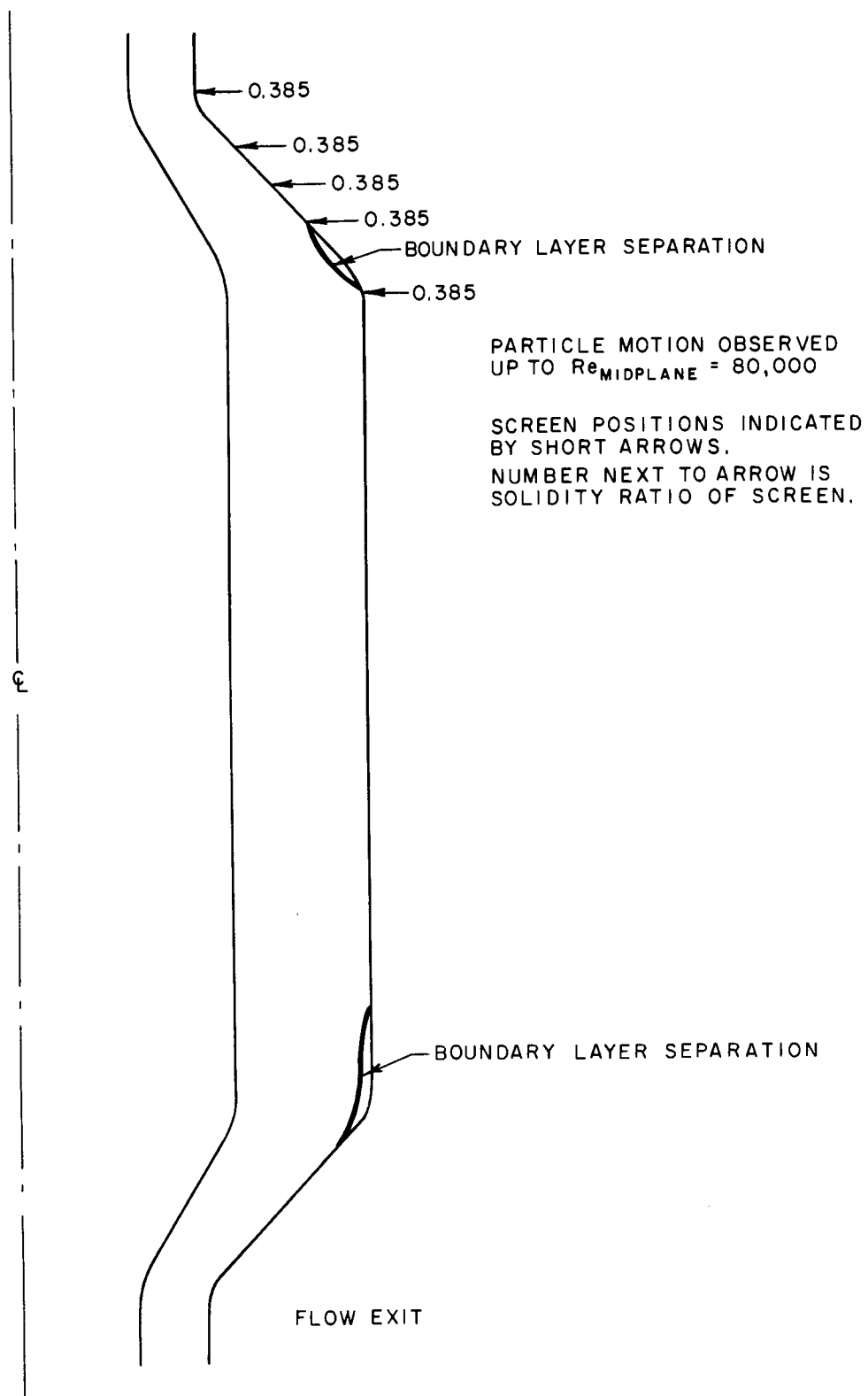
Fig. 51. General Flow Features of Axial Flow Through "21-Inch" Straight Core with Five 20 x 20 Mesh, 0.0108-in. Wire Diameter Screens.

Ornl-Lr-Dwg-17726
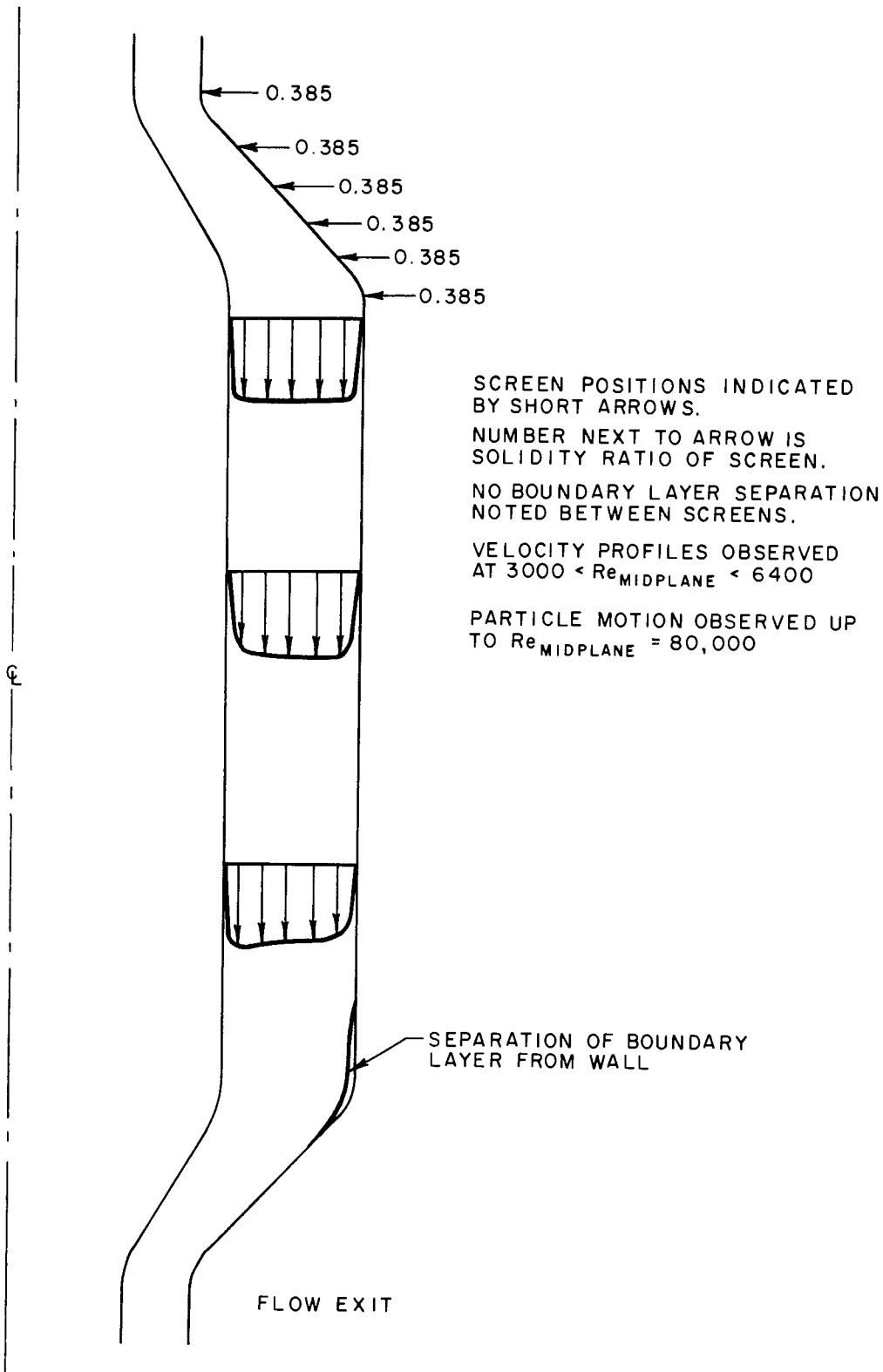
Fig. 52. Qualitative Flow Distribution in Axial Flow Through "21-Inch" Straight Core with Six 20 x 20 Mesh, 0.0108-in. Wire Diameter Screens.

ORNL-LR-DWG-17728
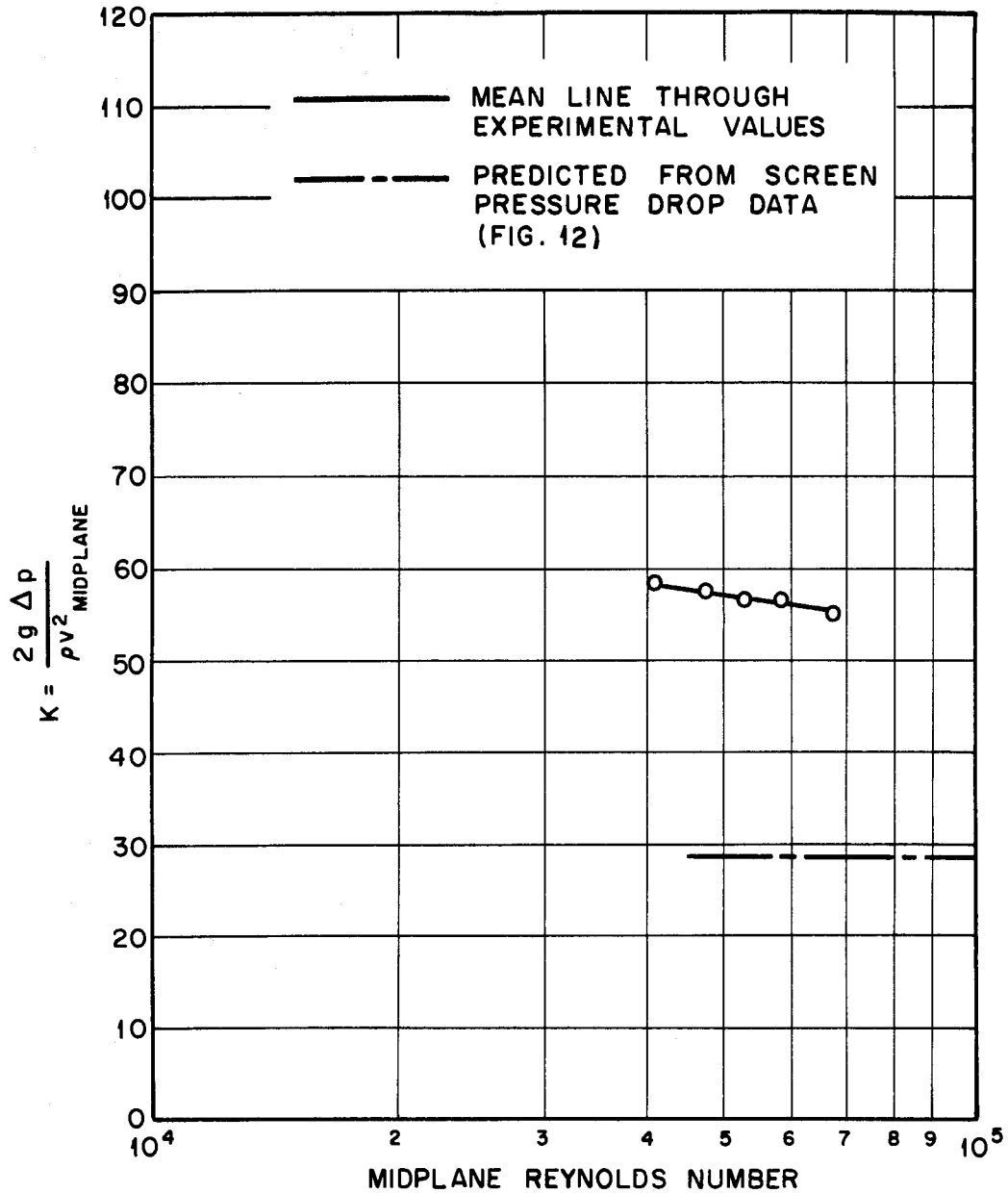
Fig. 53. Relative Core Pressure Loss for Six 20 x 20 Mesh Screens in "21-Inch" Straight Core.

Figures 54 and 55 for an average vector Reynolds modulus of 290,000.

The effect of flow velocity on fluctuation "frequency" was studied by comparing films of a high-velocity spiral flow (average vector Reynolds modulus of ~1,000,000) with the previously discussed film. The fluctuation "frequency" was observed to increase with the increased velocity.

Fluid Velocities in the Full-Scale ART "21-inch" Core

A reduction of velocity data for the full-scale "21-inch" ART core model with three different entrance conditions[6] was made to obtain mean axial and rotational components at several axial positions. These data are plotted in Figure 56 as a function of axial distance for a high-velocity rotational flow ($v_{t,avg}/v_{a,avg}$ = 11.8), a medium-velocity rotational flow ($v_{t,avg}/v_{a,avg}$ = 3.6), and a low-velocity rotational flow ($v_{t,avg}/v_{a,avg}$ = 1.7) obtained by turning vanes at the entrance. Mean velocities calculated from continuity of flow for the axial component and from conservation of angular momentum for the rotational component are plotted for comparison.

Pressure Distributions in "21-inch" ART Core

Pressure data[6] obtained with water flow through the full-size ART core model, converted to fluoride composition No. 30, are shown in Figure 57. The radial pressure difference, between the outer and inner walls, for the high-velocity rotational flow is given in relation to the axial position. Also shown for comparison are the values calculated in the previous chapter. Axial static pressure distributions in the ART core for fluoride composition No. 30 flow (1200 gpm) are plotted in Figure 58 for two entrance conditions. These curves are based on calculations made previously for entrance duct
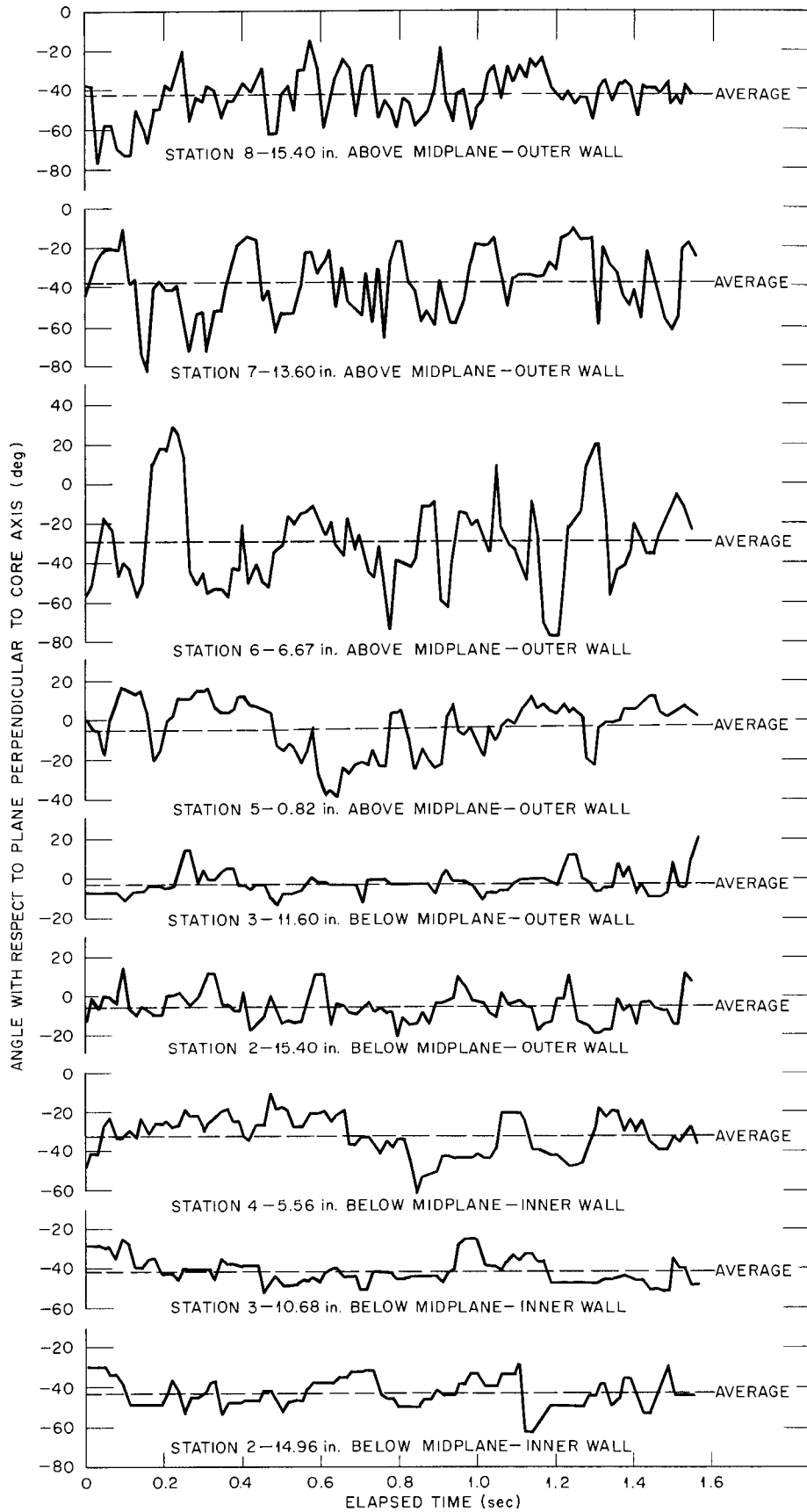
Fig. 54. Dye Filament Angular Fluctuation as a Function of Elapsed Time at Various Wall Positions for Water Flowing Through the Full-Scale Model of the "21-in." ART Core. Average resultant vector Reynolds number = 290,000.
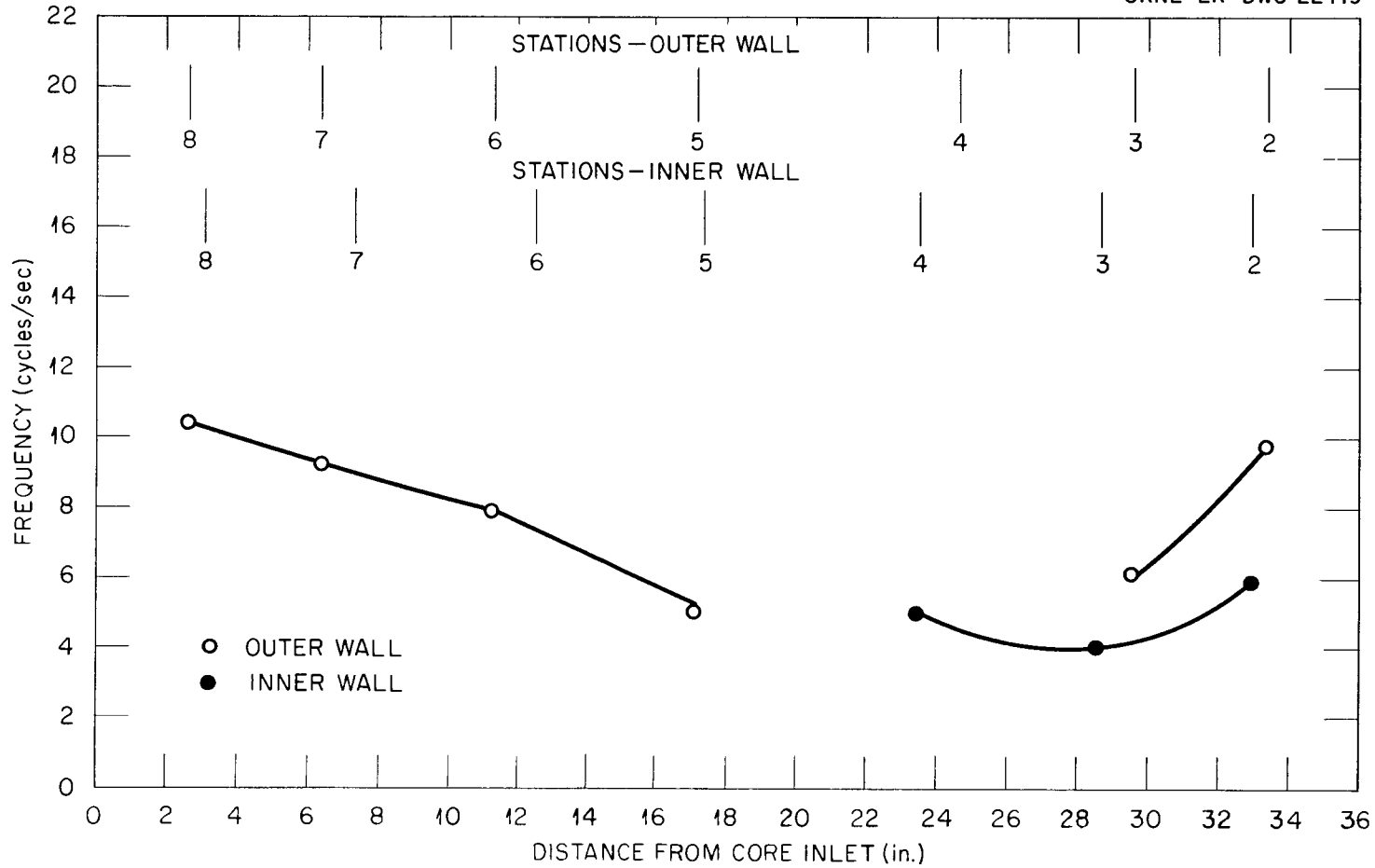
Fig. 55. Dye Filament Fluctuation Frequencies as Obtained by "Zero" Counting

ORNL—LR—DWG 22418
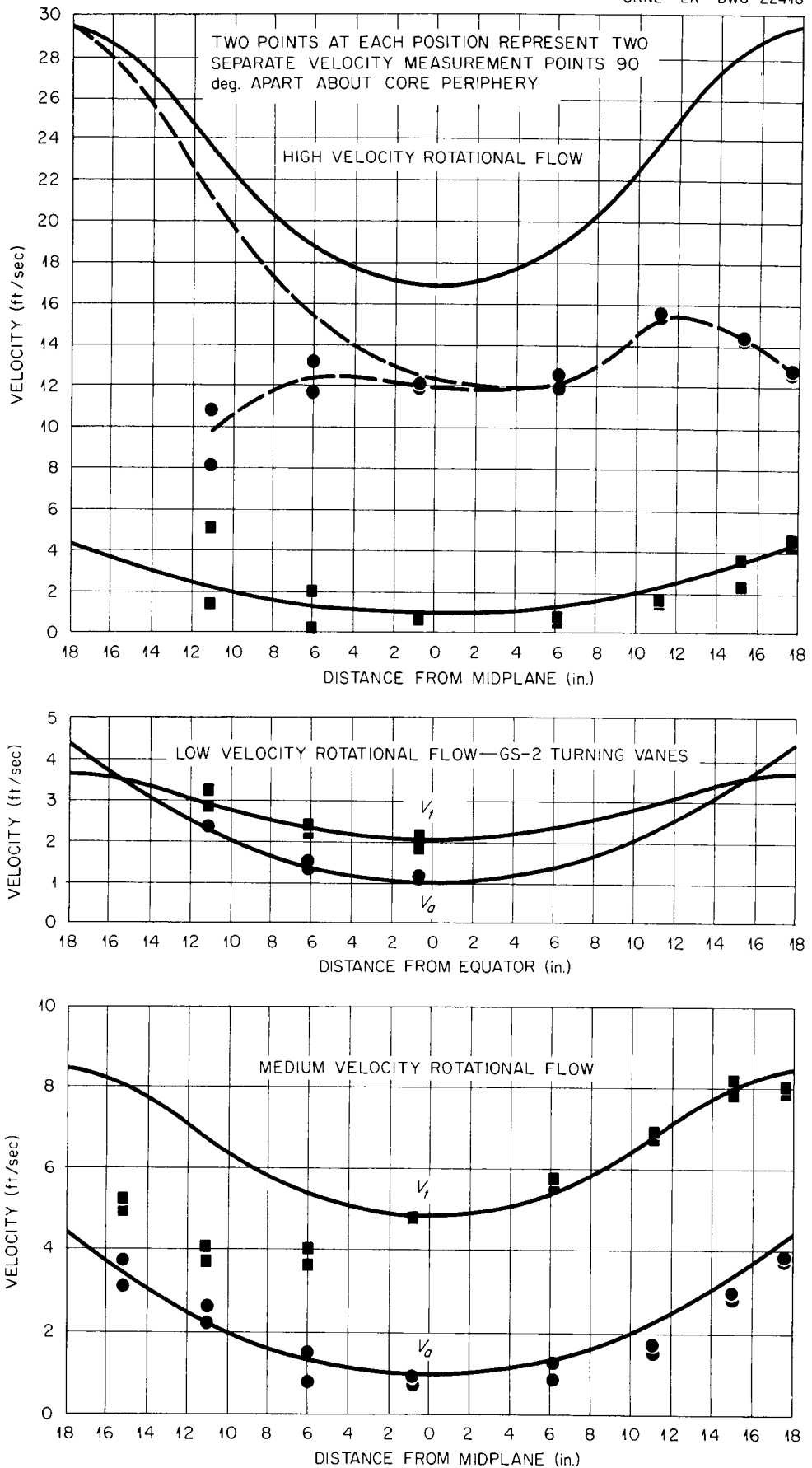
Fig. 56. Mean Axial and Rotational Components of Velocity in the "21-Inch" Full Size ART Core Model for Water Flow at ART Design Reynolds Moduli.
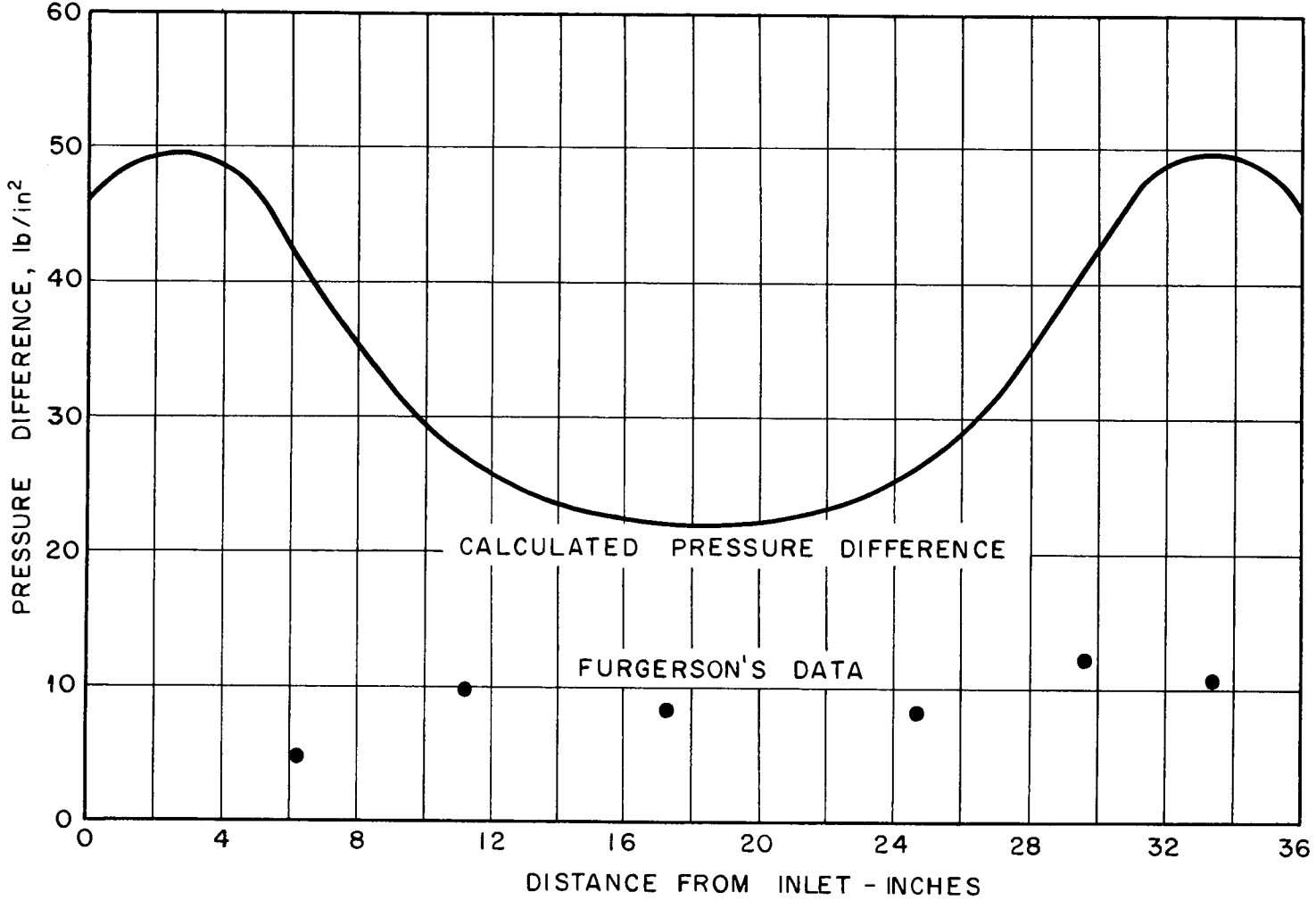
Fig. 57. Radial Pressure Difference Between Inner and Outer Walls for the High-Velocity Rotational Flow of Fluoride Mixture No. 30 at Design Reynolds Moduli in the "21-Inch" ART Core.
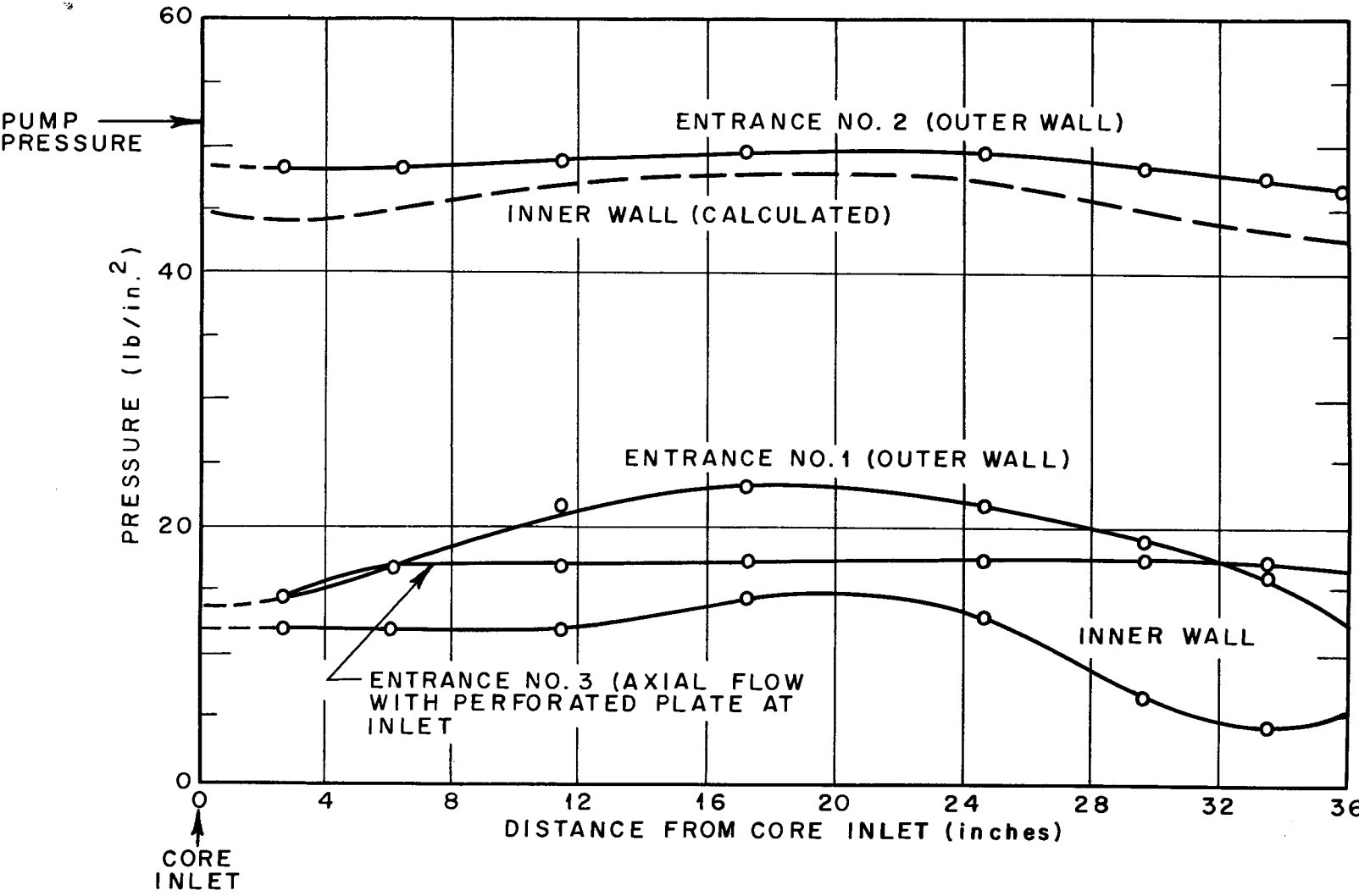
Fig. 58. Static Pressure Distributions in the "21-Inch" ART Core for Flow of Fluoride Composition No. 30 at Design Reynolds Moduli.

friction loss, entrance region turning and eddy losses, and the radial pressure differences for the medium velocity rotational flow case. Reduced data for an axial flow case achieved by turning vanes followed by a perforated plate are also included. In all cases, the pump output pressure was taken as 51.5 lb/in.^{2} (37 feet of fluoride composition No. 30).

DISCUSSION

Literature Survey

The dynamics of fluid flow through the ART and other proposed reflector-moderated reactor cores is complicated by the shape of the cores and their small length-to-hydraulic diameter ratio. A horizontal section through any of these core flow passages presented a ring-shaped, or annular, aspect. The area of this annulus was described as some function of the axial distance from the inlet. Usually this area first increased and then decreased as the distance from the inlet increased. A further complication was added when the flow was introduced such that it proceeded in a spiral fashion through the core. The length-to-diameter ratio of the cores was between 6 and 10. For spiral flows, the length of flow path to diameter ratio varied between 10 and 50, depending on the ratio of the spiral to axial velocity components.

Although the whole flow problem is enormously complicated by these factors, the problem can be clarified somewhat by considering a series of simpler problems. Disregarding the short L/D of the core and considering only axial flow, the hydrodynamic field can be described as primarily turbulent flow in a divergent-convergent annular duct.

Flow in Convergent and Divergent Channels. Consider Bernoulli's energy equation for frictionless flow,

$$h_1 + \frac{v_1^2}{2g_c} + \frac{p_1'}{\gamma} = h_2 + \frac{v_2^2}{2g_c} + \frac{p_2'}{\gamma} \quad . \tag{23}$$

Differentiating with respect to the direction of flow, x, there results,

$$\frac{dh}{dx} + \frac{v}{g_c}\frac{dv}{dx} = -\frac{1}{\gamma}\frac{dp'}{dx} \quad . \tag{24}$$

Since the body forces are balanced out by a corresponding pressure force, equation (24) can be written

$$\frac{v}{g_c}\frac{dv}{dx} = -\frac{1}{\gamma}\frac{dp}{dx} \tag{25}$$

where $\frac{dp}{dx}$ is now the pressure change with respect to flow direction due to momentum changes (friction is not considered).

Using the continuity equation for incompressible flow

$$vA_c = \text{constant} = Q \tag{26}$$

$$dv = d\left(\frac{Q}{A_c}\right) = -\frac{Q}{A_c^2}dA_c \tag{27}$$

Substituting equations (26) and (27) into equation (25),

$$\frac{Q^2}{A_c^3 g_c}\frac{dA_c}{dx} = \frac{1}{\gamma}\frac{dp}{dx} \tag{28}$$

Thus, if the cross-sectional area increases in the direction of flow, there is a corresponding pressure rise in the direction of flow.

The assumption of frictionless flow leads to the conclusion that the velocity distribution in a plane perpendicular to the flow is uniform at any plane; and, in diffusers, the diminution of velocity with distance from the inlet of the diffuser is uniform. These assumptions give a finite discontinuity at the walls. The walls do not move; and, at the wall, the velocity is that of the main stream. However, fluids are not frictionless; and the equations presented

do not give the whole picture of flow through divergent channels.

An interchange of momentum exists in all fluids that eliminates the discontinuity at the walls so that the fluid velocity at the wall is zero, and the curve of velocity versus distance from the wall rises in a continuous fashion to the main stream velocity. This interchange of momentum gives rise to a "shear" force between the various layers of fluid which is expressed in the differential equation

$$- \frac{dp}{dx} + \frac{d\tau}{dy} = \frac{\gamma v}{g_c} \frac{dv}{dx}$$

where $\frac{dp}{dx}$ is the pressure difference across the differential fluid element, between x and x + Δx as Δx $\longrightarrow$ 0; $\frac{d\tau}{dy}$ is the difference in shear stress across the element between y and y + Δy as Δy $\longrightarrow$ 0, and $\frac{\gamma v}{g_c} \frac{dv}{dx}$ is the change of momentum of the fluid in the element between x and x + Δx as Δx $\longrightarrow$ 0.

The shear force τ, in laminar flow, is proportional to the velocity gradient perpendicular to the flow direction; i.e.,

$$\tau = \mu \frac{dv}{dy} \quad .$$

In turbulent flow, however, the shear stress is not proportional to the velocity gradient; i.e.,

$$\tau = \frac{\gamma}{g_c} v'u' \quad .$$

Prandtl assumed that v' and u' are correlated to be of the same order of magnitude, thus both are proportional to $1 \cdot \frac{dv}{dy}$; and obtained

$$\tau = \rho l^2 \left(\frac{dv}{dy}\right)^2 = \left(\rho l^2 \frac{dv}{dy}\right) \frac{dv}{dy} = \epsilon \cdot \frac{dv}{dy}$$

where ε has the dimensions of a viscosity coefficient, but is not constant.
It depends on the turbulence intensity (v' and u'), indirectly.

It can be seen, in general, that if the adverse pressure gradient (pressure rise in flow direction caused by the area increase) is greater than the shear gradient, the fluid element loses momentum. Since the fluid near the wall is retarded by friction, it has much less momentum than does the rest of the stream. The adverse pressure gradient (being uniform across the channel), if sufficiently large, can cause the velocity near the wall to taken on negative values. Thus the forward flowing stream, in effect, separates from the surface.

It is also noted that if the velocity distribution is made "flat" such that large velocity gradients occur near the walls, the shear stress gradients at the walls will be larger; and the fluid can force its way against a larger adverse pressure gradient without separation. In flows in places other than in entrance regions, where the velocity is uniform to begin with, the "boundary layers"; i.e., layers of fluid moving more slowly than the main stream due to the action of the stationary walls through the viscosity (laminar or turbulent) of the fluid, have grown in thickness such that the flow is substantially nonuniform. Here, the velocity distribution can be made more uniform by mechanically increasing the turbulence level somewhat uniformly across the channel; thus increasing ε, which tends to equalize velocities in adjacent layers of fluid in the channel.

Experiments have been carried out in smooth, two-dimensional channels of rectangular cross section with varying angles of divergence between the two opposite walls which form the long sides of the rectangular cross section.[8]

The flow into the channels was essentially uniform. The velocity distributions obtained by Nikuradse in this study for established flow through channels of various divergence angles (negative angles refer to channels converging in the direction of flow) are shown in Figure 59. No backflow regions exist at either wall in Figure 59-a; separation of the forward flow is just beginning to take place at 10 degress in Figure 59-b; at 12 degrees in Figure 59-c, separation is more evident; and in Figure 59-d at 16 degrees, there is a tendency to switch from wall to wall, each configuration being maintained for some time. At still larger angles, the separation takes place at both walls. In Figure 59-a, it is also seen that as the divergence angle increases from 0 to 4 degrees the velocity tends to peak more sharply in the center of the channel; conversely, as the wall angle decreases from 0 degrees (converging channels), the flow profile is flattened out.

The maximum value of the area gradient obtained before separation of the forward flow took place was found to correspond to an included angle between the divergent walls of 8 to 9 degrees. Similar experiments done with "diffusers" of circular cross section also have roughly established the maximum included conical angle to be 8 to 10 degrees. In comparison, the included angle of a conical diffuser roughly equivalent to the divergent half of the "21-inch" ART core is ~30 degrees. From this, it is evident that separation of the forward flow from the walls of the core will occur by virtue of the core geometry alone.

That this separation of the forward flow from the walls is due to the adverse pressure gradient rather than to any other property is demonstrated
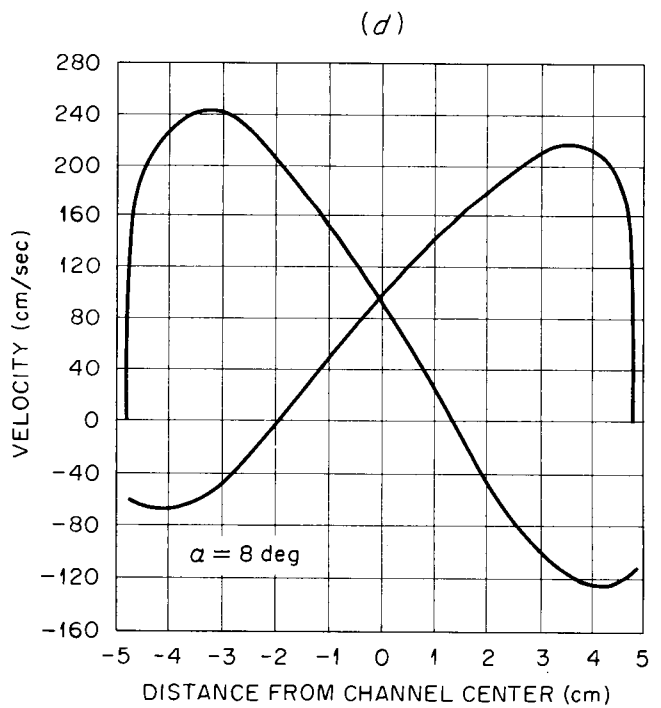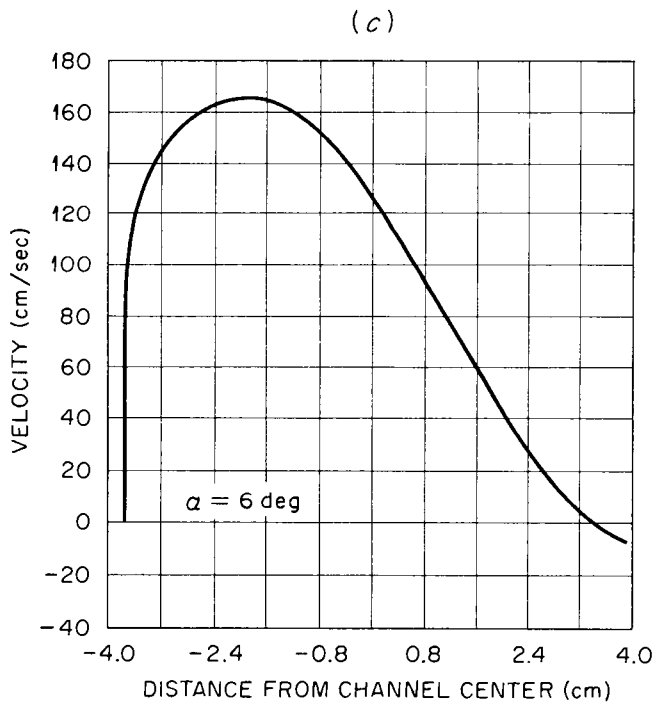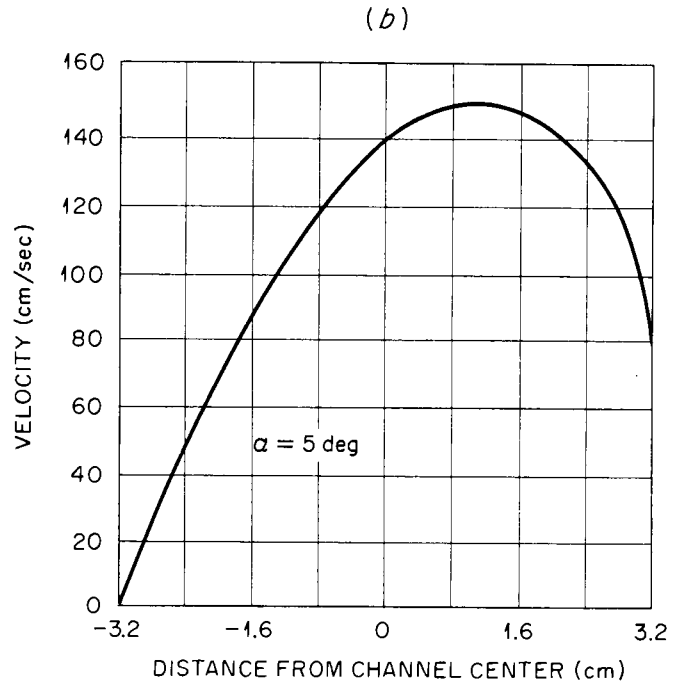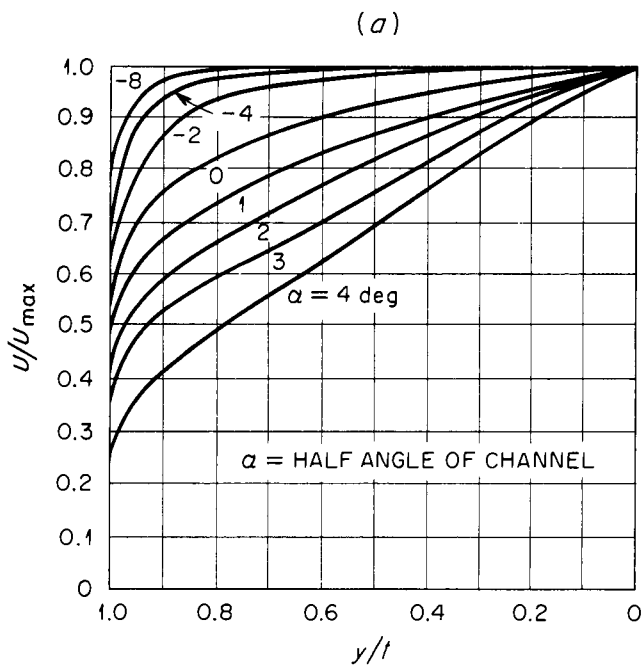
Fig. 59. Velocity Distributions in Convergent and Divergent Channels (Reference 8).

by an experiment conducted on flow through a pipe of rectangular cross section constructed such that the width of two opposite sides increased while the width of the other two sides decreased, the area remaining constant along the pipe. When fluid flows through such a pipe, there is no separation of flow from the walls[22].

The "21-inch" ART core also decreases in cross-sectional area from the midplane to the exit at the same rate as the area increases in the upper half such that the core is symmetrical about the "equator" or midplane. If separation of the flow takes place in the upper half of the core, it becomes impossible to describe quantitatively the flow distribution in the lower half of the core without resorting to experimental measurements. Therefore, no conclusions can be drawn from convergent channel data as to the flow distribution in the convergent half of the core.

Flow in Curved Channels. The effects of spiral flow through ART and other reflector-moderated reactor cores can be seen by studying the simpler case of flow in a curved channel. When curved flow is obtained, body forces due to the change in flow direction play a role in the turbulent mixing. Thus, to balance the centrifugal force, a pressure distribution is set up across the flow which decreases the turbulent momentum exchange near the convex inner wall and augments the momentum exchange near the concave outer wall.

Experiments have been conducted by Wattendorf[23] on the turbulent flow of air in a two-dimensional curved channel. The velocity distributions for fully-developed flow in curved channels of outer radius to width ratio of 5:1 and 10:1 are compared to fully-developed turbulent straight channel flow in Figure 60. It is seen that the differences between straight flow and curved flow
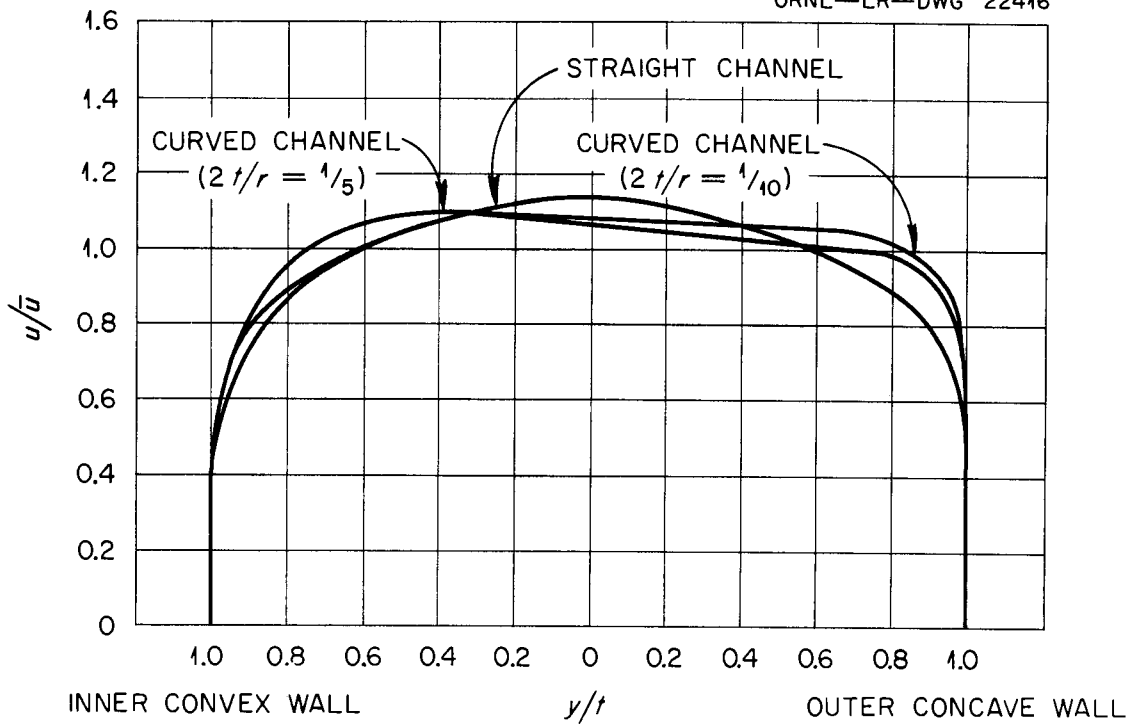
Fig. 60. Comparison of Fully-Developed Velocity Distri-
butions in Straight and Curved Channels. (Reference 23)
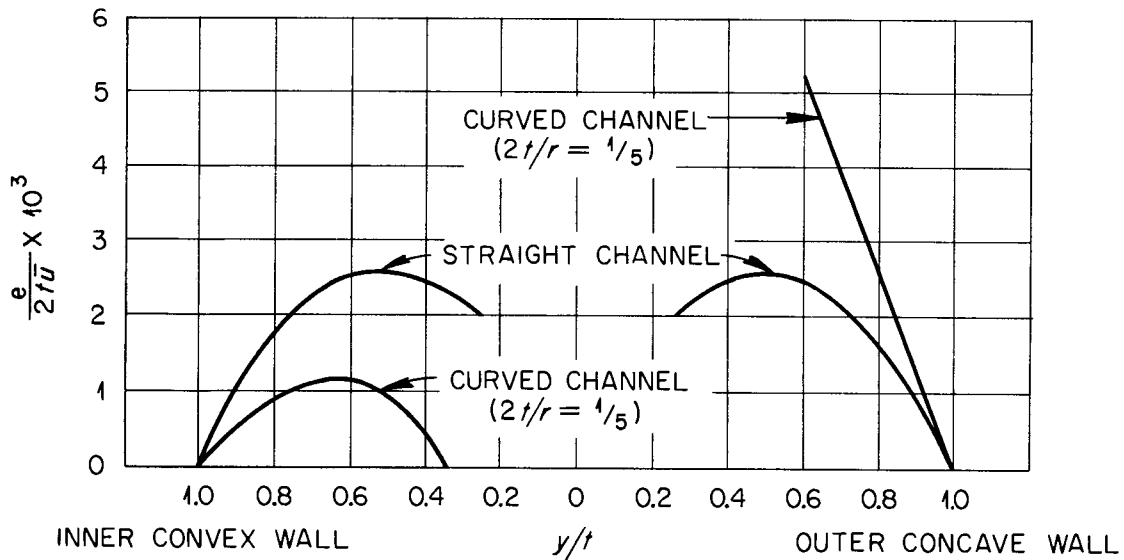
Fig. 61. Comparison of Eddy Diffusivities in Straight and
Curved Channels. (Reference 23)

become more pronounced as the ratio of channel radius of curvature to channel width is decreased.

The eddy diffusivity distribution for the 5:1 curved channel is compared with that of a straight channel in Figure 61. Two values for the eddy diffusivity can be obtained because of the difficulty in deciding whether

$$e = \frac{\frac{dv}{dr} + \frac{v}{r}}{\frac{\tau}{\rho}} \tag{29}$$

which arises from Prandtl's reasoning based on the exchange of angular momentum, or

$$e = \frac{\frac{dv}{dr} - \frac{v}{r}}{\frac{\tau}{\rho}} \tag{30}$$

which is the generalization of the equation for laminar flow where

$$\frac{\tau}{\rho} \propto \left(\frac{dv}{dr} - \frac{v}{r} \right)$$

is the valid equation.

Shear stress measurements by Wattendorf[23] give diffusivities lying between those given by the above expressions, being much closer to equation (30) than to equation (29). It is seen from Figure 61 that the eddy diffusivities are less than the straight channel diffusivities near the inner convex wall and greater, near the outer wall.

As the ratio of radius of curvature to channel width increases, the centrifugal forces decrease for a given flow rate. Thus for ratios above 5:1, the eddy diffusivities will fall somewhere between the straight-channel and the

5:1 curved-channel values. Since the curvature parameter is ~2:1, on the average, for rotational flow in the "21-inch" ART core, the differences between straight and curved flow will be even more pronounced than shown by Figure 61.

Flow Through Screens. Investigations by Baines and Peterson[24] of flow through screens show that the relative pressure loss through a screen is largely a function of the screen form (single and biplane lattices, round bars, perforated plates, woven-wire, etc.) and solidity ratio (the ratio of the obstructed area to the total area of the screen). Below a Reynolds modulus of 1,000 based on the wire diameter of the screen, the pressure loss is also a weak function of Reynolds modulus, increasing slightly as Reynolds modulus decreases. Figure 62 shows the relative pressure loss as a function of screen form and solidity ratio for $N_{Re, sc} > 1,000$.

Low solidity ratio screens tend to flatten any arbitrary velocity distribution, while screens above a solidity ratio of ~0.5 may magnify or create velocity profile asymmetries since small differences in hole sizes can cause very large differences in the pressure drops through various parts of the screen. Figure 63 shows the effects of screens of different solidity ratios on an arbitrary velocity profile.

The intensity of turbulence at distances greater than 10 wire diameters downstream from the screen is a function of wire size and distance from the screen. Therefore, a large diameter wire will create a larger velocity fluctuation (i.e., intensity of turbulence) at a given point downstream from the screen than a small wire. The fluctuation frequency will also be lower for the larger wire.
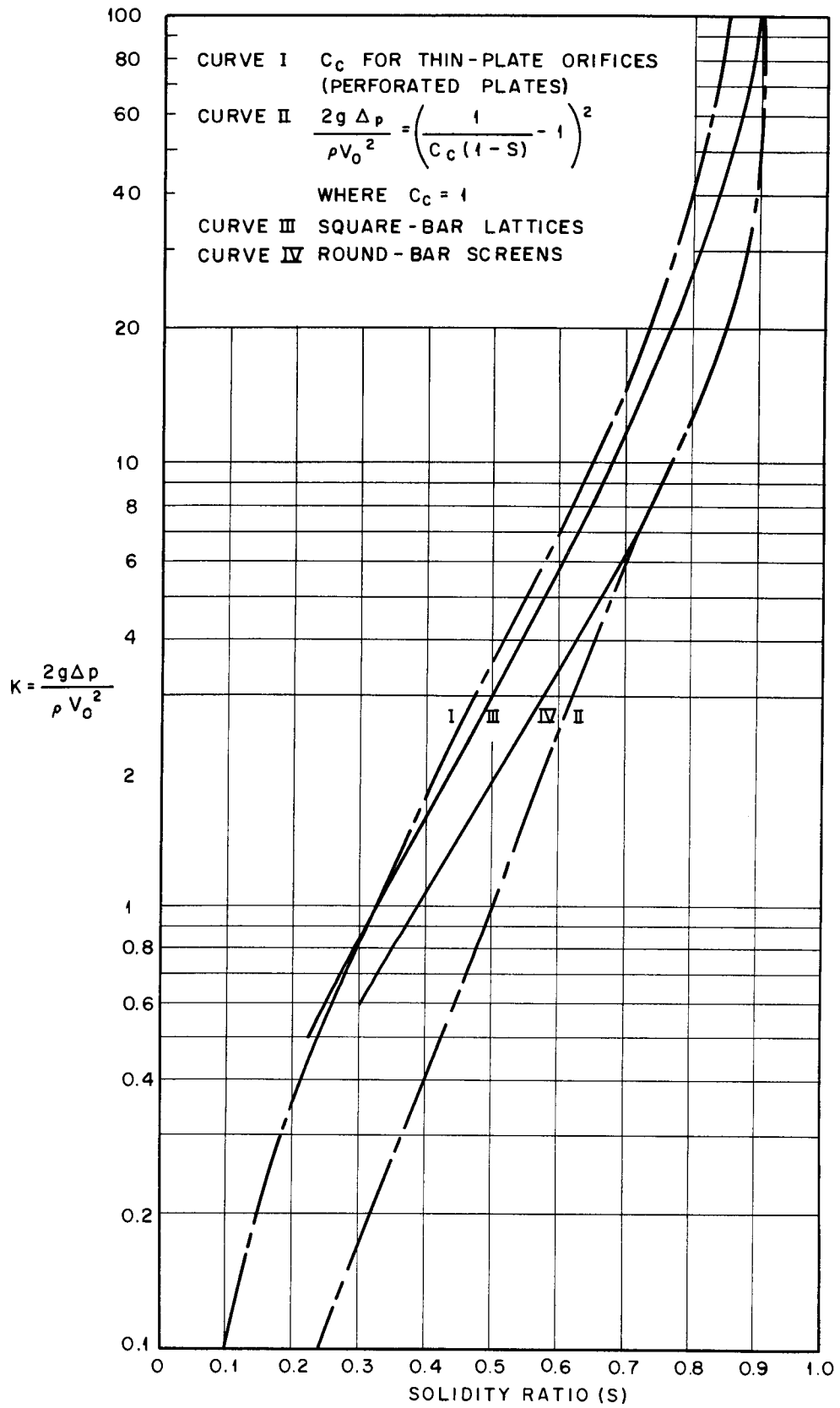
Fig. 62. Relative Pressure Loss as a Function of Screen Form and Solidity Ratio. (Reference 24)
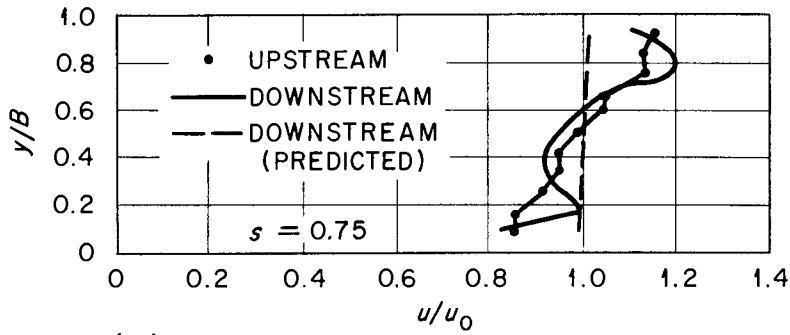
(a)
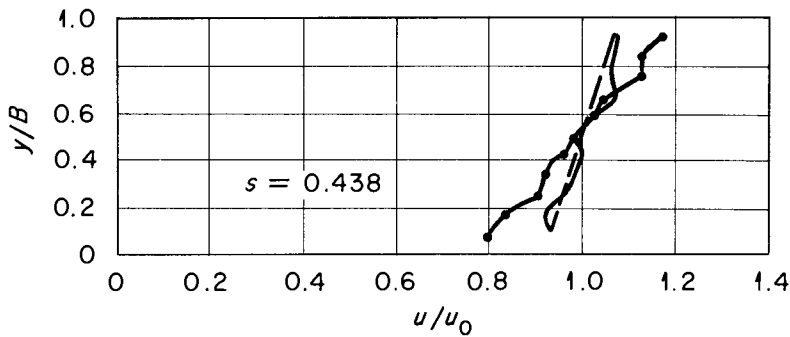
(b)
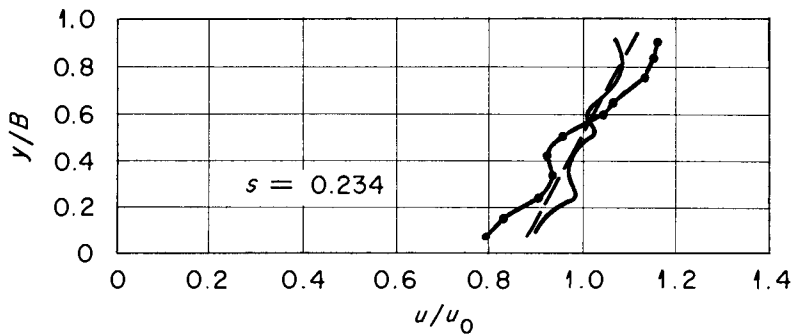
(c)   Effects of Different Solidity–Ratio Screens on
a One–Directional Velocity Variation.
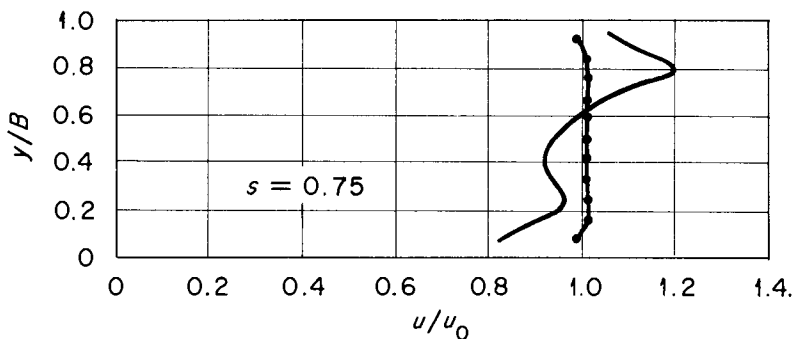
(d)   Effect of High Solidity–Ratio Screen on a
Uniform Velocity Distribution.

Fig. 63.   Effect of Screens of Different Solidity
Ratios on Arbitrary Velocity Distributions (Reference 24)

Screens in Diffusers. The equalization of velocity distribution and the turbulence promotion effects of screens have been shown to prevent separation or to restore unseparated flow in a diffuser.[25] Screens prevent separation by a combination of a number of factors: (1) increasing the velocity gradient at the wall, (2) increasing the turbulent mixing and, consequently, the shear stresses near the wall downstream from the screen, and (3) reducing the adverse pressure gradient along the wall. In studies by Schubauer and Spangenburg,[25] wide-angle diffusers were "filled" by a number of screens spaced along their length. In general, the number of screens required to "fill" the diffuser increased as their solidity ratios decreased. Figure 64 demonstrates the effect of a single woven-wire screen in a conical 30-deg included angle diffuser.
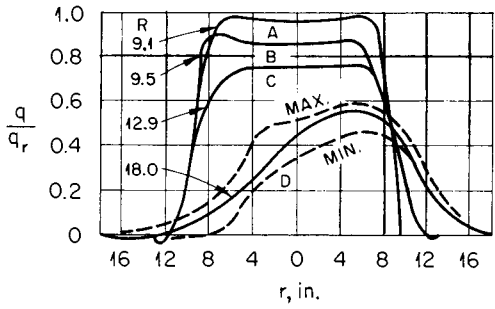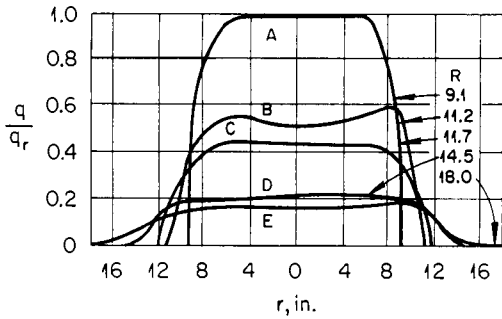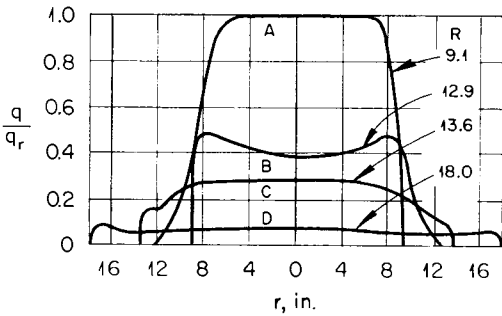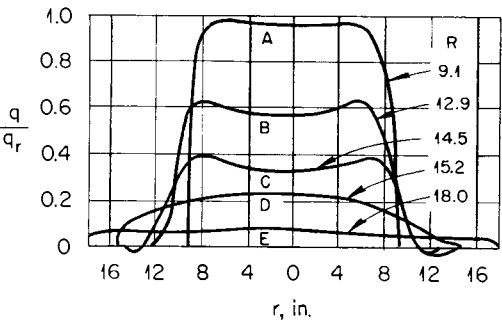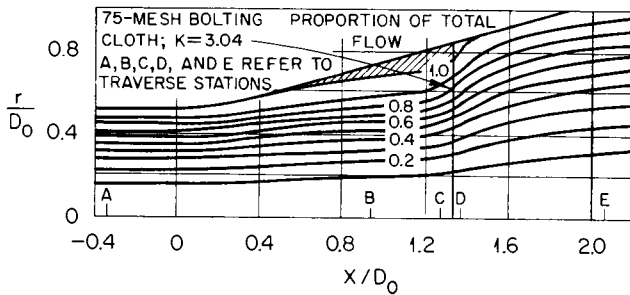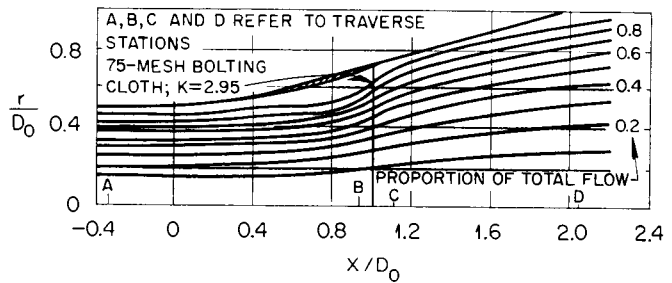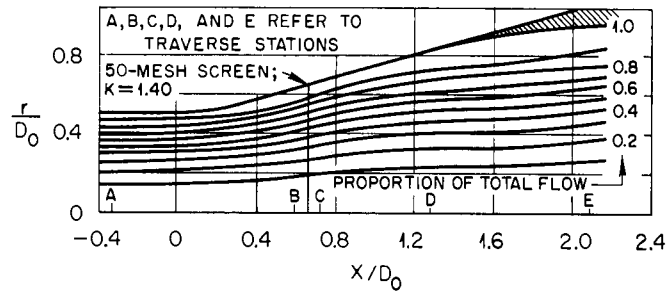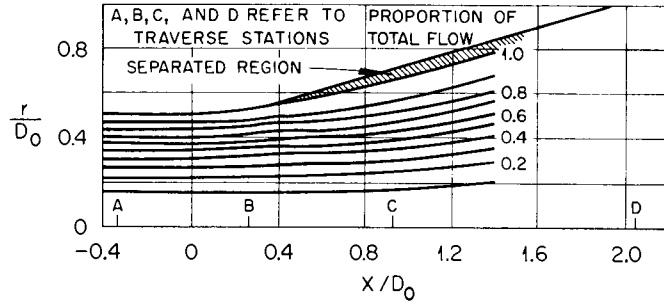
D_0 = DIAMETER OF EXIT PIPE

R = WALL RADIUS

q = DYNAMIC PRESSURE — $\dfrac{\rho V^2}{2g}$

x = DISTANCE FROM DIFFUSER ENTRANCE

K = RELATIVE PRESSURE LOSS OF SCREEN $\dfrac{2g\Delta p}{\rho V_0^{\,2}}$

r = RADIUS

q_r = REFERENCE DYNAMIC PRESSURE

Fig. 64. Effects of Screen Placed Across a Conical 30 deg. Included Angle Diffuser. (Reference 25)

Discussion of Results

Axial Flow Through ART Core Models. It was seen from the results of the experiments on the quarter-scale "18-inch" ART core model and the 10/44-scale "21-inch" ART core model with a radially and peripherally uniform axial inlet flow that axial flow was always accompanied by boundary-layer separation and reverse flow in the separation region. The separation region began at a plane 0.7 in. below the inlet plane of the "18-inch" model and covered the outer wall to a plane approximately three-fourths of the core length from the inlet. The separation region in the "21-inch" model was approximately the same size, beginning about 0.5 in. below the inlet plane.

It should be emphasized that the reverse flow in the separation region is violently unsteady, being composed of large vortex-like eddies and flow stagnations which were intermittently created and destroyed. These instabilities, in turn, created unsteadiness in the main part of the flow adjacent to the separation region. Because of the short length-to-diameter ratio of the cores (~ 10), this unsteadiness was carried practically undiminished out the exit of the core by the flow. The boundary-layer separation observed results from the large adverse pressure gradient (pressure rise in the direction of flow) caused by the velocity decrease as the fluid moves into the core. In turn, the velocity decrease is caused by the increase in the flow area through the inlet half of the core.

The comparatively lower fluid shear stress near the outer wall than the inner wall (common to flow through annular ducts) and the curvature of the channel away from the axis at the entrance probably caused the preferential

separation from the outer wall.

Axial Flow in Two Constant-Gap Core Models. The investigation of axial flow through two constant-gap core models of midplane-to-inlet area ratios of 1.443:1 and 2.133:1 revealed that boundary-layer separation occurred at the outer wall in both cases. For the 1.443:1 area ratio core, the separation region was very thin and the point of separation moved toward the inlet as the flow Reynolds modulus increased. At a core midplane Reynolds modulus of 20,000, the separation alternately occurred at the inner and outer walls; while at 30,000, separation occurred only at the outer wall. With the 2.133:1 area ratio core, the separation layer was thicker on the outer wall and began at a point closer to the inlet than in the previous core. Very little dependence of the separation point on the flow rate was noted.

These results verified the previous prediction that boundary-layer separation would occur in axial flow through cores of midplane-to-inlet area ratios greater than 1.41:1. If the 1.443:1 core had been constructed so that its rate of area increase was similar to the 1.41:1 area ratio core, instead of being zero at the inlet and midplane and reaching a maximum value half-way between, separation might have been avoided.

Rotational Flow Through ART Cores. It was found from the quarter-scale "18-inch" core model and 10/44-scale "21-inch" core model tests and from data obtained with the full-scale ART core model tests[6] that rotational flow was always accompanied by boundary-layer separation and violently unstable reverse flow in the separation region. The separation region in all cases began at the inlet on the inner wall and extended approximately three-fourths of the core length from the inlet.

The separation here was also caused by the same adverse pressure gradient as before. The preferential separation from the inner wall was probably caused by the comparatively lower fluid shear stress near the inner wall than near the outer wall (a phenomenon of flow in curved channels).

One-Pump Operation - ART Inlet Header. The same gross flow features described in the previous section were observed in one-pump simulated operation of the ART inlet header-"21-inch" 10/44-scale core model combination. In addition, a region of violent eddying was observed at the inner wall directly under the jet of fluid issuing from the tangential entrance. Peripheral flow asymmetries in the entrance half of the core were noted. The observations of the position of the eddying agreed roughly with the position of a large temperature asymmetry measured in the core volume-heat-source experiment run under the same conditions.[27]

In this study, the positions of the tangential inlets are reversed from those in the ART. However, this only results in a reversal of the flow structure without affecting any of the flow details.

Flow Through Cores with Turbulence Promotion. Three methods of turbulence promotion were tried in the "18-inch" and "21-inch" ART core models. This approach to the problem of improving the core flows was suggested by the elementary considerations presented previously. If the amount of turbulent momentum interchange in the flow can be increased between the low velocity boundary layers and the high velocity fluid in the midstream, separation could be eliminated. In terms of fluid shear stress, this would mean that the turbulent shear stress gradient near the wall would be increased and thus, the forces on a fluid element near the wall would tend to move the element forward with the flow.

It was found in the experiments that the scale of the promoted turbulence (a definition of the average size of the eddies) was also important. For example, twelve 16-mesh woven-wire screens placed in the entrance pipe of the "18-inch" core model (Figures 32 and 33) added sufficient turbulence to the flow to move the point of separation farther downstream from the core inlet than when no screens were present. A striking calming effect was also noted. In axial flow through the "18-inch" core model without screens, the flow in the separation region was very unsteady; while with the screens, the reverse flow was much more steady and streamline in character.

When turning vanes were added to give a rotational component to the flow, no differences were noticed either in the velocity profiles or in the general character of the flow for the cases of screens located before the turning vanes and no screens. It should be pointed out that the turning vanes add turbulence of a larger scale to the flow.

Contrasted with this was the flow obtained using vortex generators of the aerofoil type attached to the outer wall at the inlet (see Figures 34 through 38). Though the separation region on the outer wall was not eliminated in these cases, peripheral flow asymmetries and variable horizontal velocities of low frequency were noted in the separation region. Since these flow features had not been observed in axial flow through the "18-inch" core model, they were probably the result of the large-scale vortices generated by the aerofoils.

The flow obtained in the "18-inch" and "21-inch" core models with several vortex generators (see Figures 14 and 39 through 41) of various turning-vane angle settings was also variable in nature, the "21-inch" core exhibiting flow

variability to a much greater degree than the "18-inch" core model. Eddying

and periods of flow stagnation were visible at intervals in both cores.

It is seen from these experiments that the induced turbulence must be of

a small scale (corresponding to a high-frequency spectrum of velocity fluctua-

tions) and of high intensity (large ratio of fluctuating velocity component to

the mean velocity). If the scale of the turbulence is large enough, the fre-

quencies of the velocity fluctuations are low enough to be called variable

flow. Since turbulent flow is unstable flow, the question arises as to where

one draws the line between turbulent flow and variable flow. In connection

with high-power, high-temperature circulating-fuel reactors such as the ART,

the answer is provided by the restriction that the turbulent eddies must be of

a small enough scale to insure that the associated wall-temperature fluctua-

tions are of sufficiently high frequency and small magnitude to be considered

negligible. This is the safest assumption to make, since the effect of low-

frequency thermal cycling on the wall material is not yet fully understood.

For turbulent flow through a parallel-plates system[28] where the wall-

temperature fluctuations are negligible from the low frequency, large magni-

tude thermal cycling standpoint, the ratio of the characteristic scale of

turbulence (perpendicular to the flow) to the channel width is of the order

of 0.1, while the ratio of the scale of turbulence (perpendicular to the flow)

to the wire diameter of a turbulence-producing screen[24] is of the order of 1,

on the average. Therefore, in the ART model core channel of average width

$\sim$ 0.8 in. with screens of wire diameter $\sim$0.02 in. (for the 16-mesh screens),

the scale of turbulence produced by the screens is about one-fourth of the

scale of turbulence in the flow through a parallel-plates system of equal

channel width. The ratio of the root-mean-square lateral velocity fluctuations to the mean velocity of the flow is also much larger behind a screen (0.2 - 0.5 maximum) than the corresponding values for turbulent flow in a channel (0.03 - 0.04 maximum).

The magnitude of random turbulent velocity fluctuations established a short distance behind a screen decay at a rate predicted by Frenkiel's decay law:

$$\frac{u'}{v} = 1.12 \left(\frac{x_s}{d}\right)^{-5/7} \quad \text{for} \quad \frac{x_s}{M} > 2 \quad .$$

Since the scale of the turbulence is proportional to the screen wire diameter, it is seen that small-scale turbulence decays more quickly than large-scale turbulence.

From these considerations, it is evident that if the scale of the promoted turbulence is small - as it must be to prevent large temperature excursions - the turbulence dies out quickly behind the turbulence promoting device. This was indicated clearly by the striking calming effect of the screens placed in the inlet pipe on the flow through the "18-inch" core model.

Evidence of the effect of promoted turbulence of a large scale on the temperature structure was seen in the ART core volume-heat-source experiment[27] with a half-scale model of the guide vane and baffle plate arrangement shown in Figure 65.[29] While the boundary-layer separation regions at the core walls were eliminated by the action of the baffle plate on the flow, wakes consisting of vortices shed from the edges of the baffle plate and the trailing edges of the vanes created a low-frequency variable flow in the core.

Figures 66 through 68[30] illustrate the type of flow occurring in wakes and separation regions. Figure 66 is a photograph of flow in a separation region (in this case, behind a stalled aerofoil), Figure 67 shows the wake behind a cylinder (representative of a screen wire), and Figure 68 pictures the flow around a flat plate held perpendicular to the stream.

Flow Through Cores Packed with Screens. Due to the high rate of turbulence decay in the flow downstream from a screen and the unsteadiness induced in the flow by large-scale turbulence promoters, it became apparent that turbulence promotion at the entrance plane of the core would not be satisfactory from the standpoints of flow separation elimination and flow stabilization. The placement of screens in the core seemed to be the logical answer to the decay of the promoted turbulence.

The work of Schubauer and Spangenburg[25] noted earlier showed that when screens of low-solidity ratio (< 0.5) are placed across a wide-angle diffuser, not only was turbulence promoted by the screens; but the velocity distribution across the flow channel was made more uniform near the screen. If a sufficient number of screens were placed across the diffuser at different locations along the axis, boundary-layer separation was completely eliminated and the flow was made more steady.

The velocity redistribution effects which resulted from the screens placed across the diffuser can be explained by first considering a plane jet impinging against a solid wall perpendicular to the jet axis. As the wall is approached, the streamlines of the jet bend away from the axis and finally become parallel to the wall, the streamlines describing a family of hyperbolic curves.

Fig. 65. GS—2 Guide Vanes and Baffle Plate Mounted on Inner Wall of the 21-Inch ART Core at the Inlet. (Reference 29)

Fig. 66. Visualization of Flow in a Separation Region Behind an Aerofoil. (Reference 30)
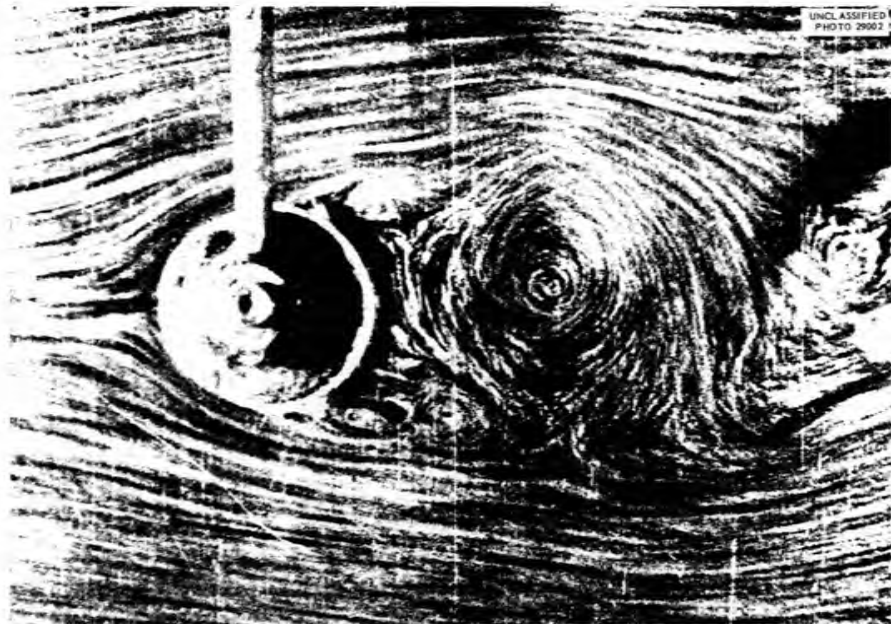

Fig. 67. Visualization of the Flow in the Wake of a Cylinder. (Reference 30)
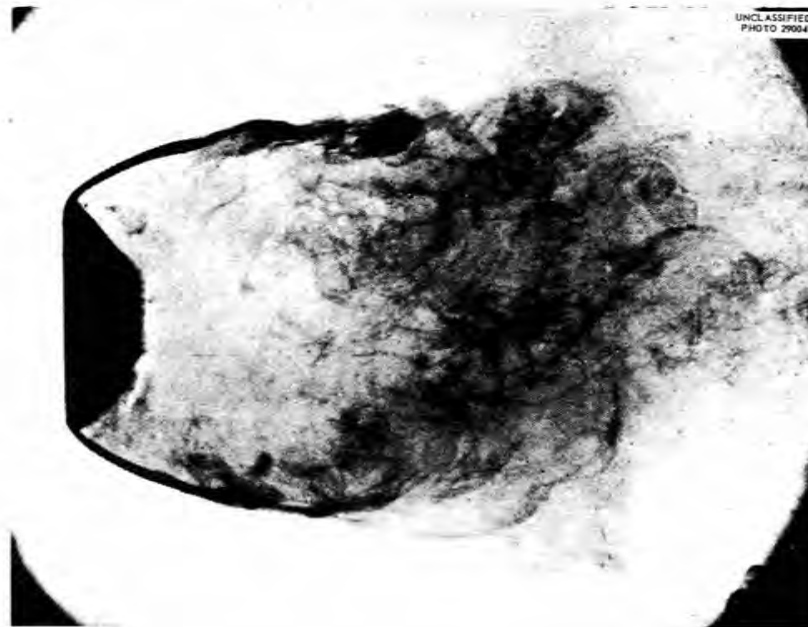
Fig. 68. Visualization of the Wake Behind a Flat Plate Held Perpendicular to the Stream. (Reference 30)

Centrifugal pressure gradients accompanying the curving flow create a pressure distribution which increases toward the jet axis and toward the wall. According to Bernoulli's law of energy conservation, the fluid velocities decrease as the pressure increases. If the wall is porous, some of the fluid passes through the wall while the rest is turned as before. The extent to which the fluid is turned decreases with increasing porosity; or, in terms of the solidity ratio (the opposite of porosity), the stream passes through the wall with more and more of its original concentration as the solidity ratio decreases.

Thus, a screen placed across a diffuser forces the high kinetic energy fluid away from the axis of the stream, where it tends to concentrate, toward the walls; and a flattening of the velocity profile occurs in the vicinity of the screen. The degree of flattening depends on the relative pressure loss of the screen, which is a function of the solidity ratio, and the form of the screen (square bars, round bars, single or biplane lattices, woven-wire screens, perforated plates, etc.). The more uniform velocity distribution plus the turbulence generated by the screen help to move the fluid near the wall behind the screen in the direction of flow, thus preventing separation of the flow.

The "filling" effect of a screen in a diffuser evidently exists only in the vicinity of the screen, the extent of the vicinity depending upon the rate of expansion of the diffuser (large rate of expansion corresponds to a small extent of the vicinity) and the relative pressure loss (large pressure loss corresponding to large extent of influence).

It was found that five screens arranged as given by combination No. 5 of Table 4 prevented separation and gave a fairly uniform flow in the ART core.

In the inlet area expansion of the straight annular core, six 0.385 solidity ratio screens gave a fairly uniform flow. It is seen that approximately the same number and type of screens were packed into the wide-angle divergence of the straight core as were spread over the upper half of the ART core to prevent separation. This bears out the considerations presented above. In addition, when a 0.510 solidity ratio screen replaced the farthest downstream 0.385 solidity ratio screen (combination No. 4 of Table 4), the resulting velocity distribution following the screen was more uniform. (See Figure 47.) This is again in accord with the above discussion.

In the straight core, the boundary-layer separation region seen in Figures 51 and 52 is a result of the abrupt curvature of the channel near the exit. The pressure must rise along the outer wall and fall along the inner wall as the curve is approached so that a radial pressure gradient is obtained to balance the centrifugal force generated by the curving flow. The adverse pressure gradient, or pressure rise in the direction of flow, along the outer wall was apparently too large; and boundary-layer separation was the result.

If the separation can be eliminated by increasing the radius of curvature of the flow path, or by eliminating entirely the flow area contraction at the exit, this core model may possess a number of advantages over the present ART core with screens. These are as follows:

(a) The screens, being in a lower neutron flux region, would absorb fewer neutrons, thus having less effect on the reactor criticality.

(b) The screens are concentrated in the coolest part of the reactor, easing the problem of screen corrosion.

(c) The volume of the core is larger (3.89 ft^3 compared to 3.23 ft^3) reducing somewhat the average power density.

(d) The fuel channel width is smaller (a maximum of 4 in. compared to 5-1/8 in.), causing a reduction in the channel wall-to-centerline power density ratio due to reduced self-shielding.

The last two considerations would reduce the uncooled wall to mixed-mean temperature differences in the fuel. A problem may exist in adequately cooling the screen packing under zero fuel flow conditions and at times when the fuel is dumped from the reactor. Investigations are indicated to specifically ascertain the extent of this problem.

A perforated-plate type of screen would have the same effect as the woven-wire screens on the flow through the cores, if its relative pressure drop and web thickness were the same as the relative pressure drop and wire diameter of a woven-wire screen. The solidity ratio of this "equivalent" perforated plate can be found by referring to Figure 62, find the pressure drop associated with a woven-wire screen of a particular solidity ratio on Curve IV; and then, using that pressure drop, obtain the perforated-plate solidity ratio from Curve I. For structural and fabrication reasons, the perforated-plate type of screen may be more desirable than the woven-wire screens used in the experiments.

Velocity Fluctuation Studies. The fluctuation "frequencies" were obtained

from the movies taken in the dye filament studies[21] with the full-scale model of the ART core. The analysis was accomplished by counting the number of times the angular deflection curve crossed the average angle curve and dividing by the elapsed time (about 1.5 sec). It will be noticed that the fluctuations have no obserable periodicity; they are completely random. No conclusions could be drawn from the magnitude of the fluctuations, since the distance of the dye filament from the wall was not exactly known; even though the angle measurements were made at the point of injection and the dye filament was known to be close to the wall at that point. The components of the velocity fluctuations influencing the dye filament were also unknown.

However, the frequencies were taken to be the frequency of changes of conditions at the walls, and the fundamental mode of the frequencies was in general agreement with the fundamental mode of the temperature fluctuations in the volume-heat-source experiments[27] after allowance for the difference in average velocities.

It is felt that, given the same conditions, the fluctuation frequencies are proportional to the flow rate. This was qualitatively ascertained by comparing movies of dye filament fluctuations for two different flow rates in the same core.

Average Fluid Velocities in the Full-Scale "21-inch" ART Core. It is observed in Figure 56 that the data are in fair agreement with the predicted average velocities except for the high-velocity rotational flow case. Here, the rotational velocities fall below the prediction. Since the axial average velocity components were in fair agreement with predicted values and since the exit

rotational velocity profiles at two peripheral stations 90 deg apart prac-
tically coincided, it was concluded that the high frictional drag had created
a noticeable "vortex decay", or slowing down of the rotation, as the fluid
passed through the core. Frictional effects were not considered in the pre-
diction. This was further substantiated by the increasing difference between
the predicted and experimental values as the core exit is approached.

A backflow occurred near the exit on the inner wall in the high-velocity
flow which also indicated the vortex decay, the backflow being induced by the
adverse pressure gradient created by the decaying rotational component of
velocity.

It was observed that a large discrepancy existed between the predicted
and experimental values for the average rotational flow component in the en-
trance half of the core for the high- and medium-velocity swirl cases. This
was noticed because the angular momentum of the flow in this region increased
as the equator was approached, which is impossible without an external force
acting upon the fluid.

The conclusion was reached that the data are erroneous in the upper half
of the core for these two cases. This conclusion is further supported by the
fact that due to separation of the flow, a large amount of cross-flow exists
in the upper half of the core. This would cause errors in the data which were
obtained by impact "claw" probes. Since the probes could not be rotated to
face the cross-flow, they would tend to read low; and since the impact tube
and "yaw" tube arrangement was not calibrated in cross-flow, an erroneous
value for the flow angle could also result.

Further support for this conclusion comes from the vaned-flow case in Figure 56. Here, separation and the accompanying cross-flow were probably eliminated, and the flow was primarily in the plane of rotation of the "claw" probe. It is seen that no such discrepancy exists in the rotational component and that the trend of what little data there is follows the predicted rotational flow curve.

Pressure Distributions in the "21-inch" ART Core. The vortex decay in the high-velocity rotational flow also explained the difference between the predicted and actual pressure differential between the inner and outer walls for that case. The prediction was based on the predicted velocity distribution. In the case of the medium-velocity rotational flow, however, the prediction of average velocities agreed well with the data; so that the prediction of the pressure distribution on the inner wall using the outer wall pressure data and the calculated difference is probably sound.

The pressure distributions shown in Figure 58 for the three cases (high- and medium-velocity rotational flow, and axial flow) showed that the total pressure loss was large for the first case (about 45 psi) and relatively small for the other two cases (about 7 psi). In the case of the axial-flow system, most of the pressure loss was caused by improperly designed turning vanes and a perforated plate placed at the core entrance.

Pressure Distributions in ART Heads. Since the pressure loss through the core is small, additional disturbances can be caused by pressure unbalances in the core entrance header. For example, the pressure loss was 2 lb/in.^{2} at a 1200 gpm fuel flow rate for the screen-packed core shown in combination No. 5

of Table 4 and less than 2 psi without screens (see Figure 58).

The calculations showed that the header shown in Figure 20(c) gave the smallest pressure unbalance, though even this unbalance was half the core pressure loss with screen packing. In an open core, these unbalances would cause a considerable amount of peripheral flow, adding to the unsteadiness already present. Since the velocity distribution in the exit half was evidently nearly uniform with periphery (see Figure 56), the cross-flow probably took place in the inlet half of the core. The actual existence of such cross-flow was masked by the low accuracy of the data in that region and the violently eddying separation region. With the large pressure differences found, the assumption of uniform fluid withdrawal from the header is no longer a good one; and the asymmetrical withdrawal of fluid will serve to lower the pressure rise somewhat.

The calculations do point up two considerations, however. One is that the header pressure unbalances, for the configurations presented, are primarily due to the average velocity level in the header. Therefore, header fluid velocities should be as low as practical. This is afforded by the header in Figure 20(c). The core pressure loss should be as large as practical to keep the relative importance of the header pressure unbalances small. This was effected by the screen packing scheme, which also eliminates separation and destroys the thermal boundary layers in the core.

CONCLUSIONS

The following conclusions were reached as a result of this series of experiments:

(a) Axial flow through the cores with sufficiently large cross-sectional area expansion rates considered here will always be accompanied by a separation of the forward flow from a point on the outer wall near the inlet and violently unsteady reverse flow in the "separated" region. This separation at the outer wall is due to the large adverse pressure gradient resulting from the large area expansion rate, the lower fluid shear stress at the outer wall than at the inner wall (common to flow through annular ducts), and the curvature of the channel. The flow into the entrance of the core models was always uniform radially and circumferentially, having passed through a calming length of 40 diameters of straight pipe into an annular "nozzle" which was mounted on the core entrance.

(b) Rotational, or spiral, flow through the same cores is always accompanied by separation of the forward flow from a point on the inner wall near the inlet and unsteady reverse flow in the separated region with a velocity component in the direction of the rotation. The separation in this case is caused by the same adverse pressure gradient and the lower fluid shear stress at the inner wall relative to the outer wall (a phenomenon of flow in curved channels). Again, the flow at the core entrance was uniform radially and circumferentially, having passed through 40 diameters of straight pipe into an

annular "nozzle" which preceded the turning-vane section which produced the rotational flow.

(c) In rotational flow, the turbulent interchange of momentum and the eddy conductivity are diminished at the inner wall due to the centrifugal force field set up by the fluid motion; and, therefore, increased temperatures due to volume heat generation can be expected at the inner wall over the temperatures obtained in straight flow at the same rate in an equivalent channel.

(d) If the spiral velocities are very high, frictional forces become of such magnitude that a decay of the spiral velocities becomes noticeable and a backflow due to spiral vortex decay will begin. This was noticed in the high spiral velocity case studied by Whitman, Stelzman, and Furgerson. Backflow occurred on the inner wall at the exit plane.

(e) Turbulence promotion within the cores has been shown to overcome the effects of adverse pressure gradients, but the promoters must be such that they do not introduce unsteady flow; i.e., the scale of the promoted turbulence must be very small. Woven-wire screens and perforated-plate screens of low solidity and small wire diameter (or web thickness) packed into the divergent part of the core flow channels are of such nature. Turbulence promoters such as vortex generators or large obstructions placed in the core entrance cause unsteady flow although they seem to eliminate the separation and the associated backflows.

(f) Straight annular cores and cores of sufficiently low expansion rates can be constructed to give a steady, unseparated flow with axial flow. Calculations show that the maximum midplane-to-inlet area ratio that

can be achieved with axial flow through a bare core is 1.33:1 within

an 18-in. length of a 21-in.-OD core with the same midplane area as

the "21-inch" ART core.

(g) Calculations have shown that a pressure unbalance (4 lb/in.^2) due to

momentum transfer exists in the header which is of the same order as

the friction losses in the core. This pressure discrepancy is in the

form of a rise in pressure as the fluid traverses the length of the

header from the inlet duct. The unbalance, plus any unsteadiness trans-

mitted to the flow by the fuel pumps, will also create peripheral flow

asymmetries and unsteady core flow.

The calculations also point up two considerations. One is that

the header pressure unbalances are primarily due to the average fluid

velocity level in the headers considered. Thus, header fluid veloc-

ities should be kept as low as practicable. The core pressure loss

should also be as large as practical to keep the relative importance

of the header unbalances small.

(h) Since screen packing in the core has been shown to eliminate the un-

steady flow, which is an inherent characteristic of the core shape, it

is proposed that this system be used in the core. An additional advan-

tage accrues from the use of the screens in an increase in core pres-

sure loss and the related velocity profile flattening. The peripheral

asymmetry due to pressure unbalances in the header will then be much

less than exists without the screens. It is felt that perforated-plate

screens with the same relative pressure loss and mesh size as the wire

screens tested would be more advantageous from the structural and fabrication standpoint than the wire screens.

The heat-transfer characteristics of the screens are in the process of being investigated to determine whether any problems exist in this regard.

(i) A header system has been designed which may afford smaller pressure unbalances than the present header system and, being used in conjunction with the screen-packed core, may allow single-pump operation without large peripheral flow asymmetries. Further experimental work is in process to establish the validity of this conclusion and conclusions (g) and (h).

APPENDIX A

VELOCITY MEASUREMENT AND FLOW VISUALIZATION TECHNIQUE

Stroboscopic Particle Photography

The measurement of velocities in the transparent "18-inch" ART core model was done by stroboscopic photography of the light scattered from a collimated plane of light parallel to the flow direction by tobacco-seed particles suspended in the water flowing through the core.[11]

The distance between two images of the same particle divided by the measured time between the flashes of light which produced the images gave the average velocity of the particle between the two positions. The particle velocity was very nearly the velocity of the water, since the density of the tobacco-seed particles was close to that of water, and the particle size was small.

Since the curved surfaces of the "18-inch" ART core model cause an appreciable apparent distortion of the relative positions within the core model, a 1/16-in. thick Plexiglas sheet scribed with co-ordinate lines was first placed inside so that it lay within the plane of the light beam.

This grid was supported by a second island which was split along its centerline and fitted with short pins to position a two-piece grid. The other half of the island was cut to fit the first with the grid halves in place.

The plastic sheet was then edge-lit from two edges in a darkened room, the lines scattering light from the interior of the plastic and identifying their position; photographed by a 4 x 5-in. Grover monorail camera equipped with a Kodak Ektar f4.7 lens facing at approximately right angles to the plane

of the light beam; and removed. The resulting photograph is shown in Figure 69.

The camera was unmoved until after the particle photographs were taken so that the two negatives could be superimposed and the actual co-ordinates of the particles determined by reference to the similarly distorted grid system.

The flash-light sources were General Electric FT-220 electronic flash-tubes operated by three 35-μf condensers in parallel and charged to about 2,360 v. A continuous light source was used so that the two images of each particle would be connected by a track, for identification on the film. This light was a General Electric H1000-B19, 1000-w mercury arc light. The light from all the sources was collimated by a pair of slits; the one farthest from the sources being common to all three sources, the sources being arranged to be in the same vertical plane.

Figure 70 is a photograph of the test section with the split island and grid in place, the camera in the foreground, and the collimator with the mercury vapor light operating. The side plate of the collimator has been removed to reveal the three slits in addition to the common one. One of the flash-tubes is in the cylindrical housing seen behind the upper collimator slit.

The flashtubes were flashed and the time interval was measured by an electronic instrument consisting of an audio oscillator whose output frequency was manually controlled. A signal was sent from the oscillator to a conventional scaler whose output was one voltage pulse for 64 input pulses. The output of the scaler was further scaled down by two more stages in a special
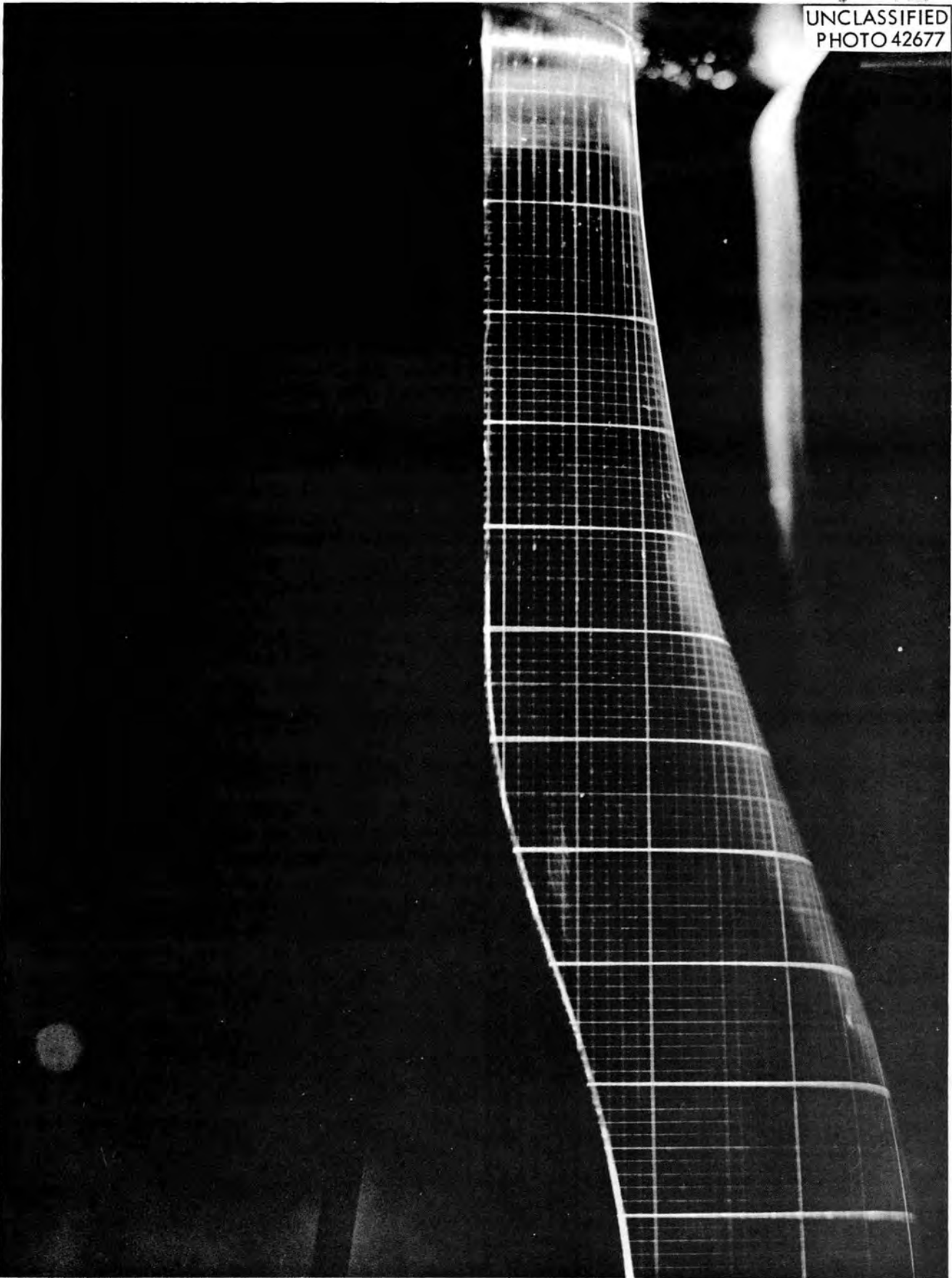
Fig. 69. Data Photograph of Cartesian Grid in 18-Inch ART Core Model.
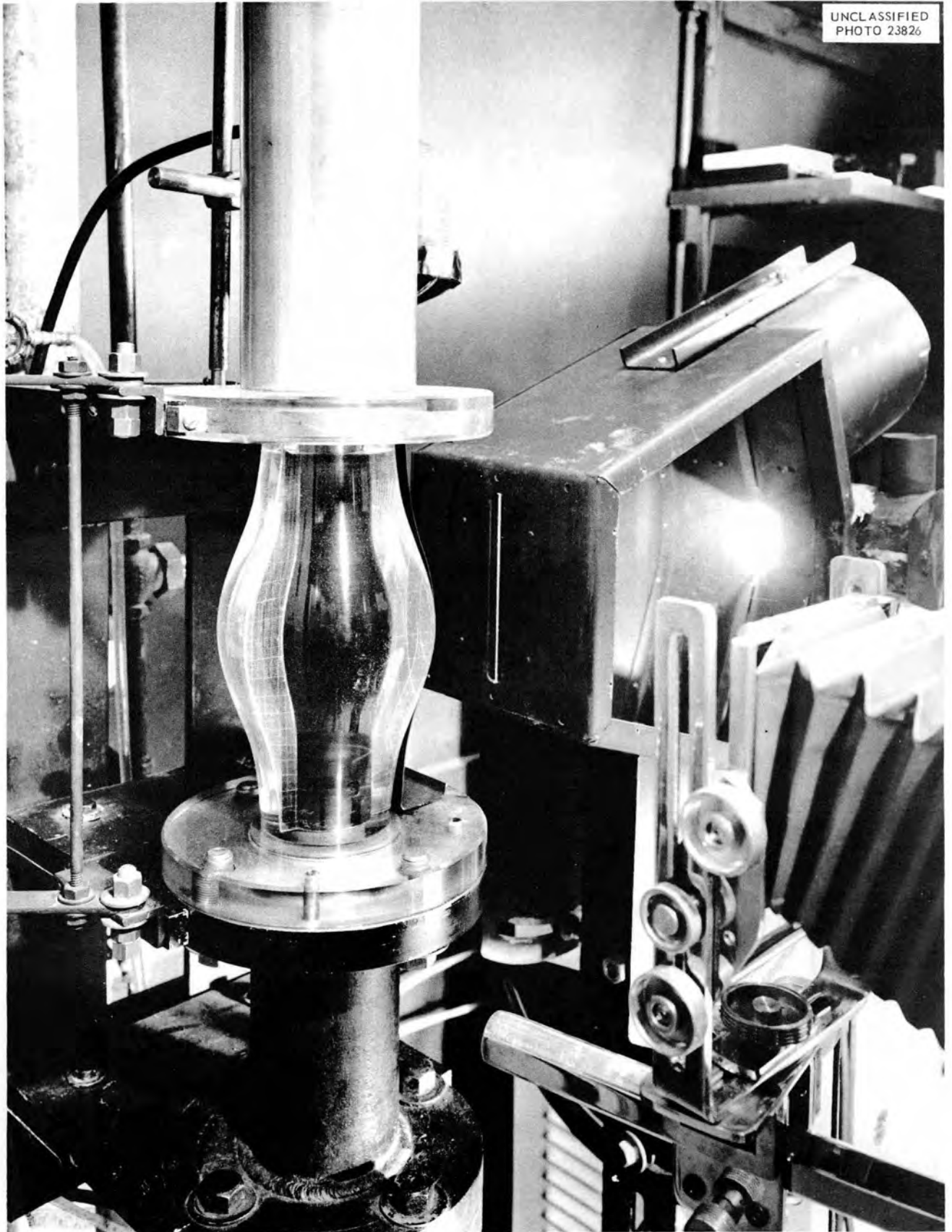
Fig. 70. Light Collimator, Test Section, and Camera Showing Relative Location. The continuous light source is operating.

"trigger unit." This unit then amplified and delivered the pulse to the first flashtube power supply which flashed its light. The second pulse, received 256 cycles from the audio oscillator later, fired the second flashtube. The cycle was not repeated until the trigger unit was reset.

When the flashtubes flashed, another signal was sent to a Hewlett-Packard Electronic Counter which was set so that the first pulse started it and the second pulse stopped it. The time between pulses was displayed on the counter front.

Figure 71 shows a photograph of the electronic instrument.

Kodak Tri-X Panchromatic and Royal Pan film were used in the camera for the recording of the light scattered by the tobacco seeds. Developing was done with Eastman DK-19a developer. However, it was found after the experiments were finished that DK-19a increased grain size and fogginess in the film, and that DK-60a was recommended.

A system of plane mirrors and a focusing lens and shutter were used to record the time displayed on the counter face on the film in the camera.

An over-all view of the apparatus is shown in Figure 72. The core model is all but hidden by the collimator.

To get particle photographs, the core model was then reassembled with the original island, the connecting inlet piping put in place, and clear water with suspended tobacco seeds was pumped through the core at a desired flow rate and temperature. The tracking light in the collimator and the automatic flashtube firing and timing equipment were turned on. The procedure was then to open the camera shutter, trigger the automatic stroboscopic equipment, and close the shutter. The time displayed on the counter face was then photographed on
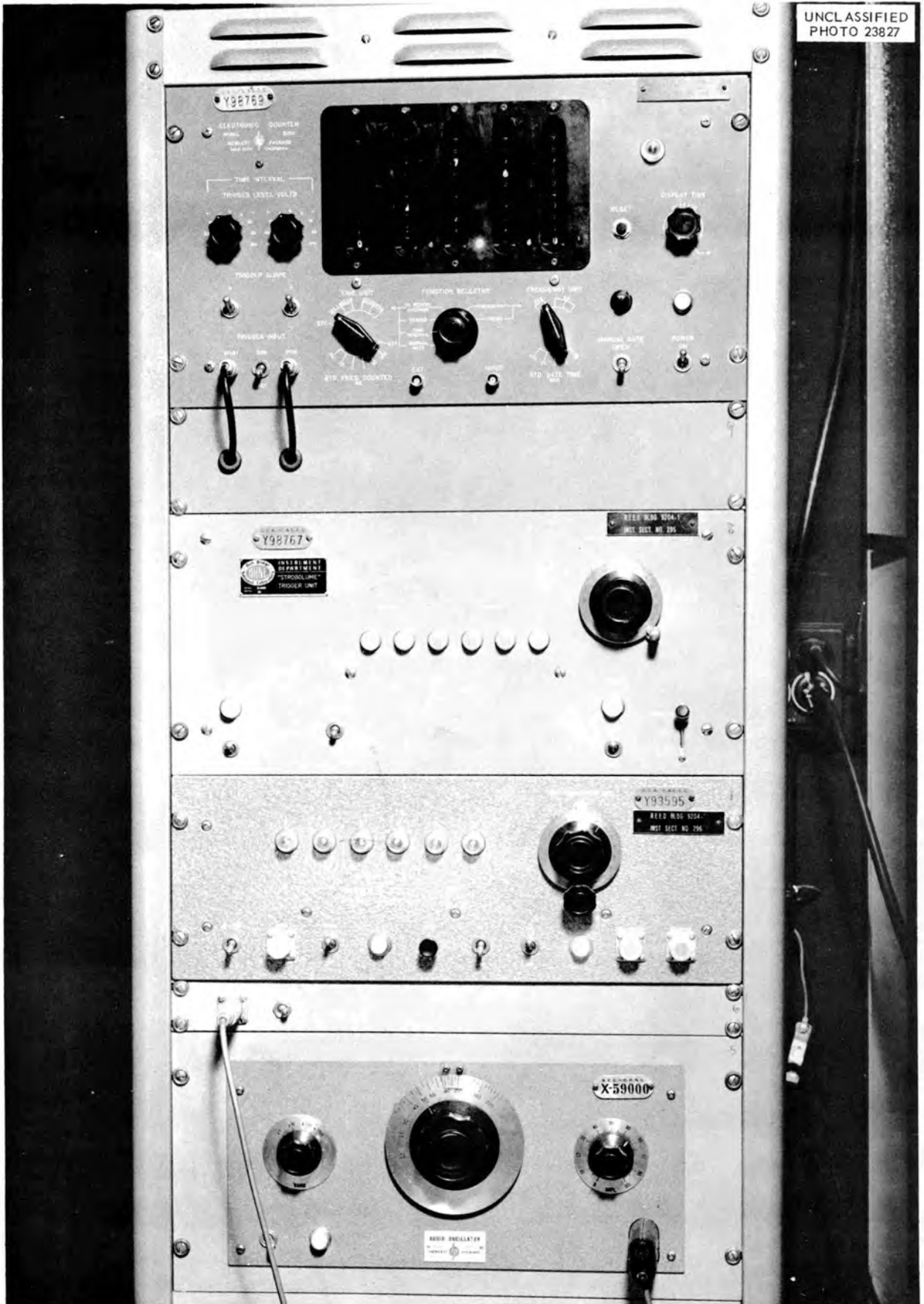
Fig. 71. Electronic Flashtube Firing and Elapsed Time Measuring Equipment.
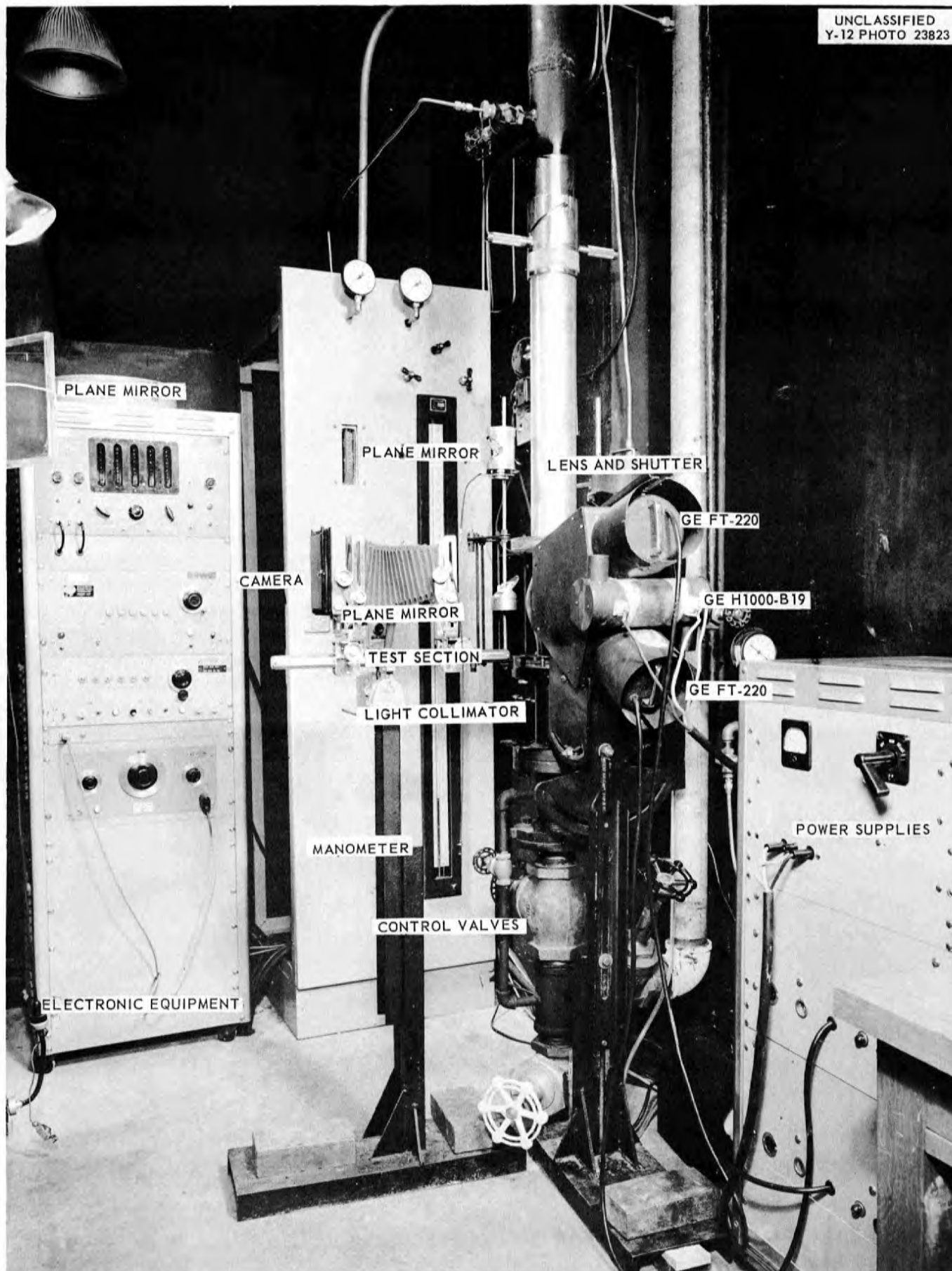
Fig. 72. Over-All View of Test Apparatus

the same film through the shuttered lens and mirror system.

This procedure was repeated at least 100 times to obtain enough data to completely map the velocity field in the core.

Typical data photographs are shown in Figures 73 and 74. The velocity data obtained was shown in Figure 23.

Phosphorescent Particle Flow Visualization

Flow visualization was accomplished by adding particles of Zn-CdS phosphor to the water in the system. Their motion, which closely followed the motion of the water, could then be observed by the light that they scattered from a collimated plane of light parallel to the flow from a continuous high-intensity light source.

By creating a beam of light of short duration, either by mechanically "chopping" the collimated light from the continuous source (a high-pressure, 1000-w mercury-arc light), or by using the collimated light pulse from a high-intensity electronic flashtube (such as the GE FT-503), the phosphor particles in the flowing water in the path of the beam could be excited at a given instant, thus "tagging" them; and, a short time later, as the band of glowing particles deformed into a shape corresponding to the velocity profile of the fluid, they could be observed.

A photograph of the mechanical chopper, which consisted of a solid rotating disk with a cut-out sector whose angle could be changed, mounted on the collimator is shown in Figure 75.

From this method, a qualitative idea of how the velocity profile looked could be obtained. At the time of the core model experiments, no film was found to be sensitive enough to register the glowing particles so that, in a
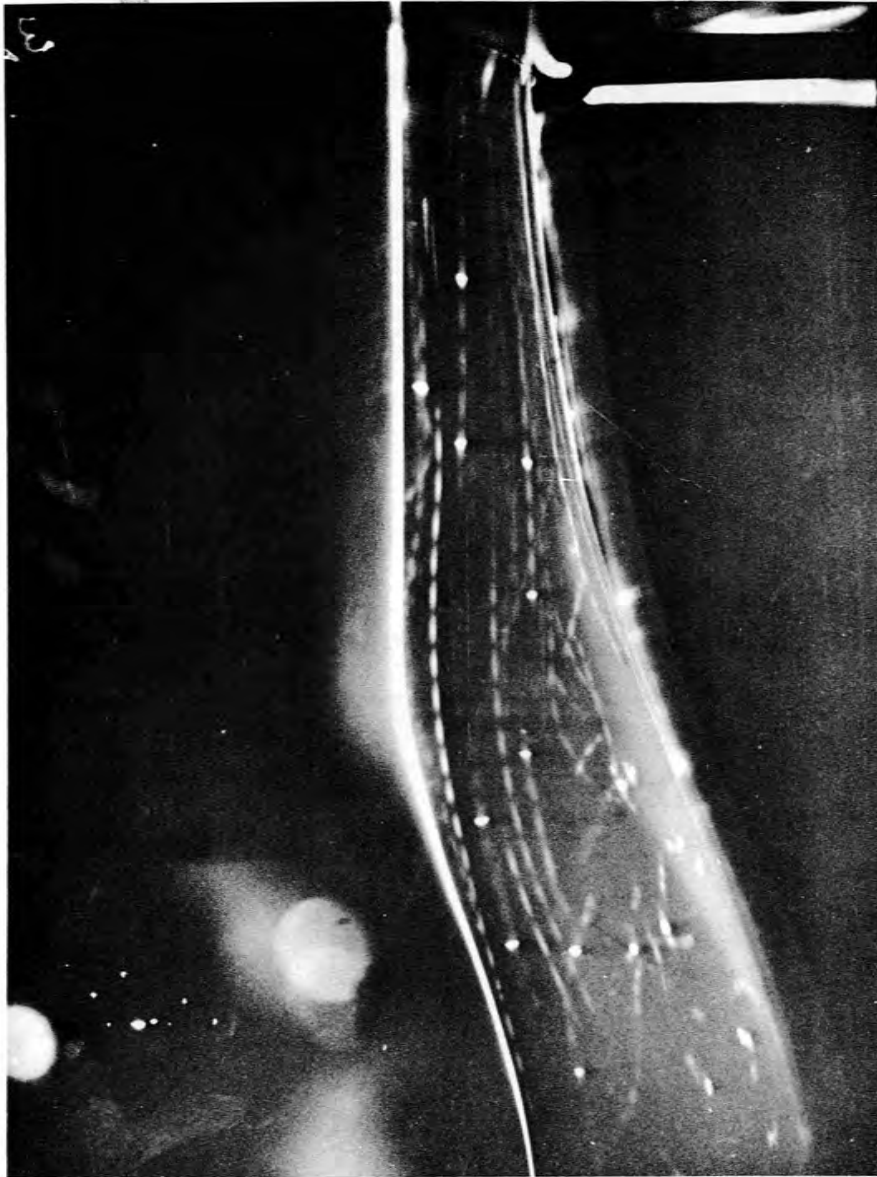
Fig. 73. Typical Data Photograph. The small light spots at the lower left are the numbers displayed on the Electronic Counter.
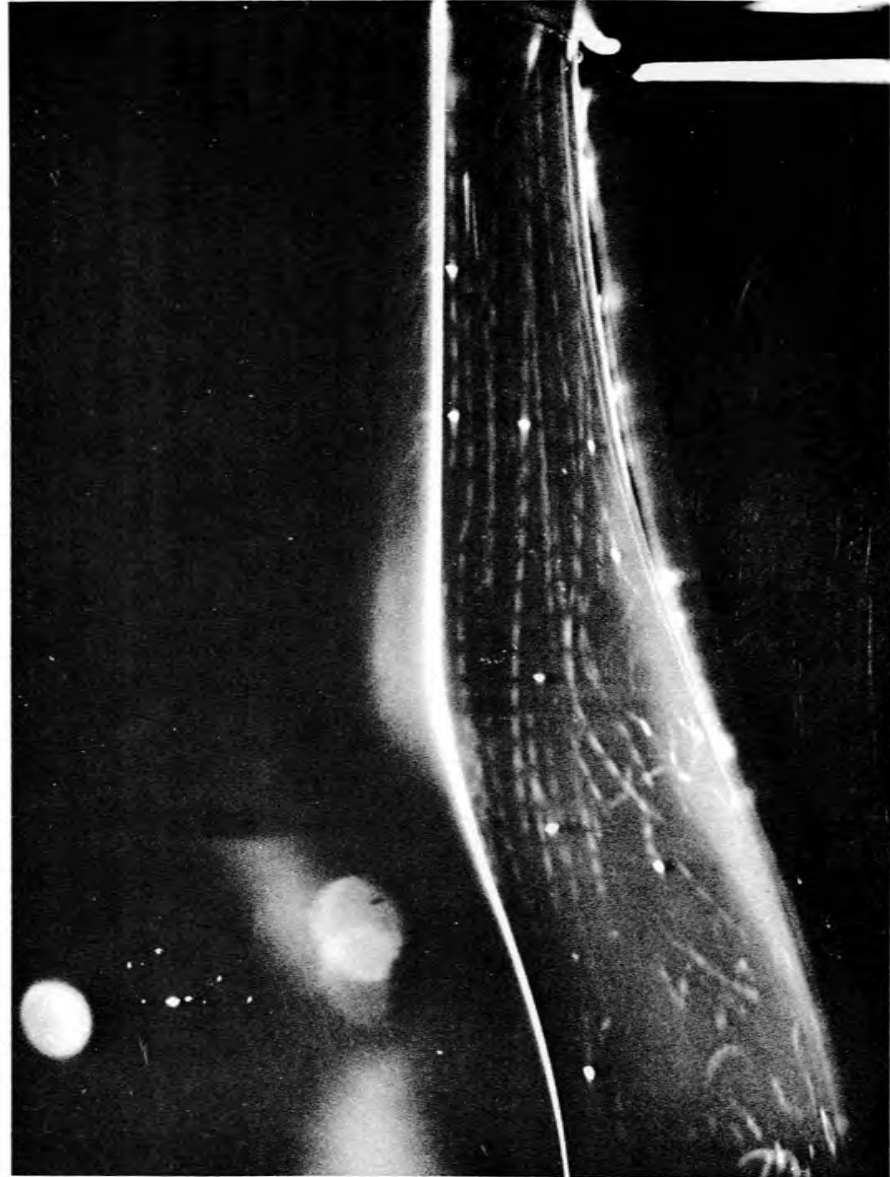
Fig. 74. Typical Data Photograph. The small light spots at the lower left are the numbers displayed on the Electronic Counter.
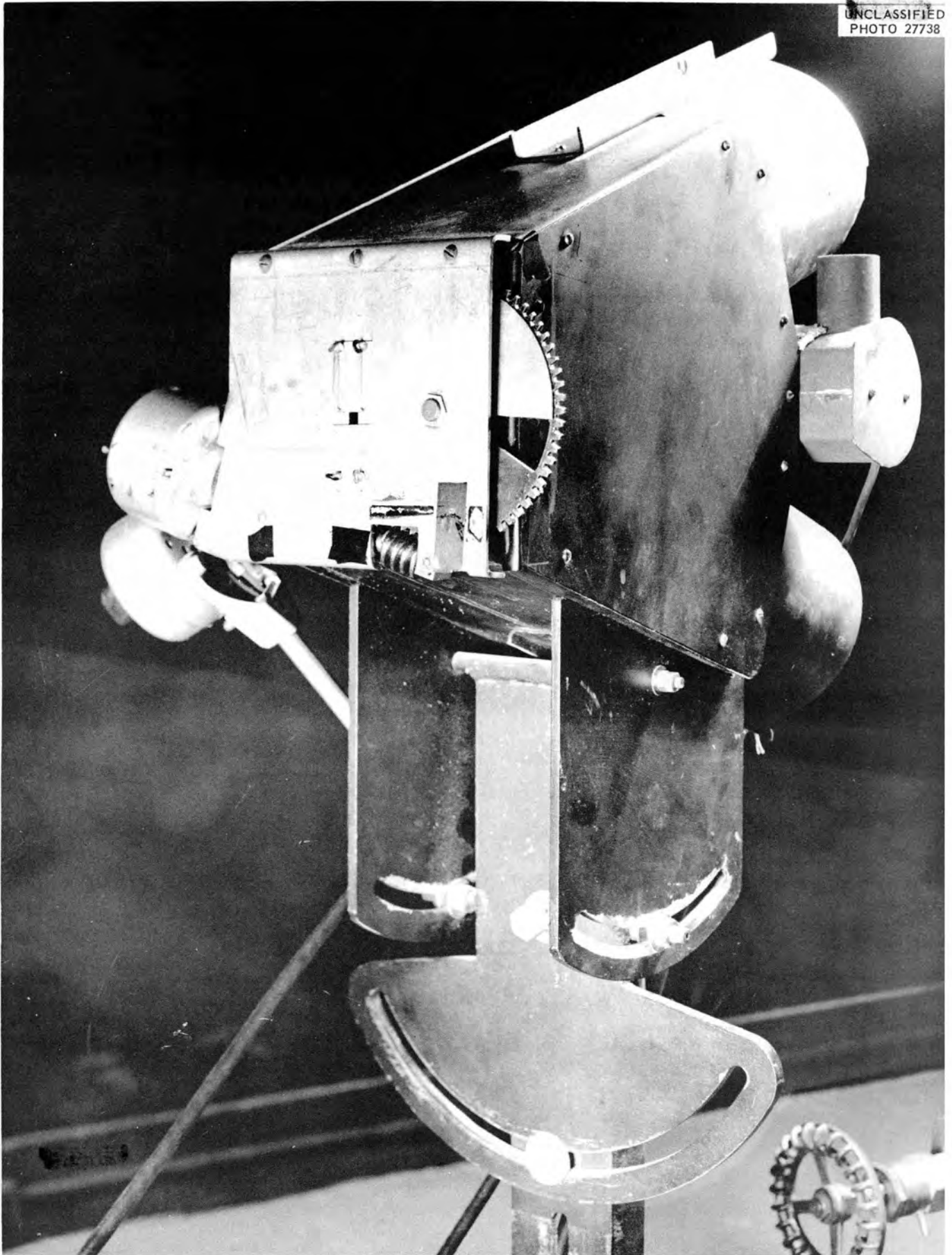
Fig. 75. Mechanical Light Chopper

manner similar to stroboscopic particle photography, the velocities could-
actually be measured. Recently, however, a feasibility study of photograph-
ing the band of excited phosphors as they distorted into a shape correspond-
ing to the velocity profile of water flowing in a tube was successful in ob-
taining photographs.[31] An experimental Eastman film with a speed of ASA 400-800
(S.O. 1177) was used in a 4 x 5-in. camera with a f1.8 lens. Eastman DK-60a
developer was used.

The method of making this method quantitative would be similar to the
stroboscopic particle photography method; the time between the excitation of
the particles and the taking of the photograph would be measured, and distances
obtained by comparison with a photograph of a similarly distorted grid, which
was previously placed in the plane of the motion of the excited particles.
Velocities are obtained from the division of distance by elapsed time.

APPENDIX B

FLOW SYSTEM COMPONENTS

Reservoir

A painted iron tank 40 in. deep and 24 in. in inside diameter served as the system reservoir. The top was open and afforded ready access for filling the system with water or adding particles for velocity measurement work. A motor-driven stirrer provided agitation to keep the particles suspended in the water. All connecting piping entered the reservoir under the level of the water maintained while the system was in operation, thus avoiding air entrainment from that source.

Centrifugal Pump

An Allis-Chalmers double-intake centrifugal pump with a 9-in. diameter impeller driven by a 5-hp electric motor was used to pump water around the flow circuit. The pump delivered 85 gpm at a 80-ft head. At shut-off, a head of 84 ft was obtained.

At a later date, a 10 3/4-in. impeller was substituted and a 7 1/2-hp electric motor was employed to drive the pump. With this arrangement, the pump delivered 100 gpm at a 100-ft head. At shut-off, a head of 120 ft was obtained. Figure 76 is a photograph of this pump and the reservoir.

Orifice Meters

Two thin-plate VDI-type orifices made by the Taylor Instrument Company having diameters of 1.530 and 0.765 in. were used alternately with a
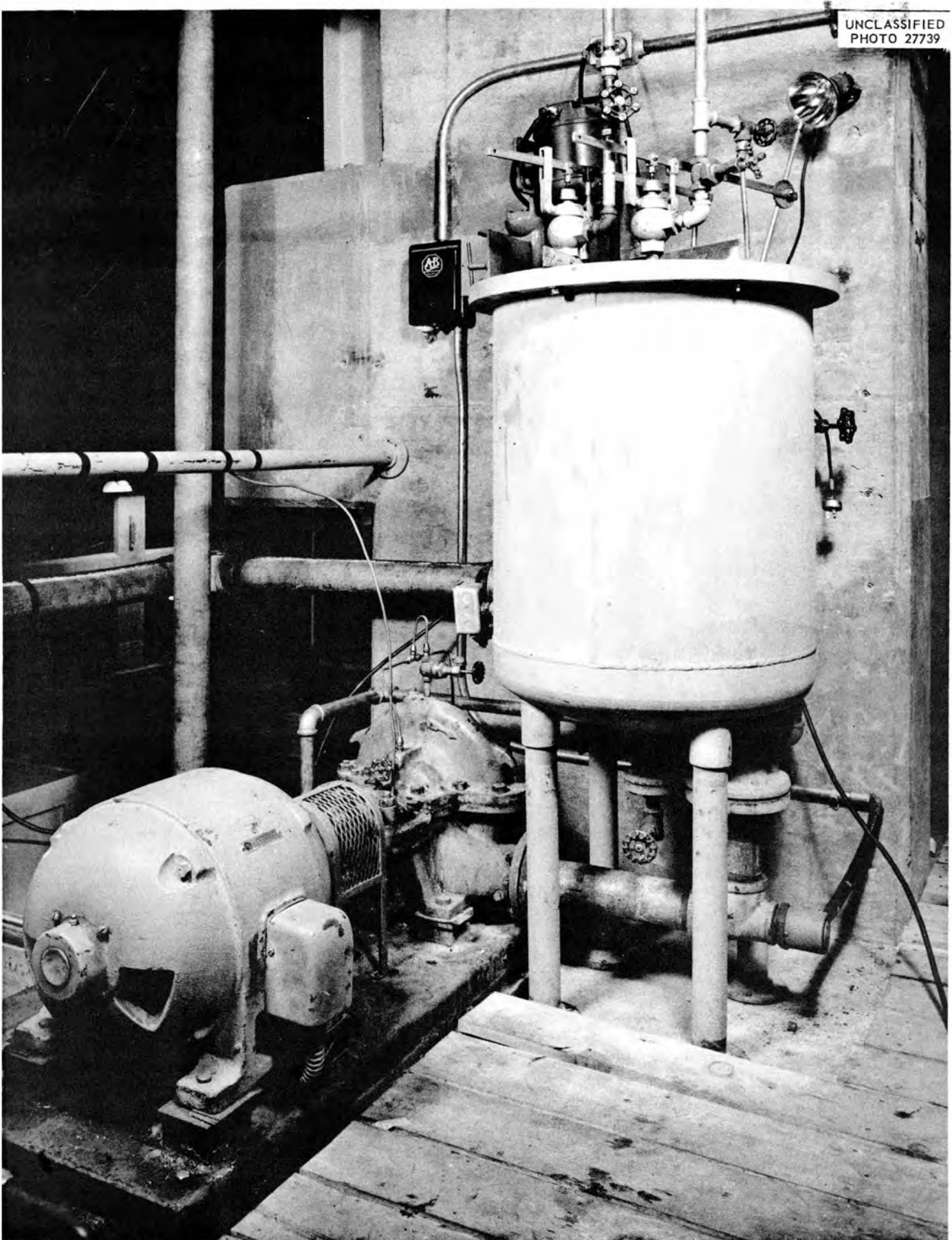
Fig. 76. Centrifugal Pump and System Reservoir

50-in. mercury-filled U-tube manometer connected across the orifice for measuring core flow rates. These diameters corresponded to 1/2-pipe diameter and 1/4-pipe diameter, respectively.

A measurable flow rate range of one to 100 gpm was obtainable.

A 30-diameter length of straight pipe preceded the orifice position.

Rotameters

A Brooks rotameter with a measurement range of 0.5 to 6.0 gpm and a Fischer and Porter rotameter of range 2 to 20 gpm were installed at a later date than the flowmeters.

Control Valves

Three globe-type valves were connected in a parallel arrangement to give good flow rate control over the entire range. A 3-in. valve, a 1-in. valve, and a 1/2-in. valve were used.

Temperature Control

A calrod immersion heater and a cooling coil made of copper tubing with cold water running through placed in the reservoir served to control the water temperature.

Core Test Stand

The core models were assembled on a support which formed part of the recirculating loop system, and which served to align the inner and outer shells.

A quickly removable section of pipe which served as the inlet to the core models facilitated access for changing or performing any alterations on the core models.

A view of the test stand with a core model in place on its support with the removable inlet pipe in place was shown in Figure 11.

REFERENCES

1. Poppendiek, H. F., Palmer, L. D., "Forced Convection Heat Transfer in Pipes with Volume Heat Sources Within the Fluids," ORNL-1395, February 1953.

2. Poppendiek, H. F., Palmer, L. D., "Forced Convection Heat Transfer Between Parallel Plates and in Annuli with Volume Heat Sources Within the Fluids," ORNL-1701, May 1954.

3. Poppendiek, H. F., Palmer, L. D., "Application of Temperature Solutions for Forced Convection Systems with Volume Heat Sources to General Convection Problems," ORNL-1933, September 1955.

4. Ball, R. E., "Investigation of the Fluid Flow Pattern in a Model of the 'Fireball' Reactor," ORNL Memo, Index No. Y-F15-11, Sept. 4, 1952.

5. Bradfute, J. O., et al, "Reactor Hydrodynamics," ANP Quarterly Progress Report, ORNL-1729, p 102, June 10, 1954.

6. Whitman, G. D., Stelzman, W. J., Furgerson, W. T., Aircraft Reactor Engineering Division, ORNL, Personal communication of unpublished velocity and pressure data for the ART "21-inch" Core.

7. Buri, "Dissertation," Zurich, 1931.

8. Nikuradse, Johann, "Untersuchungen Uber Die Stromungen Des Wassers In Konvergenten Und Divergenten Kanalen," Forschungsarbeiten, V.D.I., Volume 289, pp 1-49, 1929.

9. Keller, J. D., J. Appl. Mech. 16, pp 77-85 and p 320, (1949).

10. Bradfute, J. O., "Qualitative Velocity Information Regarding the ART Core; Status Report IV," ORNL CF 54-12-110, December 14, 1954.

11. Bradfute, J. O., Lynch, F. E., Muller, G. L., "Fluid Velocity Measured in the 18-Inch ART Core by a Particle-Photographic Technique," ORNL CF 55-6-137, June 21, 1955.

12. Muller, G. L, "Qualitative Estimates of the Velocity Profiles in the 21-Inch ART Core," ORNL CF 55-7-92, July 20, 1955.

13. Muller, G. L., Lynch F. E., "Qualitative Velocity Information Regarding Two Constant-Gap Core Models," ORNL CF 55-10-49, October 3, 1955.

REFERENCES (Continued)

14. Muller, G. L, Bradfute, J. O., "Qualitative Velocity Profiles with Rotation in 18-Inch ART Core," ORNL CF 55-3-15, March 1, 1955.

15. Lynch, F. E., and Muller, G. L., "Qualitative Velocity Profiles with a Rotational Component at the Inlet of the 21-Inch Core Model; G. F. Wislicenus Design," ORNL CF 55-10-50, October 3, 1955.

16. Lynch, F. E., and Bradfute, J. O., "Qualitative Velocity Profiles in 18-Inch ART Core with Increased Turbulence at its Inlet," ORNL CF 55-5-132, May 10, 1955.

17. Muller, G. L., "Qualitative Velocity Information Regarding the 18-Inch ART Core with Turbulator Vane Set No. 1 in Entrance," ORNL CF 55-6-174, June 27, 1955.

18. Lynch, F. E., "Qualitative Velocity Information Regarding the 18-Inch ART Core with Vane Set No. 2 in Entrance," ORNL CF 55-6-173, June 27, 1955.

19. Muller, G. L., and Lynch, F. E., "Qualitative Velocity Information Regarding the Quarter-Scale Model of the 18-Inch ART Core and the 5/22-Scale Model of the 21-Inch ART Core with the Pratt and Whitney Swirl Nozzles at the Inlet," ORNL CF 55-10-48, October 3, 1955.

20. Muller, G. L., Lynch, F. E., "Effects of Screen Packing in the ART 21-Inch Core and in an RMR Core Designed to Concentrate the Packing in the Core Entrance Region," ORNL CF 56-12-5, December 20, 1956.

21. Stelzman, W. J., Whitman, G. D., Furgerson, W. T., Personal communication of photographic data on dye filament fluctuations in full-size model of ART Core.

22. Goldstein, S., Modern Developments in Fluid Dynamics, Corrected Impression, Oxford University Press, Amen House, London, E. C. 4, 1950, Vol 1, pp 58-59.

23. Wattendorf, F. L., "A Study of the Effect of Curvature on Fully Developed Turbulent Flow," Proc. Roy. Soc. A, Vol 148, 1935, pp 565-598.

24. Baines, W. D., and Peterson, E. G., "An Investigation of Flow Through Screens," Trans. ASME, July 1951, pp 467-480.

25. Schubauer, G. B., and Spangenburg, W. G., "Effect of Screens in Wide-Angle Diffusers," NACA Report 949, 1949.

REFERENCES (Continued)

26. Stumpf, H. J., and Wilner, B. M., *ANP Quarterly Progress Report*, March 10, 1954, ORNL-1692, pp 37-39.

27. Poppendiek, H. F., et al., *Analytical and Experimental Studies of the Temperature Structure within the ART Core*, ORNL-2198, January 1957.

28. Laufer, J., "Investigation of Turbulent Flow in a Two-Dimensional Channel," *NACA Report 1053*, 1951.

29. Stelzman, W. J., Furgerson, W. T., *ANP Quarterly Progress Report*, September 10, 1956, ORNL-2157, Parts 1-5, p 28 (Figure 1.1.10).

30. Goldstein, S., *Modern Developments in Fluid Dynamics*, Corrected Impression, Oxford University Press, Amen House, London, E. C. 4, 1950, Vols. 1 and 2, plate 12-c, opp. p 76; plate 17-a, opp. p 82; plate 33-d, opp. p 552.

31. Palmer L. D., Lynch F. E., Winn, G. M., *Instantaneous Velocity Profile Measurement by Photography*, ORNL-2257 (to be published).

32. Mills, C. B., and Reese, H., "Design Study of an ANP Circulating-Fuel Reactor," WAD-1930, November 30, 1954.

33. *Nuclear Propulsion Program, Engineering Program Report No. 12, April 1 - June 30, 1954*, PWAC-542, pp 63-64.

34. *Nuclear Propulsion Program, Engineering Program Report No. 13, July 1 - September 30, 1954*, PWAC-543, pp 63-64.

35. *Nuclear Propulsion Program, Engineering Program Report No. 14, October 1 - December 31, 1954*, PWAC-544, pp 52-53.

36. *Nuclear Propulsion Program, Engineering Program Report No. 15, January 1 - March 31, 1955*, PWAC-551, pp 42-44.

37. *Nuclear Propulsion Program, Engineering Program Report No. 16, April 1 - June 30, 1955*, PWAC-552, pp 45-46.

38. *Nuclear Propulsion Program, Engineering Program Report No. 17, July 1 - September 30, 1955*, PWAC-553, pp 48-49.

39. *Nuclear Propulsion Program, Engineering Program Report No. 18, October 1 - December 31, 1955*, PWAC-554, pp 56-58.

REFERENCES (Continued)

40. Nuclear Propulsion Program, Engineering Program Report No. 19, January 1 - March 31, 1956, PWAC-561, p 66.

41. Nuclear Propulsion Program, Engineering Program Report No. 20, April 1 - June 30, 1956, PWAC-562, pp 62-63.

42. Nuclear Propulsion Program, Engineering Program Report No. 21, July 1 - September 30, 1956, PWAC-563, p 65.

43. Nuclear Propulsion Program, Engineering Program Report No. 22, October 1 - December 31, 1956, PWAC-564, p 64.

44. Nuclear Propulsion Program, Engineering Program Report No. 23, January 1 - March 31, 1957, PWAC-565, pp 61-64.

-141

ORNL-2199
C-84 - Reactors-Special
Features of Aircraft Reactors
M-3679 (20th ed. Rev.)

INTERNAL DISTRIBUTION

1. C. E. Center
2. Biology Library
3. Health Physics Library
4-5. Central Research Library
6. Reactor Experimental
   Engineering Library
7-11. Laboratory Records Department
12. Laboratory Records, ORNL R.C.
13. A. M. Weinberg
14. L. B. Emlet (K-25)
15. J. P. Murray (Y-12)
16. J. A. Swartout
17. E. H. Taylor
18. E. D. Shipley
19. M. L. Nelson
20. S. C. Lind
21. F. L. Culler
22. A. H. Snell
23. A. Hollaender
24. M. T. Kelley
25. J. H. Frye, Jr.
26. K. Z. Morgan
27. C. P. Keim
28. R. S. Livingston
29. A. S. Householder
30. C. S. Harrill
31. C. E. Winters
32. D. W. Cardwell
33. D. Phillips
34. A. J. Miller
35. R. A. Charpie
36. J. A. Lane
37. R. R. Dickison
38. R. B. Gray
39. J. Moshman
40. J. A. Amos
41. B. Cottrell
42. C. W. Cunningham
43. J. H. DeVan
44. W. K. Ergen
45. A. P. Fraas
46. W. T. Furgerson
47. A. G. Grindell
48. W. H. Jordan
49. M. E. Lackey

50. E. S. Bettis
51. C. J. Barton
52. F. F. Blankenship
53. W. R. Grimes
54. F. Kertesz
55. H. W. Savage
56. G. M. Kinyon
57. H. G. MacPherson
58. J. D. Manly
59. J. L. Whitman
60. J. L. Koch
61. J. T. Long
62. J. L. Gregg
63. D. E. Ellington
64. E. P. Blizard
65. C. M. Clifford
66. L. Doney
67. L. B. Holland
68. S. E. Beall
69. R. B. Briggs
70. S. I. Cohen
71. C. M. Copenhaver
72. W. R. Gall
73. W. R. Gambill
74. N. D. Greene
75. J. J. Keyes
76. A. I. Krakoviak
77. H. W. Hoffman
78. F. E. Lunch
79. R. N. Lyon
80. J. D. Powers
81. D. C. Thomas
82. J. L. Wantland
83. R. E. MacPherson
84. F. L. Bagley
85. E. R. Mann
86. L. A. Mann
87. W. B. McDonald
88. R. V. Meghreblian
89. A. M. Perry
90. A. W. Savolainen
91. R. D. Schultheiss
92. W. L. Scott
93. W. J. Stelzman
94. D. B. Trauger

95. G. D. Whitman
96. M. Yarosh
97. J. Zasler
98. M. Skinner
99. A. D. Callihan
100. G. W. Wilhöltz
101. O. Sisman
102. L. G. Alexander
103. E. J. Breeding
104. W. F. Boudreau
105. H. C. Claiborne

106. D. A. Douglas
107. D. A. Garrison
108. R. B. Lindauer
109. W. R. Osborn
110. M. W. Rosenthal
111. G. Samuels
112. I. Spiewak
113. A. Simon
114. C. S. Walker
115. ORNL Y-12 Technical Library,
    Document Reference Section

EXTERNAL DISTRIBUTION

116. Division of Research and Development, AEC, ORO
117-119. Air Force Ballistic Missile Division
120-121. AFPR, Boeing, Seattle
122. AFPR, Boeing, Wichita
123. AFPR, Curtiss-Wright, Clifton
124. AFPR, Douglas, Long Beach
125-127. AFPR, Douglas, Santa Monica
128. AFPR, Lockheed, Burbank
129-130. AFPR, Lockheed, Marietta
131. AFPR, North American, Canoga Park
132. AFPR, North American, Downey
133-134. Air Force Special Weapons Center
135. Air Materiel Command
136. Air Research and Development Command (RDGN)
137. Air Research and Development Command (RDTAPS)
138-151. Air Research and Development Command
152. Air Technical Intelligence Center
153-155. ANP Project Office, Convair, Fort Worth
156. Albuquerque Operations Office
157. Argonne National Laboratory
158. Armed Forces Special Weapons Project, Sandia
159. Armed Forces Special Weapons Project, Washington
160. Assistant Secretary of the Air Force, R&D
161-166. Atomic Energy Commission, Washington
167. Atomics International
168. Battelle Memorial Institute
169-170. Bettis Plant (WAPD)
171. Bureau of Aeronautics
172. Bureau of Aeronautics General Representative
173. BAR, Aerojet-General, Azusa
174. BAR, Convair, San Diego
175. BAR, Glenn L. Martin, Baltimore
176. BAR, Grumman Aircraft, Bethpage
177. Bureau of Yards and Docks
178. Chicago Operations Office
179. Chicago Patent Group
180. Curtiss-Wright Corporation

181. Engineer Research and Development Laboratories
182-185. General Electric Company
186. General Nuclear Engineering Corporation
187. Hartford Area Office
188. Idaho Operations Office
189. Knolls Atomic Power Laboratory
190. Lockland Area Office
191. Los Alamos Scientific Laboratory
192. Marquardt Aircraft Company
193. Martin Company
194. National Advisory Committee for Aeronautics, Cleveland
195. National Advisory Committee for Aeronautics, Washington
196. Naval Air Development Center
197. Naval Air Material Center
198. Naval Air Turbine Test Station
199. Naval Research Laboratory
200. New York Operations Office
201. Nuclear Development Corporation of America
202. Nuclear Metals, Inc.
203. Office of Naval Research
204. Office of the Chief of Naval Operations (OP-361)
205. Patent Branch, Washington
206-227. Pratt and Whitney Aircraft Division (1 copy each to G. Beardsley, C. C. Bigelow, A. I. Chalfant, W. Corliss, R. A. Doak, E. R. Dytko, H. C. Gray, M. Hoenig, C. E. Holtsinger, K. J. Kelley, R. W. Kelley, A. Y. Overman, B. A. Schmickrath, R. Dettrough, R. N. Wallace, D. P. Gregory, T. J. Woods, and G. L. Mulder)
228. San Francisco Operations Office
229. Sandia Corporation
230. School of Aviation Medicine
231. Sylvania-Corning Nuclear Corporation
232. Technical Research Group
233. USAF Headquarters
234. USAF Project Rand
235. U. S. Naval Radiological Defense Laboratory
236-237. University of California Radiation Laboratory, Livermore
238-255. Wright Air Development Center (WCOSI-3)
256-280. Technical Information Service Extension, Oak Ridge